11. ANALOGUES TO THERMALLY COUPLED PROCESSES

11.1 INTRODUCTION

Numerous igneous-intrusion contact zones have been examined with the objective of understanding chemical reactions and migration of elements away from the heated contact zone, as well as understanding thermal-hydrologic-chemical (THC) effects. A number of these studies are described in CRWMS M&O (2000 [141407]; 2000 [151945], Section 13), as summarized by the following.

The effects of shallow (<500 m) magmatic intrusions into unsaturated host rocks can be quite different from effects associated with deeper hydrothermal systems. Deeper, saturated hydrothermal systems may display evidence that a large-scale hydrothermal cell was established (Brookins 1986 [109877], p. 337). In contrast, both the Banco Bonito study (Stockman et al. 1994 [117820], p. 88) and the Grants Ridge basalt intrusion study (WoldeGabriel et al. 1999 [110071], p. 409) indicate that the effects of high-temperature (~850°C; Stockman et al. 1994 [117820], p. 88) intrusions into these unsaturated environments appear to have been slight, to have been limited to within 10 m or so of the contacts, and to show no evidence of fluid-driven convective heat transfer or pervasive hydrothermal alteration of the country rock. These field studies, along with the Paiute Ridge field studies (see Section 11.4), provide limiting high-temperature-case natural analogues for evaluating THC processes resulting from the heat released by the decay of radioactive waste in an unsaturated environment.

A good analogy for understanding future water-rock interactions at the mountain scale is the fossil hydrothermal system at Yucca Mountain itself. Most zeolitic alteration occurred 13 to 11.6 Ma, at about the same time as tuff emplacement (Bish and Aronson 1993 [100006], p. 148). After formation of the major zeolitic horizons, deep-seated hydrothermal activity persisted until about 10 Ma. This activity was evidently limited to temperatures of 90–100°C, because at prolonged exposure to temperatures greater than 90°C, the sorptive zeolites clinoptilolite and mordenite are altered to the nonsorptive minerals analcime plus quartz and/or calcite, and this transformation did not occur.

Section 11 reports analyses conducted since CRWMS M&O 2000 [141407] of THC and thermal-hydrologic-mechanical (THM) natural analogue studies. Section 11.2 presents the results of an extensive survey of geothermal literature for the purpose of obtaining insights from coupled processes operating in geothermal fields. Section 11.3 then provides a detailed examination of THC processes relevant to the Yucca Mountain drift-scale system, observed at the Yellowstone, Wyoming, geothermal field. Section 11.4 presents results of a field investigation and modeling study of evidence left in a fossil hydrothermal system at Paiute Ridge, Nevada. Next, examples are given in Section 11.5 of evidence for THC effects on transport. Section 11.6 reports THM effects to a potential repository from a number of settings with analogous conditions. Finally, Section 11.7 summarizes what can be learned about THC and THM coupled processes relevant to a potential high-level waste repository at Yucca Mountain. Information found in Sections 11.2 through 11.5 may help to support arguments associated with KTI KUZ 0407 listed in Table 1-1.

11.2 GEOTHERMAL ANALOGUES TO YUCCA MOUNTAIN THERMAL-HYDROLOGIC-CHEMICAL PROCESSES

11.2.1 Objectives

The goal of Section 11.2 is to demonstrate the utility of geothermal systems as natural analogues for processes that are expected to occur in the potential Yucca Mountain repository. The primary objective of Section 11.2 is to use geothermal systems as natural analogues for illustrating coupled processes that impact permeability, fluid flow, and chemical transport. The introduction to this section notes some of the key THC processes observed in geothermal systems, and how these processes might impact the potential Yucca Mountain repository. A summary of key components of geothermal systems is then presented, followed by a description of the potential Yucca Mountain repository and a discussion of limitations of geothermal analogues for the Yucca Mountain system. The main body of this report consists of descriptions of geothermal analogues for each of the key THC processes identified. This is followed by a discussion of how these processes could impact the total site performance. Finally, suggestions are made for additional work that would further extend the use of geothermal systems in the validation and confirmation of Yucca Mountain models. The initial stages of a literature survey identified the Yellowstone geothermal system as particularly relevant for the Yucca Mountain system. Detailed analysis of core samples from Yellowstone was conducted to supplement previous studies of the Yellowstone geothermal system. The results of this work are described in detail in Section 11.3 of this report.

11.2.2 Introduction

Geothermal systems can be used as a natural laboratory for examining many of the coupled THC processes expected for the potential nuclear waste repository at Yucca Mountain, Nevada (Simmons and Bodvarsson 1997 [126511]; CRWMS M&O 2000 [141407]). Key processes that are expected to occur in the potential high-level nuclear waste repository at Yucca Mountain, such as boiling and condensation and mineral dissolution and precipitation, and their effects on permeability, fluid flow, and radionuclide transport, can be observed in many geothermal systems. Prior use of geothermal systems as natural analogues has focused on the verification of geochemical models (e.g., Meijer 1987 [101345]; Apps 1995 [154615]; Bruton et al. 1995 [117033]). However, active and fossil geothermal systems can also yield important insights into the consequences of processes such as boiling, condensation, fluid mixing, and water-rock interaction associated with fluid flow in matrix and fractures (Figure 11.2-1). These systems allow observation of the effects of processes over much longer time scales than are possible in laboratory or field testing, and provide a benchmark for coupled process modeling. Characterization of the effects of water-rock interaction (such as mineral precipitation and dissolution) on matrix and fracture permeability in geothermal systems can then be used to estimate potential changes in fluid flow resulting from the thermal impact of storing high-level nuclear wastes in fractured ash flow tuffs.

This study builds upon an earlier review of geothermal systems as natural analogues (Simmons and Bodvarsson 1997 [126511]; CRWMS M&O 2000 [141407]). This study expands the scope of the earlier review by including additional THC processes that are observed in geothermal systems and incorporates the results of new geothermal studies as part of a literature review.

Because no single geothermal analogue is suitable for all elements of Yucca Mountain, the geothermal analogues are used to evaluate the effects of individual THC processes, with multiple geothermal examples examined for each process of interest.

11.2.3 Similarities between Geothermal Systems and Yucca Mountain

There are many similarities between geothermal systems and an anthropogenic (man-made) hydrothermal system that would be created by the emplacement of high-level nuclear waste. For most geothermal systems, intrusion of magma at shallow crustal levels results in high heat flow and the formation of a convective hydrothermal system with associated water-rock interaction. In the anthropogenic system, heat-generating nuclear waste would induce changes in the ambient system. Both types of systems are subjected to coupled THC processes (Table 11.2-1) such as conductive and advective heating, fluid flow and chemical transport through matrix and fractures, boiling and condensation, and mineral dissolution and precipitation. These processes can result in important changes in the fluid flow properties of the rocks surrounding the heat source over time.

The use of geothermal systems as natural analogues for THC processes is most applicable for the higher temperature (above boiling) operating mode, because many of the processes mentioned in Table 11.2-1 would have little effect on a cooler, sub-boiling repository. These processes will have a greater impact in the near-field area, where the effects of heating (and associated THC processes) are expected to be most pronounced. For all cases, the magnitude of the effects of many THC processes (such as boiling, condensation, mineral dissolution, and precipitation) is envisioned to be significantly reduced at Yucca Mountain as a result of the much lower anticipated fluid and thermal flux rates than those observed in active geothermal systems. Key differences between geothermal systems and Yucca Mountain are described in Section 11.2.7. However, geothermal systems provide well-constrained examples of how THC processes can modify important hydrogeologic properties (such as porosity, permeability, and sorptive capacity) that would affect the total system performance of a geologic high-level radioactive waste repository.

11.2.4 Key Physical Components of Geothermal Systems

Prior to providing detailed evaluation of geothermal systems of natural analogues, it is worthwhile to examine the key components of these systems. While geothermal systems are found in a variety of geologic and tectonic environments and have many different characteristics, they all share a number of common traits. These include: (1) heat source, (2) fluids, (3), permeable flow paths, and (4) impermeable boundaries. Another important feature present in many vapor-dominated geothermal systems is a heat pipe, consisting of a boiling zone and condensation zone. Each of these features is discussed below.

11.2.4.1 Heat Source

Most active geothermal systems have magmatic heat sources, consisting of shallow intrusions that provide a high-level heat source for periods ranging from 100,000 to over 1,000,000 years. These intrusive bodies also supply magmatic components (such as water, CO_2, SO_2, and HCl) that often control the chemistry of the reservoir fluids. For example, the granitic pluton

underlying The Geysers geothermal field in California was emplaced around 1.2 Ma (Dalrymple et al. 1999 [156374], pp. 293–297), serving as a long-lived heat source for the still-active geothermal field. The Krafla and Námafjall geothermal fields, located along the Mid-Atlantic Rift Zone in Iceland, are much younger systems, where recent ongoing volcanic activity (1975–1984) led to the injection of magma into an existing geothermal well bore (Larsen et al. 1979 [155885]).

11.2.4.2 Fluids

Geothermal energy is extracted from local thermal anomalies in the earth's crust through the withdrawal of heated fluids. These fluids have a number of origins: connate (formation) waters, surface (meteoric) waters, juvenile (magmatic) waters, and seawater. The relative amounts of these fluids depend greatly on the geology and tectonic environment, the groundwater hydrology, the local climate, and the size and composition of the cooling and degassing intrusive heat source. The origin and abundance of these fluid types in geothermal systems can be determined through isotopic and geochemical study of fluid compositions (e.g., Giggenbach 1997 [156338]; Kennedy and Truesdell 1996 [156339]; Arnórsson 1995 [156321]).

11.2.4.3 Permeable Flow Paths

The development of a convecting geothermal reservoir (and the successful exploitation of such a resource) depends on the presence of high-permeability pathways. Many geothermal reservoirs are hosted by rocks with low matrix permeabilities, resulting from either intrinsically low permeabilities (i.e., intrusive igneous rocks and welded ash flow tuffs) or from hydrothermal alteration. The presence of a high-permeability fracture network in many geothermal systems allows for the heated fluids to flow convectively within the reservoir. Such permeable fracture networks may be generated by faulting occurring within tectonically active areas (Moore et al. 2001 [156320]; Forster et al. 1997 [156355]).

11.2.4.4. Impermeable Seals

The longevity of a geothermal resource depends on the presence of an impermeable cap above the reservoir. Without such a cap, heated fluids would buoyantly rise to the surface, rapidly dissipating the heat of the source. This impermeable barrier may result from a pre-existing low-permeability formation, but often develops as a result of extensive argillic alteration occurring at temperatures of 100–200°C. Lateral permeability barriers along the margins of geothermal systems can form by precipitation of retrograde solubility minerals, such as anhydrite and calcite, from descending (and heating) fluids along the margins of a geothermal system (Allis and Moore 2000 [156316], p. 215).

11.2.4.5 Heat Pipes

Geothermal heat pipes have been described for a number of vapor-dominated geothermal systems (Ingebritsen and Sorey 1988 [137537]; Allis and Moore 2000 [156316]). In a geothermal heat pipe (Figure 11.2-1), water boils at the heated (lower) end, and water vapor migrates to the cooler region where it condenses and the heat of vaporization is released. The condensed water then flows back to the heated end by gravity or capillary forces. The region within the heat pipe will be at a nearly uniform temperature near the boiling point of water. The

condensate water will be undersaturated with respect to the host rock minerals and will begin to dissolve constituents from the rock and gases locally present. Some of the water containing the dissolved constituents will flow through the fractures back down towards the heat source. Water flowing back towards the heat source will boil again, precipitating the formerly dissolved solids. The repeated dissolution and precipitation will affect fracture permeability by locally widening apertures where dissolution takes place, or narrowing apertures where precipitation occurs.

The heat-pipe features observed in geothermal systems have also been demonstrated in smaller-scale laboratory experiments. A heat-pipe reactor was built using tuff chips from Yucca Mountain and operated for 30 days (Rimstidt et al. 1989 [142190]). In the top region (condensation zone), etching and dissolution were observed. In the center region, few indications of dissolution or precipitation were observed. In the bottom region, extensive precipitation was observed with silica, iron oxyhydroxides, stilbite, and possibly clays forming. A layer of rock grains tightly cemented with amorphous silica formed at the face of the heater; this mineralization would result in reduced permeability. Similar heat-pipe features were also observed in the column tests reported in Lowry (2001 [157900]).

11.2.5 Characteristics of the Potential Yucca Mountain Repository

The potential nuclear waste repository is sited within a section of crystal-poor, devitrified, moderately to densely welded Topopah Spring tuff that forms part of a 1,000 m (3,300 ft) thick section of 11–14 Ma ash flow tuffs at Yucca Mountain (CRWMS M&O 1997 [100223], Figure 35). The repository horizon is overlain by 300 m (980 ft) of nonwelded to densely welded tuff, and underlain by a sequence of nonwelded to densely welded Miocene ash flow tuffs, older Tertiary volcanic and sedimentary rocks, and Paleozoic dolomites. The repository would be located within the unsaturated zone (UZ), 350 m (1,150 ft) above the regional water table (Figure 11.2-2). The potential repository is located in fractured unsaturated host rock with very low matrix permeability. The combination of low matrix permeability and unsaturated rock helps keep water from waste packages, thus retarding unwanted processes such as corrosion of the waste packages, dissolution of the waste materials, and transport of radionuclides to local aquifers. Fluid flow along high-permeability fractures may, however, result in seepage.

The higher-temperature operating mode (BSC 2001 [155950], Section 2.3) consists of a drift spacing of 81 m (266 ft), with drip shields, line load waste packaging, and 50 years of drift ventilation after the waste has been emplaced. These design attributes (see also Section 2 of this report) are used to minimize seepage onto the waste containers, limit peak temperatures in the drifts, and reduce the likelihood of the development of coalescing boiling zones, thus permitting drainage to occur in the pillar regions between the drifts. For the higher-temperature operating mode, maximum temperatures of around 120°C are predicted for the drift wall (BSC 2001 [155950], Section 4.3.5.3.3), with temperatures greater than 100°C predicted to persist in the waste package and near-field for 1,000–2,000 years. Other design possibilities also under consideration include a lower-temperature operating mode in which the maximum temperature at the drift wall will never exceed 85°C (BSC 2001 [155950], Section 3.2.5).

The near-field repository environment is predicted to undergo two distinct phases resulting from the thermal loading: dryout and rewetting. Dryout is predicted to occur as the waste packages transfer their heat to the surrounding environment. The size of the dryout zone will vary with

time and may extend up to 13 m (43 ft) away from the drift walls, depending on waste package configuration (BSC 2001 [154677], Section 6.4.5.1). During the dryout phase, liquid water will be converted to water vapor, which will effectively displace air from this zone. This is important because the oxygen necessary for many corrosion reactions will be present only in low concentrations. As the heat output from the waste package diminishes with time, dryout zones are predicted to gradually undergo rewetting from reflux of CO_2-replenished condensate and ambient percolation. The rewetting will be accompanied by an influx of air back into the near-drift environment as temperatures drop below the local boiling point and slowly approach ambient (pre-repository) thermal conditions (BSC 2001 [154677], Section 6.6.5).

Subsurface fluid flow for the Yucca Mountain area is controlled by the permeability and unsaturated hydraulic properties of the Miocene ash flow tuff sequence. Densely welded sections of the tuff have very low matrix permeabilities, and fluid flow through these sections is controlled by faults and fractures. Nonwelded tuffs have significantly higher matrix permeabilities and fewer fractures, and thus matrix flow appears to be the dominant process in these sections. These differences in matrix and fracture permeability as a function of welding (Figure 11.2-3) are characteristic of ash flow tuff deposits (Winograd 1971 [156254]). The potential repository is located within a densely welded devitrified tuff (Figure 11.2-2), and thus bulk permeability for this horizon is controlled by fractures.

Fracture permeability depends on a variety of fracture characteristics, including fracture orientations relative to the regional stress field, fracture density and spacing, fracture apertures, and the presence or absence of mineralization within the fractures. Field permeability measurements have been made at the Yucca Mountain Exploratory Studies Facility (ESF) to evaluate the variability of permeability and identify controlling factors. The matrix permeability of the welded Topopah Spring tuff (TSw) is 3 to 6 orders of magnitude lower than the fracture permeability (LeCain 1997 [100153], pp. 28–29), so fluid flow within this formation should be highly focused along fractures.

11.2.6 Time Scales of Geothermal Processes

Time scales of processes expected to occur in a geologic nuclear waste repository are compared with processes that occur in geothermal systems shown in Table 11.2-2. Because of these very long and variable time scales, it is not possible to create a scale model of a potential nuclear waste repository, study all of these processes for a short while, and then extend this knowledge to real repository future behavior. Laboratory and field-scale studies have been conducted and others are currently underway to study some of these processes for the purpose of model validation. Computer-based numerical modeling is being used to interpret and extend these results within a framework of well-understood physical laws and data. The same processes expected to occur at a geologic high-level nuclear waste repository at Yucca Mountain have been occurring over the long-term in geothermal systems, making the study of geothermal systems highly relevant to the long-term understanding of possible repository behavior.

11.2.7 Limitations of Geothermal Analogues

It is important to note several important differences between most geothermal analogues and the potential Yucca Mountain repository:

- The potential Yucca Mountain repository is located within unsaturated rocks, while most geothermal systems have saturated conditions. While the repository may develop locally saturated areas (such as the condensation zone), this difference should result in reduced water-rock interaction for the thermally loaded repository system. Convective liquid flow will not develop under unsaturated conditions, and thus thermal and fluid fluxes for the Yucca Mountain system will be significantly lower than those found in high-temperature geothermal systems. Advective transport will still occur within the fracture network, and thus chemical transport rates could be fairly rapid along the fast flow paths within the UZ at Yucca Mountain. Several natural analogues that have experienced elevated temperatures under unsaturated conditions (Banco Bonito, New Mexico, and Paiute Ridge intrusive complex, Nevada) exhibit very little hydrothermal alteration resulting from the heat pulse event (Stockman et al. 1994 [117820]; Lichtner et al. 1999 [121006]; and Section 11.4 of this report).

- Liquid-dominated geothermal systems have increasing hydrostatic pressures with depth, reflecting the presence of a hydrostatic column. Boiling within a geothermal system at depth thus occurs at progressively higher temperatures (following the boiling point-depth curve). Because Yucca Mountain is an unsaturated system, fluid pressures will typically not exceed atmospheric pressure, and thus boiling should occur at temperatures around 96°C throughout the system.

- The higher-temperature operating mode for the potential Yucca Mountain repository is predicted to have an areally restricted and short-lived (1,000–2,000 yrs) higher temperature (>100°C) pulse, thus limiting the time when boiling and condensation processes could occur. In addition, because of the unsaturated nature of the Yucca Mountain system, dryout zones should develop around the high-temperature repository drift areas, also serving to reduce the potential impact of water-rock interaction.

- For the lower-temperature operating mode, drift-wall temperatures will never exceed boiling point values, and thus precipitation of dissolved species resulting from boiling will not occur. Some increase in the concentration of dissolved species may result from evaporation in this case. The lower predicted temperatures in this operating mode will also result in less extensive water-rock interaction, with reduced amounts of mineral alteration, dissolution, and precipitation.

- Speciation and transport of dissolved species may be affected by the redox state of the system. Geothermal systems are typically somewhat reducing in nature (as evidenced by the presence of H_2S rather than SO_2 in most geothermal fumarolic gases), whereas the Yucca Mountain system is expected to be more oxidizing (owing to the presence of atmospheric oxygen in the gas phase). This difference in oxidation state could affect the transport and precipitation of chemical components with multiple oxidation states (such as Fe^{2+}/Fe^{3+} and U^{4+}/U^{6+}), but should not significantly impact the behavior of important sealing species such as silica.

- Gas compositions of geothermal systems differ significantly from that predicted for Yucca Mountain, which lacks a magmatic fluid component. While both systems will contain CO_2 and air, most geothermal systems also contain significant amounts of sulfur-

bearing gases (typically H_2S) that can lead to the development of acidic fluid compositions when oxidized.

11.2.8 Geothermal Examples of Heat and Fluid Flow

Many geothermal systems worldwide have been the subject of heat and fluid flow studies. Fluid flow in geothermal systems is controlled in part by thermal buoyancy effects, chemically controlled density contrasts, and channelized flow resulting from permeability barriers. Drilling of exploration and production wells in developed geothermal fields facilitates the collection of downhole temperature and pressure data. Production flow and tracer tests also permit the determination of formation permeability and fluid flow paths and rates. Reservoir simulation models have been widely used along with such data to predict future heat and fluid flow behavior in commercial geothermal reservoirs under production (e.g., Bodvarsson et al. 1993 [138618]; Steingrimsson et al. 2000 [156686]; also see Section 11.2.8.2). The ability of these models to accurately forecast changes in reservoir behavior provides confidence that similar models developed for Yucca Mountain will reasonably simulate future repository performance. Two aspects of heat and fluid flow in geothermal systems are discussed in detail below. The first topic is the role of faults and fractures in providing high-permeability pathways for fluid flow within the convecting geothermal reservoir. The second topic is the use of numerical models to create natural-state models and to simulate the effects of production and reinjection on geothermal reservoirs.

11.2.8.1 Fracture-Dominated Fluid Flow

Many geothermal systems have reservoir rocks with relatively low matrix permeabilities, but high overall formation permeability caused by the presence of a high-permeability fracture network (Bodvarsson and Witherspoon 1989 [156337], p. 3). For some systems, this network is dominated by a few large-scale faults that control both the location of surface thermal features as well as fluid flow in the subsurface. Several examples of these geothermal systems are described below.

Dixie Valley, Nevada

The Dixie Valley geothermal field is located along the active Stillwater normal fault, in an area of high regional heat flow in the Basin and Range province of Nevada. The production wells are targeted to intersect strands of this fault at depth. Interference and tracer tests conducted in this field demonstrate that the high-permeability wells are well connected by a high-permeability fracture network. In a tracer test at Dixie Valley, three tracer combinations were introduced into three wells (Adams et al. 1989 [156348], pp. 215–217). Pre-test modeling based on the porous medium approximation identified seven well pairs that were expected to show tracer breakthrough. Only one well produced tracer, identifying a connected fracture network between the injection site and the producing well. The minimum velocity (based on a straight line between injection and the producing well) for the tracer front was 5 m/hr, and the minimum velocity for the tracer peak was 1.4 m/hr. As part of another investigation at Dixie Valley, a series of four tracer tests was performed (Rose et al. 1998 [156341]). Tracers were introduced in pulses in target injection wells located in the southern and central portions of the field. The tracers were detected only in a cluster of seven wells located between the injection wells. The

amount of short-circuiting between the wells differed for each injection well, with one of the wells having a much shorter residence time than the others, indicating heterogeneity in the fracture network. Breakthrough curves presented by Rose et al. (1998 [156341], Figure 2) can be used to calculate tracer-front minimum velocities ranging from about 0.7 to 3 m/hr (average = 1.6 m/hr) and peak minimum velocities ranging from about 0.4 to 0.8 m/hr (average = 0.6 m/hr).

Silangkitang, Indonesia

The Silangkitang geothermal field is one of several geothermal systems located along the Great Sumatran fault zone. The main thermal features are located along surface traces of this major strike-slip fault (Gunderson et al. 1995 [156361], p. 691). Exploration wells drilled directionally to penetrate the main trace of the fault encountered extremely high fluid flow rates within the fault zone (Gunderson et al. 2000 [156310], Figure 4, pp. 1184–1185). In contrast, nearby vertical wells that do not intersect the fault have very low formational permeabilities, thus underscoring the importance of the fault in providing high-permeability flow paths. Higher temperatures and increased alteration were encountered near the fault, which serves as an upflow zone for this geothermal system (Moore et al. 2001 [156320], pp. 1190–1191).

Wairakei, New Zealand

The Wairakei geothermal field is located in the Taupo Volcanic Zone, a tectonically active area that has been the site of voluminous Quaternary volcanism. Normal faults cutting the area appear to be the primary conduits for high-volume fluid flow. Grindley (1965 [154663]) identified three groups of wells based on their relative deliverabilities. Wells intersecting faults have very high permeabilities (>1 darcy) that cannot be precisely quantified because of a lack of pressure drawdown during production tests. Wells drawing on reservoir storage have pronounced drawdown, with calculated permeabilities ranging from 5–30 millidarcies. Nonproductive wells typically intersect hydrothermally cemented rocks with intrinsically low (<1 millidarcy) permeabilities. The intensely altered, impermable rocks serve to protect the producing reservoir from cold water encroachment. Tracer tests conducted at Wairakei (Jensen and Horne 1983 [156643], Table 1) suggest minimum flow velocities along fractures that are as high as 38 m/hr. These flow velocities result from high-pressure gradients within the system; similar gradients are not expected for Yucca Mountain.

Relevance to Yucca Mountain

These geothermal examples show the importance of high-permeability fractures in the circulation of geothermal fluids. Numerous normal faults (i.e., Solitario Canyon, Bow Ridge, Dune Wash, Drill Hole Wash, Pagany Wash, Sever Wash, Sundance, Ghost Dance) have been identified at Yucca Mountain, but little is currently known about their permeability (BSC 2001 [155950], Section 3.3.4.5.1). If these faults are permeable, then they could serve as fast fluid flow paths for infiltrating surface waters reaching the repository level, as well as pathways for dissolved radionuclide transport from the waste packages down to the water table.

The presence of bomb-pulse tritium and ^{36}Cl in water samples collected from core samples from the potential repository horizon within Yucca Mountain suggests that fault and fracture pathways have experienced relatively fast rates of fluid flow (Fabryka-Martin et al. 1997 [100145]). Based

on these results, minimum fluid-flow velocities calculated using a distance of 300 m (distance from the surface to the sampled areas) and a maximum time of 50 years (first generation of bomb-pulse tritium and ^{36}Cl) are on the order of 0.0007 m/hr; these rates are much slower than those observed in geothermal fields. Because the bomb-pulse tracer flow rate estimate is poorly constrained, a number of fluid flow experiments have been conducted along faults within the ESF at Yucca Mountain with the goal of obtaining better estimates of flow velocities. A series of *in situ* flow tests was conducted in Alcove 4 between two boreholes 1.07 m apart that intersected a minor normal fault (Salve and Oldenburg 2001 [157316], Figure 8, p. 3049). Measured flow velocities along the fault ranged from 0.08–0.58 m/hr. In another test between Alcove 8 and Niche 3, the time (~840 hr) between water release and the onset of seepage along a fault that intersects both the main drift and cross-drift tunnels (Figure 11.2-4) and the distance between these two areas (~25 m) can be used to calculate a flow velocity of about 0.03 m/hr (Salve et al. 2001 [156848]). The measured fluid velocities from these field experiments are significantly higher than those obtained from the bomb-pulse data and may reflect the need for surface infiltration rates to be high enough to initiate and sustain fracture flow (Flint et al. 2001 [156351], pp. 19–21, 24, 25).

The percolation flux at Yucca Mountain is much lower than the fracture flow rates described above. The percolation flux depends on the magnitude and spatial distribution of surface infiltration rates, as well as other factors, such as the presence of fast flow paths and lateral diversion within low-permeability intervals. Present-day infiltration rates are estimated to vary from 0–80 mm/yr, with an average value of about 5–10 mm/yr, for the potential Yucca Mountain repository block area (Flint et al. 2001 [156351], pp. 22–23). Thus, it is critical to understand the role of faults and fractures at Yucca Mountain and how these features could serve to accelerate and/or focus fluid flow within the potential repository.

11.2.8.2 Heat and Fluid Flow Simulations for Geothermal Systems

Numerical simulation of geothermal fields has been performed successfully for more than three decades. The Code Comparison Study (Molloy 1981 [156407]) evaluated several geothermal simulators with six test problems. The codes tested all performed reasonably well, indicating that the physics of the test problems were correctly represented. Numerical simulation of geothermal fields has proved to be of great economic importance in aiding geothermal companies to understand where to drill and to predict production capacity (Simmons and Bodvarsson 1997 [126511]). In a recent examination of geothermal simulations, more than 100 field simulations have been carried out worldwide since 1990 using a variety of simulators (O'Sullivan et al. 2001 [156353]).

Over the decades of geothermal reservoir simulation, a robust modeling process has been developed. The process includes data collection and evaluation, conceptual model development, numerical model design, natural-state modeling, history matching, prediction, and postauditing. Each step is dependent on the preceding steps, and thus changes in any preceding step require modifications in all subsequent steps.

In the first step, all available data are evaluated. The data may be from several sources, including flow tests, well logs (temperature, lithology, electrical resistivity), fluid chemistry, self-potential surveys, measurements on core samples, topography, location and flow rates from hot springs

and fumaroles, seismic data, precision gravity surveys, and other techniques. The data evaluation may be performed by individuals from many disciplines, yielding a conceptual model that is typically distilled into a few plan- and cross-sectional schematics providing an understanding of how the reservoir works.

The numerical model is constructed to resemble the conceptual model. Region size, gridblock sizes, boundary conditions, fluid chemistry, and equations of state are selected and parameters are assigned for each gridblock. The first step in model calibration is natural-state modeling. In natural-state modeling, the numerical model is tested by placing a heat source into the system at some time in the past (usually thousands to millions of years ago) and running the model forward to obtain a match with current measurements. If an adequate match is not obtained, parameters are altered within reason and the process is repeated. Many iterations are often required, and this procedure may be partially automated (White et al. 1997 [156340]; Bullivant and O'Sullivan 1998 [144410]; Finsterle 1999 [104367]). The importance of field features may be identified in this step, often leading to inferences of fluid inflows and faults.

The second step in model calibration is history matching, which can be performed when fluids have been produced from the geothermal system. In history matching, the field perturbation (caused by fluid extraction) is modeled, with the results compared to field measurements (temperature, pressure, enthalpy, brine composition). Again, parameters are adjusted until a reasonable match is obtained. Since natural-state modeling is performed for long time frames and history matching over significantly shorter time frames (years to decades), different types of parameters can be inferred. In natural-state modeling, parameters such as permeability are inferred. In history matching, storage-type parameters like porosity are inferred. Changes in parameters at any stage require verification in earlier stages. Calibration of a model using both natural-state modeling and history matching is a significant milestone in the creation of a viable reservoir model and becomes increasingly difficult as the amount of data increases.

Upon completion of successful natural-state modeling and history matching, the model is used for predictive purposes. Geothermal fields are modeled for a variety of reasons, but generally to devise a strategy for energy extraction. These models are generally evaluated and updated when development is planned. Few postaudits of geothermal field models have been published (post audits of two fields were found in the literature), although model performance is often monitored and demonstrated. The postaudit of Olkaria East Geothermal Field, Kenya (Bodvarsson et al. 1990 [136384], pp. 399–407) showed that the field-wide decline in steam rate agreed very well with predictions. A well-by-well comparison identified adequate predictions for 75% of the wells. Many of the wells for which prediction was inadequate had limited production when the initial model was constructed, and thus there was insufficient history on which to base the predictions for these wells. In a postaudit of the Nesjavellir Field, Iceland, Bodvarsson et al. (1993 [138618]) evaluated predictions made with a 1986 model for pressure decline and enthalpy changes. Acceptable agreement was reported between modeled and measured data (Figure 11.2-5), particularly considering that the prediction time (6 years) was longer that the 1–3 yr calibration period. A second audit was performed of the Nesjavellir geothermal system (Steingrimsson et al. 2000 [156686]) because the model underestimated enthalpy decline in some wells. Recalibration led to slight changes in the conceptual model within the producing region of the reservoir. The new model matched well data better, but the larger-scale reservoir performance predictions remained unchanged.

The geothermal industry relies heavily on the use of models, and at many fields several generations of models have been used. Beginning in the early 1980s, UNOCAL developed and maintained 3-D models of U.S., Philippine, and Indonesian geothermal fields (e.g., Williamson 1992 [156613]; Strobel 1993 [156614]; Murray et al. 1995 [156612]). The Wairakei geothermal field (New Zealand) has been modeled since the late 1960s, including many types of models and levels of complexity (O'Sullivan et al. 1998 [154567]). The Kawerau geothermal field (New Zealand) has also been extensively modeled for more than a decade (White et al. 1997 [156340]). These models have been upgraded over time as new information, codes, and techniques became available. The accumulated longevity of the models at a particular field indicates a significant degree of confidence in geothermal reservoir modeling.

Application to Yucca Mountain

There are a number of similarities and differences between modeling geothermal reservoirs and modeling the potential high-level nuclear waste repository at Yucca Mountain. The volume and number of dimensions modeled at Yucca Mountain are similar to those employed for geothermal reservoir modeling. The number of gridblocks in Yucca Mountain models ranges from hundreds to millions. The time scale for Yucca Mountain THC coupled process models is similar to the time scales of natural-state geothermal modeling, but significantly exceeds the time scale of history-matching reservoir models used to predict future reservoir behavior. The temperature and pressure conditions expected at Yucca Mountain are well within the range observed and modeled for geothermal reservoirs.

The aims of modeling geothermal fields and modeling Yucca Mountain are different. Geothermal reservoirs are generally modeled to optimize energy extraction for economic gain. To that end, fluid extraction and injection rates, enthalpy, and the number and location of replacement wells are needed. Modeling for the potential Yucca Mountain repository is performed to describe the environment within the repository drifts and to assess the potential for release of the emplaced radionuclides and their fate. Data collection at Yucca Mountain to constrain these models has been extensive; however, much of it is related to small-scale measurement and requires scaling to be adequately represented in the numerical models. Repository performance depends on: (1) the amount of water that may seep into the repository, (2) the temperature and humidity near the waste packages, and (3) the ability of the natural system to sorb and retain radionuclides possibly escaping the repository (Bodvarsson et al. 1999 [120055], pp. 3, 5). As understanding geothermal systems requires modeling at various scales (i.e., well scale, zone scale, and field scale), so modeling for Yucca Mountain requires modeling at multiple scales (drift scale, mountain scale), but in addition requires an understanding at smaller scales, because flow on smaller scales may impact repository performance.

Prediction time frames for geothermal fields range from 10–50 years. It is generally accepted in the geothermal-modeling community that predictions for a well-studied geothermal field are valid only for a time scale on the order of magnitude of the history-matching data (Bodvarsson et al. 1993 [138618]), because of uncertainties in assigning parameters to the model. It is not realistic to collect history-matching data for a 10,000-year period of model confidence for the thermal system at Yucca Mountain. Tests applying thermal perturbations to Yucca Mountain are planned for as long as eight years. Because of this, the modeling efforts for the potential repository have investigated potential behavior for a large range of possible conditions, including

higher and lower percolation fluxes resulting from climate changes, different heat loads, and different waste package arrangements. Sensitivity analyses have been performed for a variety of model parameters (Bandurraga and Bodvarsson 1999 [103949]).

Modeling for the Yucca Mountain repository has benefited greatly from the foundation produced from the robust modeling techniques developed in geothermal modeling. Wu et al. (1999 ([117161], pp. 186–188) reviewed many of the earlier thermal-hydrologic (TH) modeling efforts. These coupled, multiphase, multicomponent models simulate the flow and distribution of moisture, gas and heat at Yucca Mountain for use in predicting current and future conditions in the UZ. For example, Tsang and Birkholzer (1999 [137577]) used a 3-D coupled TH numerical model to predict the results of the Single Heater Test at Yucca Mountain. They obtained good agreement between measured temperatures and model results, and the simulated dryout and condensation zones were consistent with radar tomography and air-permeability data.

More recent Yucca Mountain modeling efforts (e.g., BSC 2001 [154677]) have utilized the TOUGHREACT code (Xu and Pruess 2001 [156280]), which couples reactive chemistry and transport to the TOUGH2 code used to create many of the TH models. The coupled THC models incorporate heat and fluid flow, chemical transport, kinetic and equilibrium mineral-water reactions, and coupling between mineral dissolution and precipitation, porosity, and permeability for a fracture-matrix system. Three heater tests have been performed (the Large Block Test, the Single Heater Test, and the still-active Drift-Scale Test [DST]) to allow assessment of the numerical models. These tests provide data (for validation of Yucca Mountain numerical models) that are analogous to production data used for history-matching exercises performed on geothermal reservoir models. The duration of these thermal-perturbation tests is short relative to the time scale of the potential repository, with the DST having a four-year heating phase followed by a planned four-year cooling phase. These thermal tests have been used to validate the THC model by comparing measured gas and water chemistry from the DST to the results of simulations obtained using the DST THC model (BSC 2001 [154677]). The THC model captures the observed changes in pH, Ca, Cl, and CO_2 concentrations over time for areas that have different thermal histories, and is consistent with the results of TH modeling (BSC 2001 [154677], Sections 6.2.7 and 6.2.8).

Simulations of the anticipated system at Yucca Mountain have been performed using coupled-process modeling to assess THC effects on seepage and fluid flow within the near-field environment (BSC 2001 [154677]). Fracture porosity reductions in the near-field environment resulting from the precipitation of calcite and silica are predicted to be less than 3% (for the homogeneous model; higher fracture porosity reductions of 5% were obtained for heterogeneous fracture permebility models), and thus only minor changes in permeability and fluid flow caused by THC processes are expected to occur (BSC 2001 [155950], Section 4.3.6.4.2). Similar to postaudit reviews of geothermal reservoir models, Yucca Mountain models should be regularly updated, as new data become available, to maximize their effectiveness as a repository management tool.

11.2.9 Chemical Transport in Geothermal Systems

The transport of chemical species in geothermal systems is intimately linked to advective fluid flow. Chemical constituents of geothermal fluids are commonly used to infer deep reservoir

temperatures, identify sources of fluids (such as magmatic, meteoric, connate, and condensate waters), and monitor important processes such as injectate breakthrough and influx of ground waters into producing portions of geothermal reservoirs. Because fluid velocities are rapid (and often faster than chemical reequilibration rates) within most geothermal systems, the chemistry of reservoir fluids sampled at surface thermal features can be used to estimate reservoir conditions. For example, chloride springs found at many geothermal systems are typically derived in large part from deep reservoir fluids. The chemical compositions of geothermal waters are commonly used to determine reservoir temperatures using a variety of silica and alkali geothermometers (Fournier 1991 [105419]). Natural and introduced chemical tracers are used to monitor fluid velocities, estimate flow paths, examine fracture-matrix interaction, and identify the sources of fluids within geothermal systems. The presence of hydrothermal minerals along veins and fractures in fossil geothermal systems is evidence for chemical transport (and subsequent mineralization) in these systems.

11.2.9.1 Geothermal Tracer Tests

For conservative tracers (such as iodine and chloride), tracer travel time represents the flow rate of advecting fluid within the geothermal reservoir. Tracer tests at Dixie Valley and Wairakei (previously summarized in Section 11.2.8.1) indicate minimum tracer velocities ranging from 0.7 to 38 m/hr. In some Japanese fields, tracer returns have been observed at rates of up to 100 m/hr, indicating high-conductivity fractures. Observed tracer speeds in the Hatchobaru field are as high as 80 m/hr (Horne 1982 [156362], p. 501).

Naturally occurring tracers are commonly used in geothermal fields to evaluate important processes such as heat flow, groundwater influx, and reinjectate breakthrough. Measurements of the total amounts of chloride and boron (nonreactive components that are often magmatic in origin) associated with surface feature discharges have been used to estimate heat flow values of geothermal systems (e.g., Fournier et al. 1976 [156817]; Sorey and Lewis 1976 [156809]). Because reinjected fluids have higher chloride contents than produced fluids (due to the concentration of chloride in the liquid phase resulting from the removal of steam), the arrival of reinjected waters in production zones can be detected and monitored by tracking chloride contents of production well brines. Chloride generally behaves in a conservative fashion (it is nonsorbing and is not involved in mineral precipitation, except in very saline water), and thus generally reflects the effects of mixing and boiling only.

Bulalo, The Philippines

Tracer tests conducted at the Bulalo geothermal field have been used to monitor the dispersal of injected fluids within the reservoir, track the influx of groundwater influx, and identify high-permeability flow paths (Villadolid 1991 [156656]). Changes in chloride contents and fluid enthalpies were used in production wells to identify the contribution of reinjected fluids in production wells. Elevated concentrations of tritium were interpreted to indicate zones where downflux of groundwater along permeable flow paths occurred. Rapid increases in magnesium concentrations following acid stimulation in neighboring wells were used to identify fast flow paths between wells.

11.2.9.2 Application to Yucca Mountain

Gravity-driven fracture flow is predominant through the fractured units with low matrix permeability at Yucca Mountain. Chemical transport accompanying percolation flux and associated seepage into cavities over time is evidenced by the precipitation of calcite and opal along fracture and cavity surfaces. Textural observations and fluid inclusion, isotopic, and geochronologic data on the coatings suggest that these secondary minerals were deposited from infiltrating meteoric water under unsaturated conditions (Whelan et al. 2001 [154773], p. 6). Using an equilibrium evaporation model to predict calcite and opal precipitation associated with seepage into lithophysal cavities, Marshall et al. (2000 [151018], p. 4) calculated that the total seepage volume over the past 10 million years (m.y.) is approximately 5×10^4 times greater than the volume of secondary calcite precipitated over the same time period at Yucca Mountain. This model assumes that all water is calcite-saturated, and no significant dissolution of calcite has occurred. The seepage flux estimated from this model (4×10^{-6} mm/yr (Marshall et al. 2000 [151018], p. 5)) may be used to calibrate predicted rates of seepage into drifts for numerical models (e.g., Birkholzer et al. 1999 [105170]) as well as provide insights relating to chemical transport rates and mechanisms at Yucca Mountain.

A key factor affecting chemical transport at Yucca Mountain involves possible interaction between minerals and dissolved constituents. The effects of ion exchange are demonstrated by the marked difference in strontium concentrations of perched waters in the Topopah Spring and Calico Hills tuffs. The strontium contents of perched waters in the UZ-14 and WT-24 boreholes (that sample the stratigraphically higher Topopah Spring tuff) range from 169–240 ppm (Sonnenthal and Bodvarsson 1999 [117127], Table 3). Much lower strontium concentrations (3–11 ppm) were measured for perched waters from the SD-7, SD-9, and NRG-7A boreholes in the Calico Hills tuff. The lower strontium values from these samples were interpreted by Sonnenthal and Bodvarsson (1999 [117127], pp. 119–120) to result from ion exchange between the perched waters and Ca-rich zeolites, which are abundant in the Calico Hills tuff (see Figure 7-2). These zeolite-rich tuffs form an important part of the geologic barrier inhibiting radionuclide transport from the repository down to the water table at Yucca Mountain.

11.2.10 Geothermal Examples of Boiling and Dryout

Many geothermal systems have localized boiling zones resulting from upward flow of high-enthalpy fluids, or from depressurization induced by geothermal production. Dryout zones (areas where fluids have boiled to dryness) are much less common, and typically are associated with the transition between liquid-dominated to steam-dominated geothermal systems. The effects of boiling on fluid chemistry, mineral precipitation, and reservoir permeability have been documented for a number of natural-state and producing geothermal systems. Dryout zones are more transient features, and thus are more difficult to characterize. However, as discussed in Section 11.2.10.2, detailed study of cores from the Karaha-Telaga Bodas geothermal field provides some insights as to how these zones develop and their significance. Summaries of some relevant geothermal examples of boiling and dryout are presented below.

11.2.10.1 Boiling in Geothermal Systems

Boiling is a common phenomenon in high-enthalpy geothermal systems. Many of these systems have high-temperature (≥100°C) thermal features (boiling hotsprings and superheated fumaroles) resulting from the depressurization of high-enthalpy fluids ascending to the surface. Localized boiling within the reservoir can also occur as a result of production of geothermal fluids, which decreases reservoir pressure. The process of boiling results in increased concentrations of dissolved constituents in the residual liquid phase, as well as the partitioning of volatile species (such as CO_2) into the gas phase. These changes often lead to the precipitation of phases such as amorphous silica and calcite. Several examples of the observed effects of boiling in geothermal systems are given below.

Waiotapu, New Zealand

The Waiotapu geothermal system is the largest of the 20 major geothermal systems located in the Taupo Volcanic Zone on the North Island of New Zealand (Hedenquist 1991 [156315]). Surface thermal features include fumaroles and associated acid sulfate springs along the flanks of dacite cones, and numerous chloride, acid-sulfate and mixed composition hot springs located in Waiotapu Valley. The chloride springs represent the liquid component of the hot (≥230°C) reservoir fluid that feeds these surface features.

Champagne Pool, one of the largest of the chloride springs at Waiotapu, has a surface temperature of 75°C (Hedenquist 1991 [156315], Table 1, pp. 2756, 2758–2764). It derives its name from the outgassing of CO_2 near the surface, thus giving it the appearance of champagne. The elevated chloride contents of this feature (1,898 ppm) suggest that it has experienced minimal dilution from meteoric fluids. The effects of boiling and evaporation on the waters from this feature can be seen by the isotopic enrichment in deuterium and ^{18}O resulting from the loss of vapor. The dissolved silica concentration of 445 ppm is much higher than the equilibrium solubility concentrations of both quartz and amorphous silica at the pool temperature, and results from the processes of boiling and cooling of a hot (≥230°C) reservoir fluid as it ascends to the surface. An extensive silica sinter deposit surrounds this thermal feature, and similar deposits are common for many of the other chloride springs at Waiotapu.

Cerro Prieto, Mexico

Localized aquifer boiling occurs in the shallow two-phase reservoir at Cerro Prieto (Truesdell et al. 1984 [156350]). Boiling increases the total dissolved solids (TDS) concentrations in the residual liquid through steam production, but also causes a decrease in fluid temperatures, thus reducing the solubility of most mineral phases. The increase in dissolved silica concentrations and decrease in silica solubility often results in the precipitation of silica polymorphs. Boiling also results in the partitioning of CO_2 into the gas phase, thus causing pH to increase and calcite to precipitate.

Large decreases (up to 70%) in discharge rates from wells located in the boiling zone at Cerro Prieto (Figure 11.2-6) have been interpreted to result from the precipitation of quartz and calcite, which decreased permeability for these zones (Truesdell et al. 1984 [156350], Table 2, p. 226).

This interpretation is supported by the observed decrease in silica and bicarbonate contents of the produced fluids of these wells with time.

Relevance to Yucca Mountain

For the higher-temperature operating mode at Yucca Mountain, a heat pipe may form above the repository when temperatures reach boiling. Water originally stored in the rock matrix, combined with water infiltrating from the surface, would boil near the margins of the heated drifts and migrate (as vapor) to cooler surrounding areas, where condensation would occur. Similar to the cases mentioned above, boiling will lead to increases in the concentration of dissolved species in the residual liquid phase, resulting in supersaturation and subsequent precipitation of phases such as amorphous silica.

The impact of boiling on mineral precipitation at Yucca Mountain should be significantly less than that observed in most geothermal systems because of the restricted area where boiling would occur, the much smaller quantities of fluid involved, and the lower initial concentrations of dissolved silica. A simple calculation using the matrix porosity, saturation, and pore-water silica concentrations and fracture volume can be made to estimate the maximum amount of silica that could potentially precipitate in adjoining fractures (Simmons 2002 [157578], SN-LBNL-SCI-190-V2, p. 79). Assumptions for this model include a matrix porosity of 10%, a matrix fluid saturation of 90%, a silica pore-water concentration of 70 mg/L, and a fracture volume of the rock of 0.5%. Also assumed is that with boiling, the water and associated dissolved silica are completely transferred from the matrix pore space into the fractures, where the water is subsequently boiled to dryness so that all of the dissolved silica precipitates as amorphous silica. For a 1 m^3 block of rock undergoing this process, that would correspond to a matrix water volume of 90 L and a dissolved silica amount of 6.3 g. The fracture volume for this block would be 5 L, and using a density of 2100 g/L for amorphous silica, the volume of amorphous silica available for precipitation is thus equivalent to 0.003 L. This corresponds to 0.06% of the available fracture volume. This very minor reduction in fracture porosity would result in a negligible reduction in fracture permeability.

Another bounding calculation can be made by estimating the amount of silica precipitation resulting from transport of additional dissolved silica to the boiling zone resulting from continued influx of infiltrating water from the surface (Simmons 2002 [157578], SN-LBNL-SCI-190-V2, p. 80). This calculation uses the same 1 m^3 block as a starting point, with a fracture volume of 0.5%, a fluid infiltration rate of 5 mm/yr, a fluid composition of 70 mg SiO_2/L, and assumes that: (1) all infiltrating water is focused into the fractures and (2) all of the water entering this zone from above undergoes complete boiling, resulting in the precipitation of dissolved silica as amorphous silica. For a boiling zone duration of 1,200 years, this translates into an infiltration fluid volume of 6000 L with a corresponding silica amount of 420 g. Using the density and fracture volumes given above, this corresponds to 4% of the available fracture volume. This simplistic bounding calculation is meant to illustrate the potential for fracture sealing at Yucca Mountain. Migration of the boiling front with time at Yucca Mountain would result in a larger area with reduced porosity and permeability, but with smaller average reductions. Variability in fracture apertures could lead to sealing of small aperture fractures and focussing of flow into larger aperture fractures. A fracture sealing experiment conducted in a block of ash flow tuff and accompanying numerical simulations demonstrate that similar

amounts of total fracture sealing could result in large (up to two orders of magnitude) reductions in permeability in the case where mineralization is highly focused (BSC 2001 [155950], Section 4.3.6.7.4).

One factor that could significantly increase the amount of silica precipitation in the fracture zone is the transport of additional dissolved silica to the boiling zone through reflux of fluids associated with a heat pipe. The return of condensed vapor that has dissolved silicate minerals back into the boiling zone could effectively transport significant amounts of silica into the fractures of the boiling zone. However, it is difficult to quantify the impact of this process. THC coupled-process modeling of the near-field environment, using a homogeneous fracture-permeability model, predicts that porosity reduction caused by precipitation of silica and calcite will be less than 3% over the 100,000-year simulation of the higher-temperature operating mode (BSC 2001 [155950], Section 4.3.6.4.2). This fairly small change relative to geothermal systems is in part due to the much lower fluid fluxes and lower temperatures expected at Yucca Mountain.

Boiling would not occur for the lower-temperature operating mode at Yucca Mountain. Moderately elevated temperatures (~80°C) around the drift area for this case would lead to higher amounts of evaporation, and thus result in higher concentrations of dissolved constituents in the remaining fluids in the area around the heated drifts. However, the amount of silica precipitation calculated above for the higher-temperature operating mode would be much reduced for the lower-temperature operating mode. THC simulations performed for the near-field environment for the lower-temperature operating mode predict that less than 1% porosity reduction will occur, because amorphous silica will remain undersaturated except in areas adjacent to the drift wall, where substantial evaporation will take place (BSC 2001 [155950], Section 4.3.6.5).

11.2.10.2 Dryout Zones in Geothermal Systems

Dryout is less common than boiling in geothermal systems, because most systems are liquid-saturated, and thus always contain some water. However, dryout zones do occur in steam-dominated geothermal systems, and evidence of these zones in such a system is presented in the summary below.

Karaha-Telaga Bodas, Indonesia

The Karaha-Telaga Bodas geothermal system, located on the island of Java in Indonesia, consists of a horizontally zoned reservoir with an upper condensate layer, an intermediate vapor-dominated zone, and an underlying deep liquid-dominated zone (Allis et al. 2000 [156317], Figures 4 and 5, pp. 220–221). Mineralogic and fluid inclusion studies of core samples from the T-8 corehole reveal a complex history, with calcite and quartz (after chalcedony) veins present at shallower depths, and veins containing epidote, actinolite, albite and quartz (after chalcedony) present in deeper samples (Moore et al. 2000 [156319], pp. 260–262). The precipitation of chalcedony (revealed by botryoidal textures) at elevated temperatures is unusual (Figure 11.2-7) and is interpreted to result from extreme silica supersaturation resulting from decompressional boiling (Moore et al. 2000 [156319]). The abundance of vapor-rich inclusions in the vein

minerals is consistent with this model. Many of the hydrothermal minerals are coated with scale (consisting of Ti- and K-bearing phases along with iron chloride, and halite) with desiccation

cracks (Figure 11.2-8). These minerals are thought to have formed as a result of dryout (Moore et al. 2000 [156319], pp. 260-261). The youngest fluid inclusions, associated with scale-coated anhydrite, have extremely high salinities (31% NaCl equivalent), and Moore et al. (2000 [156319], pp. 262–263) interpreted that the inclusions and scale formed as a result of condensate boiling to dryness. The high solubility of the chloride minerals suggests that the rocks containing the scale have not been subjected to rewetting after they were formed.

Relevance to Yucca Mountain

Dryout is predicted to occur in the rock mass around the potential repository drifts at Yucca Mountain (for the higher-temperature operating mode) as the waste packages transfer their heat to the surrounding environment. The size of the dryout zone will vary with time and may extend up to 13 m away from the drift walls (as previously mentioned in Section 11.2.5), depending on the waste package configuration (BSC 2001 [154677], Section 6.4.5.1). During the dryout phase, liquid water will be converted to water vapor, which will effectively displace air from this zone. This is important because the oxygen necessary for many corrosion reactions will only be present in low concentrations. As the heat output from the waste package diminishes with time, dryout zones will gradually undergo rewetting from influx of condensate and precipitation infiltration as temperatures drop below the local boiling point. The rewetting process will be accompanied by an influx of air (BSC 2001 [154677], Section 6.6.5).

In the dryout zone near repository drifts, water will be driven from the pore space in the rocks. The rock in the potential repository has a porosity of about 10%, which is about 90% filled with water in the natural condition (90% water saturation). This water is expected to be an important source of circulating water near the repository. Heating of the matrix rock, even to temperatures below boiling, may cause dryout in fractures. As the rock mass heats following waste emplacement, the volume of the dryout zone may increase to include regions formerly altered in the heat pipe. Mineralogic changes expected in this region will include precipitation of minerals in fractures (see discussion above), dehydration of naturally present sorbing clay minerals, carbonate mineral decomposition, and deposition of minerals on fracture faces from liquid driven from the rock.

With rewetting of the dryout zone, some of the more soluble mineral salts are likely to be redissolved. This could initially result in the formation of fairly saline fluids that could cause corrosion problems with the waste package in the drift. However, with continued seepage into the former dryout area, the resulting fluids will become increasingly more dilute. Dryout will be much less pronounced for the lower-temperature (sub-boiling) operating mode.

11.2.11 Geothermal Examples of Condensation and Mineral Dissolution

The processes of condensation and mineral dissolution and their effects can also be detected in many geothermal systems. Condensation of upflowing steam, when it comes into contact with cooler meteoric waters in the shallow portions of geothermal systems, results in the production of steam-heated waters (e.g., Hedenquist 1991 [156315], pp. 2756–2757). These dilute fluids often have fairly distinct chemical compositions and often reflect the effects of the gas phase accompanying the steam. Waters that receive an influx of CO_2 are typically bicarbonate fluids,

whereas those interacting with H_2S become acid-sulfate waters. The acid-sulfate waters are often associated with acid-sulfate alteration, where feldspars readily alter to kaolinite.

Mineral dissolution is not as readily evident in geothermal systems, but can be detected in core samples. At The Geysers geothermal field, corroded faces of quartz crystals found in hydrothermal veins indicate that these crystals underwent partial dissolution prior to being coated in later chalcedony (Moore et al. 2000 [156318], Figure 9, pp. 1722–1723). Similar dissolution features are also observed for calcite. These textural features (Figure 11.2-9) are interpreted to represent dissolution resulting from the downward percolation of condensate near the site of condensation in the upper portion of a vapor-dominated heat pipe (Moore et al. 2000 [156318], Figure 11, pp. 1731–1732).

11.2.11.1 Relevance to Yucca Mountain

Condensation and dissolution are processes that are likely to occur at Yucca Mountain. A tuff dissolution experiment was conducted to simulate mineral dissolution by condensate water in fractured tuff (Kneafsey et al. 2001 [154460]). Deionized water containing dissolved CO_2 was flowed through a column containing crushed Topopah Spring tuff at a temperature of 94°C. The reacted water exiting the column was regularly collected and analyzed. The experiment achieved a pseudo-steady-state flow composition after 11 days. Silica (92 ppm) was the dominant dissolved consituent. A similar plug-flow reactor experiment (using higher temperature conditions) was conducted by Johnson et al. (1998 [101630]), and a series of unsaturated nonisothermal vertical column tests were conducted by Lowry (2001 [157900]). These experiments demonstrate the ability of condensate waters to dissolve (and subsequently transport) significant quantities of dissolved constituents. As mentioned in the discussion on boiling, reflux of condensate fluids containing dissolved silica could serve as an important source for the generation of fracture-plugging minerals precipitated at the boiling front.

11.2.12 Geothermal Examples of Mineral Alteration and Precipitation

Mineral alteration and precipitation are ubiquitous in geothermal fields. The nature and extent of alteration depends on a variety of factors, including temperature, initial rock mineralogy, initial water and gas chemistry, fluid/rock ratios, and the rock surface area exposed to fluids. Many geothermal systems show a series of mineral assemblages that corresponds to different temperature and fluid chemistry regimes (e.g., Muffler and White 1969 [156650]; Arnórsson 1995 [156321]). Mineral alteration and precipitation can significantly affect porosity, permeability and sorptive properties (at least locally) of both matrix and fractures, resulting in the sealing of former fluid flow pathways.

Precipitation of new minerals in vugs, pore spaces, and fractures can occur when fluids reach supersaturation with respect to dissolved constituents. The rate of precipitation is often controlled by kinetic processes, and thus is highly dependent on factors such as nucleation sites and temperature. Supersaturation can be caused by processes such as boiling, cooling, heating (in the case of minerals with retrograde solubility, such as anhydrite and calcite), degassing, and mixing of two distinct fluids. The effects of boiling have previously been discussed, so this section will focus on the other processes mentioned.

11.2.12.1 Hydrothermal Alteration and Seal Formation in Geothermal Systems

Imperial Valley

The effects of water-rock interaction have been studied at a number of geothermal fields (Salton Sea, East Mesa, Heber, Brawley, Cerro Prieto, and the Dunes) within the Imperial Valley (e.g., Muffler and White 1969 [156650]; Schiffman et al. 1985 [154644]; Cho et al. 1988 [154599]). Elders (1987 [154632]) examined the Salton Sea geothermal field as a potential natural analogue for evaluating processes related to radioactive waste storage. One of the features examined was the impact of water-rock interaction and mineralization on fluid flow and solute transport. While primary lithology plays a major role in the distribution of permeability and porosity within the field, processes such as compaction and hydrothermal alteration have significantly modified these rock properties. Carbonate-cemented sandstones form the primary caprock for the Salton Sea geothermal system, and represent the first of four distinct mineralogic zones related to hydrothermal alteration. Within this sealed zone, calcite cement fills up to 50% of the pore space, resulting in very low matrix permeabilities for this interval (Elders and Cohen 1983 [157502], p. 100). Matrix permeability appears to favor horizontal fluid flow, as low permeability shale interbeds serve as barriers to vertical fluid flow. Fractures provide fluid flow pathways that can cut across these lithologic barriers. Complex sequences of fracture mineralization observed at the Salton Sea indicate that fractures have been episodically opened and sealed throughout the life of the geothermal system (Elders 1982 [154602] pp. 63–64).

Silica sealing has been documented at the Dunes geothermal system (Bird and Elders 1976 [154601], Figure 3, p. 289). An exploration well drilled at this prospect (DWR No. 1) has a depth of 612 m, with a maximum temperature of 104°C. Fluids sampled from this well are NaCl brines with up to 4,000 ppm TDS. Seven distinct zones of sandstones and conglomerates have undergone intensive silicification, which significantly reduced porosity and permeability. These silicified zones (Figure 11.2-10) are located in what originally were the most permeable strata within the sedimentary section. Silicification appears to be most intense near the upper portions of these units, immediately below low-permeability shale interbeds. The silicified zones have mineral assemblages of quartz + adularia + hematite and quartz + adularia + pyrite, reflecting enrichments of silica and potassium to these zones caused by mass transfer accompanying hydrothermal alteration. Brittle fractures developed in the silicified zones. The precipitation of silica is thought to be caused by the lateral migration of hot brine to a cooler environment. Smectite and kaolinite have reacted with potassium-rich brines to form adularia.

Wairakei Geothermal Field, New Zealand

Fluid chemistry and mineralogy data from the Wairakei field were used to test the EQ3/6 geochemical modeling codes and the GEMBOCHS thermodynamic databases (Bruton 1995 [100105]). Water and gas compositions obtained from well samples were used to reconstruct reservoir fluid compositions, and these fluid compositions were used as input for the EQ3/6 code to calculate equilibrium mineral assemblages. These calculated assemblages were then compared to the observed downhole mineralogy for these wells to help identify which thermodynamic datasets produced the best match between the observed and calculated mineralogy. Lower temperature portions of the reservoir exhibit similar mineralogy (including zeolites such as mordenite, clinoptilolite, stilbite, and dachiardite) to that observed in the Yucca Mountain tuffs.

Vein mineral assemblages contain fewer phases than those found associated with the matrix. Bruton (1995 [100105], p. 18) inferred that the fracture, vein, and vug minerals are the product of a fluid-dominated system, whereas the more complex matrix alteration mineralogy results from high rock-water ratios.

Medicine Lake Geothermal Field, California

The Quaternary Medicine Lake volcano in northern California is host to a high-temperature geothermal system. Exploratory drilling has revealed that the geothermal reservoir is capped by hydrothermally altered rock rich in smectite-group swelling clays that form a barrier to fluid flow (Hulen and Lutz 1999 [154600], pp. 217, 219). Glassy dacitic to rhyolitic tuffs and pumiceous lavas have been strongly altered to smectites, calcite, zeolites, quartz, potassium feldspar, hematite, and pyrite. This argillic alteration mineral assemblage also fills fractures and vugs, and forms a hydrologic barrier between a shallow, cool groundwater zone and a deeper, hot geothermal reservoir.

Fossil Systems

Fossil hydrothermal systems also demonstrate the impact that water-rock interaction has on permeability. Figures 11.2-11 and 11.2-12 illustrate variations in permeability for interbedded siliceous diatomite and pumiceous tuff from northern Japan (Chigira and Nakata 1996 [156349], Figure 2, Table 1; Chigira et al. 1995 [156364], pp. 75–76). An andesite dike intruded these bedded rocks, inducing a hydrothermal system that resulted in the alteration of the tuffs and diatomite, thereby reducing permeability up to four orders of magnitude. While the initial temperatures immediately adjacent to the dike probably approached those of the andesite magma (~1000ºC), conductive and convective heat transfer resulted in a significantly lower temperature (<150ºC) alteration assemblage (opal-CT, quartz, and several zeolite minerals) near the heat source (Nakata et al. 1998 [156365], p. 334).

11.2.12.2 Scale Formation in Geothermal Reinjection

Reinjection of geothermal water is necessary in many fields because of the need to dispose of produced water and maintain reservoir pressure. The precipitation of minerals can pose a serious problem in the reinjection of geothermal fluids. Reinjection occurs following energy extraction, thus the resulting geothermal fluid has been cooled and concentrated (owing to steam extraction) from its original, in-reservoir condition. This often results in silica concentrations exceeding saturation values, causing scale formation in reinjection pipelines, wells, and the receiving formation (Corsi 1986 [156344], pp. 839–840).

Silica behavior in geothermal environments has been studied in great detail (Bohlmann et al. 1980 [156363]; Weres and Apps 1982 [156644]; Rimstidt and Barnes 1980 [101708]), but the scaling behavior of a particular geothermal fluid is still difficult to predict. This is because traces of contaminants can significantly affect the rate of silica polymerization and deposition (Mroczek and McDowell 1990 [156342], p. 1619). Additionally, quantitative data on other factors such as pH, temperature, and supersaturation may not be known for the conditions for which one desires to predict. Reduction in the ability to inject these fluids has been noticed at several geothermal fields (for example, Hatchobaru and Otake, Japan) (Horne 1982 [156362];

Itoi et al. 1984 [156347]) and is considered a delicate problem with reinjection (Stefánsson 1997 [156343]).

Otake Geothermal Field, Japan

In an effort to understand silica precipitation in the Otake geothermal field, Japan, an extensive research effort was undertaken including field-scale reinjection, laboratory experiments, and numerical modeling. In the field, Itoi and colleagues (Itoi et al. 1987 [156346], pp. 541–542; 1989 [156345], pp. 153–155) injected geothermal waters into two wells over 656 days. The 120–162°C waters were extracted and cooled to temperatures between 50 and 80°C to cause silica supersaturation ratios between 2 to 3.2, and were reinjected. Over the course of the experiments, the permeability of the two wells declined unsteadily to 4% and 0.35% of their initial values, respectively (Figure 11.2-13). Under the conditions of the injection, the volume of silica, if all precipitated, would have been about 170 and 196 m^3 for the two wells. Borehole televiewer and caliper logs indicated that little of the total mass of injected silica was deposited in the well bores; however, the well screens were strongly fouled by silica scale.

Of interest in the Otake geothermal field is the likely occurrence of formation sealing, over both gradual and punctuated temporal intervals, probably resulting from the plugging of narrow fracture and pore apertures. Yet, there are significant differences between this reinjection study and the potential anthropogenic system at Yucca Mountain. First, supersaturation ratios at Yucca Mountain will only be high near the boiling front. In the field experiments at Otake, the supersaturation ratios were controlled by cooling the water, resulting in the entire reinjected volume being supersaturated with respect to silica. Supersaturation in the Yucca Mountain system will be controlled either by boiling off water as water approaches the drifts, or by cooling as water flows away from the repository below the drifts. Second, water flow rates will be much lower at Yucca Mountain. Flow at Otake is hydraulically saturated, and large volumes of water were reinjected into the wells over the test duration. Flow at Yucca Mountain will be hydraulically unsaturated with a flow rate many orders of magnitude less than at Otake, considering the spatial scale of the experiment at Otake. Permeability at Otake was dramatically reduced as a result of silica precipitation from injection of large (5×10^5 m^3) volumes of water into each well over the test duration (Itoi et al. 1989 [156345], pp. 153–155). If we assume that this water affects a spherical shell 50 m in diameter within the reservoir, this provides a fluid flux of several m/yr, which is three orders of magnitude larger than expected fluxes at Yucca Mountain (order of ten mm/yr) (Flint et al. 2001 [156351], pp. 22–23).

Laboratory experiments were run to evaluate permeability changes caused by silica precipitation using water from the Otake geothermal field. In these experiments, geothermal water at about 92°C was run through a column (50 cm × 5 cm diameter) of 2 mm aluminum beads or rock particles (Itoi et al. 1984 [156347] pp. 301–302; 1986 [156352], p. 229). Silica was deposited primarily in the top 10 cm of the column. Specific deposits of silica (defined as the ratio of silica weight to bead weight) of less than 0.02 caused a two-orders-of-magnitude permeability decrease. These results were compared to the drilling of a replacement injection well next to a fouled well at the Hatchobaru Geothermal Field, Japan. The new well had the same injectability as the original old well, indicating that silica precipitation is occurring near the source.

Reinjection at New Zealand Geothermal Fields

A variety of studies of silica precipitation from geothermal waters from the Taupo Volcanic Zone has been performed (Mroczek and Reeves 1994 [156360]; Mroczek and McDowell 1990 [156342]; Mroczek 1994 [154621]; Carroll et al. 1998 [124275]). Field experiments conducted at several of the geothermal fields in this area measured scale deposition rates under different process conditions in pipes, open channels, and gravel beds to determine the conditions under which the scaling could be tolerated in piping, wells, and reinjection aquifers. Data were collected at the Rotokawa well RK4, Ohaaki wells BR20, BR22, BR11, and Wairakei well 61. Geothermal fluid, being pretreated to the proper initial condition by cooling, aeration, and flashing, was then flowed through packed beds or pipes, and the amount of silica deposited was measured, generally by weighing.

The main conclusions drawn from the field studies are: (1) silica deposition occurs prior to the beginning of polymerization when all the silica is present as monomers; (2) only a small fraction of total silica deposits as scale, such that the total silica concentration is relatively unchanged; (3) deposition remains constant or increases with increasing fluid residence time; (4) deposition rates from lower-temperature, low-silica and poorly buffered Wairakei water exposed to the atmosphere were up to more than an order of magnitude higher than unaerated water; however, aeration had little effect on Ohaaki BR22 water; (5) nucleation appears slow in nonhomogeneous nucleation systems, but once started, scale will continue to grow rapidly; (6) scale appeared to be denser and deposition rates lower at higher velocities; (7) deposition onto clean iron pipes decreases after some time, presumed to be after the surface is uniformly coated with silica, and deposits formed at higher temperature were tougher and more adherent than those formed at lower temperatures.

11.2.12.3 Application to Yucca Mountain

The potential effects of fracture mineralization on fluid flow have already been discussed in the section on boiling. Other potential impacts to consider include alteration and precipitation of hydrothermal minerals that would impact the sorptive properties of the Yucca Mountain unsaturated zone and affect transport of fluids below the drift areas.

Below the potential repository, regions containing zeolites are present. Zeolites are hydrous secondary minerals that are well known for having sorptive properties. Heating of the zeolites may cause dehydration or transformation to phases (such as the less-sorptive zeolite analcime) that will reduce the sorptive capacity of the subrepository horizons. The zeolites at Yucca Mountain were formed by diagenetic alteration of vitric tuff in response to a magmatically induced thermal pulse (Broxton et al. 1987 [102004], pp. 107–108). The increase in temperature caused by waste emplacement could result in the formation of additional zeolites in the vitric tuffs below the potential repository horizon. Because of heat conduction, the temperatures will decrease with distance from the repository. Many dissolved components, such as silica, decrease in solubility as the temperature decreases. However, the precipitation of amorphous silica below the potential repository is expected to be limited in extent (BSC 2001 [155950], Section 3.3.6.3.2).

11.2.13 General Observations and Conclusions

Geothermal systems illustrate a variety of THC processes that are relevant to Yucca Mountain. They include advective and conductive heating, fracture-dominated fluid flow, chemical transport, boiling and dryout, condensation, and mineral alteration, dissolution, and precipitation. Some of the more pertinent observations made regarding these processes are listed below:

- Fluid flow in low-permeability rocks (such as the welded ash flow tuffs found at Yucca Mountain) is controlled by interconnected fractures. Alteration in low-permeability rocks is typically focused along fracture flow pathways. Only a small portion of the fracture volume needs to be sealed in order to retard fluid flow effectively. At Yucca Mountain, fluid flow and low-temperature water-rock interaction over the past 10 m.y. have resulted in the precipitation of minor amounts of opal and calcite on fracture and lithophysal cavity surfaces. More extensive water-rock interaction may occur in fractures in the near field if a heat pipe is generated after waste emplacement occurs.

- The main sealing minerals in geothermal systems are silica polymorphs (amorphous silica, chalcedony, cristobalite, and quartz), swelling clays (smectite and saponite), zeolites, anhydrite, and calcite. These minerals typically form an impermeable cap above the high-temperature geothermal reservoir where convective fluid flow occurs. The main minerals predicted to precipitate in the near field of the potential Yucca Mountain repository are amorphous silica and calcite.

- Sealing can occur in geothermal systems over a relatively short time frame (days to years). Precipitation of minerals can be triggered by a variety of processes, including boiling, water-rock interaction, heating and cooling of fluids, and fluid mixing. Mineral solubilities, reaction rate kinetics, and the flux and chemistry of circulating fluids control the rates and volumes of mineralization. The unsaturated conditions, lower temperatures, and much lower fluid flow rates predicted for the Yucca Mountain system in comparison to geothermal systems, should result in less extensive water-rock interaction than is observed in geothermal systems. Current THC models for Yucca Mountain (BSC 2001 [155950], Section 4.3.6.4.2) predict that significant fracture sealing in the near field is unlikely.

- Fracturing and sealing occur episodically in geothermal systems. Different generations of fracture mineralization indicate that there are multiple pulses of fluid flow, recording distinct temperature conditions and fluid compositions, throughout the lifespan of a geothermal system. Most mineralization at Yucca Mountain is predicted to occur soon after waste emplacement (1,000 to 2,000 years), when temperatures would reach boiling (for the higher-temperature operating mode) above the emplacement drifts. The absence of boiling for the lower-temperature operating mode would result in reduced amounts of fracture mineralization.

- The effects of processes such as boiling, condensation, dissolution, and precipitation for the higher-temperature operating mode for Yucca Mountain will be most significant in the near-field environment. Changes in permeability and porosity are expected to be relatively minor at the mountain scale, where thermal perturbations will be reduced; this

also applies to the lower-temperature (sub-boiling) design. Relatively small changes in zeolite concentrations (<1% volume) were predicted within the nonwelded zeolite-bearing Paintbrush and Calico Hills tuffs resulting from precipitation and dissolution reactions (BSC 2001 [155950], Section 3.3.6.3.2), and thus the sorptive properties of the potential repository would not be greatly modified.

- TH reservoir models have been effectively used for many producing geothermal systems to model initial state conditions and to predict changes in field performance resulting from production and injection activities. The successful use of these models provides confidence that they can be applied to predict fluid and heat flow at Yucca Mountain. Incorporation of chemical reactions and transport processes into these models has not been done extensively for geothermal systems.

- THC coupled-process modeling approaches used at Yucca Mountain can be validated by applying the technique to a number of well-constrained geothermal systems. A simplified model of a portion of the Yellowstone geothermal system is currently under construction. The goal of these simulations will be to reproduce the observed variations in alteration mineralogy, porosity, and permeability and to demonstrate the effects of THC processes on fluid flow and chemical transport.

Detailed reviews of selected geothermal systems improve understanding of fluid flow in fractured rocks, the timing and episodicity of alteration, and the effects of alteration on permeability. A number of geothermal systems hosted by rhyolitic ash flow tuffs such as Long Valley, California (Mariner and Willey 1976 [156811]; Flexser 1991 [156815]; Sorey et al. 1991 [156816]), and Baca, New Mexico (Hulen and Nielson 1986 [156813]; White 1986 [156814]; Goff et al. 1992 [156808]; Goff and Gardner (1994 [156812]) have been the subject of earlier studies of core and fluid samples. Further examination of the zonation, distribution, and ages of alteration minerals, and porosity and permeability variations as a function of degree of welding, alteration, and fracture intensity, can serve as additional validation of THC models. To construct an integrated time/temperature/fluid composition/alteration history of these systems, it may be necessary to supplement existing information with new fluid inclusion data, permeability and porosity measurements, and radiometric age determinations. In the next section, a detailed review of the Yellowstone geothermal system is presented, with attention focused on silica mineralization and sealing, geochemical modeling, and their relevance to the Yucca Mountain system.

11.3 YELLOWSTONE AS A NATURAL ANALOGUE FOR THC PROCESSES

11.3.1 Introduction and Objectives

The Yellowstone geothermal system has previously been utilized as a natural analogue for Yucca Mountain (CRWMS M&O 2000 [141407]). During the course of the current review of geothermal natural analogues (Section 11.2), Yellowstone was identified as a particularly useful example of a number of important THC processes of interest. The Yellowstone geothermal system has reservoir rocks very similar in mineralogy and chemistry to rhyolitic tuffs found at Yucca Mountain. Important processes such as boiling, mineral dissolution and precipitation, and changes in permeability caused by self-sealing have been documented at Yellowstone. An added

benefit is the availability of rock and fluid samples collected from surface and subsurface locations (see Section 11.3.5). In addition to reviewing the existing body of literature on Yellowstone, permeability and porosity variations were also studied in two Yellowstone coreholes (Dobson et al. 2001 [154503]; [154547]).

In this section, several aspects of the Yellowstone geothermal system are reviewed in the context of coupled THC processes. These include: (1) observed changes in surface thermal feature chemistry and associated mineralization; (2) a study of the role of lithology and alteration on porosity and permeability in the reservoir rocks of the Yellowstone geothermal system; and (3) the validation of water-rock geochemical modeling through study of fluid chemistry and alteration mineral assemblages. The objective of this review is to illustrate how such processes can affect fluid flow behavior, and ultimately, apply these observations to the potential Yucca Mountain repository.

11.3.2 Introduction to the Yellowstone Geothermal System

Yellowstone National Park is the site of one of the largest active geothermal systems in the world (Figure 11.3-1), with hundreds of thermal features located both within and outside of the 0.6 Ma Yellowstone caldera (Fournier 1989 [156245], p. 16). The Yellowstone volcanic center has had three major caldera-forming ash flow tuff eruptions (at 2.0, 1.3, and 0.6 Ma); these eruptions have been interspersed with lesser eruptions of lavas and tuffs that are predominantly rhyolitic in composition (Hildreth et al. 1984 [156248], pp. 8339–8350; Christiansen 2001 [156739], pp. G11–G68). While the most recent eruptive activity at Yellowstone occurred at about 70 ka, the high heat flow at Yellowstone suggests that magma currently underlies much of the Yellowstone caldera.

Studies of the active hydrothermal features at Yellowstone suggest that the geothermal system consists of two distinct reservoirs: a liquid-dominated reservoir in the western portion of the caldera and a steam-dominated system in the eastern portion (Fournier 1989 [156245], p. 17). The chemistry of chloride-rich waters sampled from the Upper, Midway, Lower, West Thumb, Shoshone, and Norris Geyser Basins indicates that the reservoirs feeding these features have temperatures ranging from 180 to 325°C, with a fairly dilute (<2,000 ppm TDS) neutral chloride brine (Fournier 1989 [156245], pp. 18–20; Fournier et al. 1992 [156247], p. 1289).

The U. S. Geological Survey drilled 13 research core holes in Yellowstone National Park in 1967–1968, with the objectives of determining the temperature and pressure gradients and describing the nature of water-rock interaction at the Yellowstone geothermal system (White et al. 1975 [154530], Table 3, pp. 1–2). These holes range in depth from 66–332 m, with most holes having depths of 150 m. Pressure and temperature measurements were made as the drilling progressed, with additional pressure and temperature surveys conducted in most wells after completion. The highest measured temperature (237.5°C) was obtained at the bottom of the deepest hole; most of the wells have maximum temperatures of 165–200°C. Continuous core samples collected from each well were subsequently subjected to detailed mineralogic study to characterize the primary lithologies and the alteration phases formed by water-rock interaction.

11.3.3 Silica Mineralization at Porkchop Geyser

Numerous studies at Yellowstone have focused on hydrothermal silica sealing and its effect on permeability (Keith et al. 1978 [106316]; Sturchio et al. 1986 [156253]; Fournier et al. 1991 [156246]). Mechanisms for silica precipitation include: (1) cooling of silica-saturated waters; (2) mixing of fluids with different chemistries and temperatures; and (3) boiling. Silica sinter is a commonly observed trait of many of the thermal features at Yellowstone National Park. Porkchop Geyser, located in the Norris Geyser Basin, provides a natural laboratory to evaluate rapid changes in permeability due to amorphous silica sealing caused by boiling (Fournier et al. 1991 [156246] pp. 1118–1119).

Porkchop Geyser has been the subject of chemical monitoring for over 50 years. Early changes in flow characteristics were attributed to the 1959 magnitude 7.5 Hebgen Lake earthquake, which caused many observed changes in thermal activity throughout Yellowstone (Marler 1964 [156249]). Since the earthquake, flow properties of this thermal feature have evolved from a quiescent hot spring (1960–1971) to an infrequently geysering pool (1971–1985) to a perpetually spouting geyser (1985–1989). The geyser eruption height increased significantly (from 6–9 m to 20–30 m) immediately preceding a small hydrothermal eruption that occurred on September 5, 1989. This eruption consisted of a single blast that formed a crater measuring 13.9 by 11.7 m (Figure 11.3-2), surrounded by ejecta blocks of siliceous sinter (Fournier et al. 1991 [156246], p. 1115). Some of the ejected sinter blocks (Figure 11.3-3) had coatings (up to 1 cm thick) of clear to translucent botryoidal masses of silica; a few of these masses were still pliable shortly after the eruption, suggesting that the amorphous silica formed as a colloidal coating on subsurface cavity walls just prior to eruption.

The observed temporal changes in flow properties were accompanied by systematic changes in the chemistry of the Porkchop Geyser fluids (Figure 11.3-4). Sodium-potassium-calcium (NKC) geothermometry temperatures increase with time from 214°C in 1961 up to 273°C a few months prior to the hydrothermal eruption (Fournier et al. 1991 [156246], Figure 4, Table 1, pp. 1116–1118). These increases in calculated reservoir temperatures are accompanied by increasing silica concentrations (from 420 ppm in 1961 to 741 ppm in 1989). No colloidal silica was either detected by observation (via the presence of an opalescent color to the water) or by analysis (comparison of colorimetric and total silica measurements) prior to the time that the thermal feature became a perpetual geyser. While the lack of standing water precluded such measurements during the time when Porkchop Geyser was a perpetually spouting feature (1985 to 1989), the presence of colloidal silica during this time can be inferred from posteruption conditions. The boiling water partially filling the eruption crater has an opalescent color, and 18% of the total silica measured on January, 1990, consisted of colloidal silica.

The above observations were interpreted by Fournier et al. (1991 [156246], p. 1118–1120) to reflect changes in the upflow water chemistry and in the amount of boiling occurring during upflow. The increasing NKC geothermometry temperatures since 1961 suggest that the waters for this feature were derived from an increasingly hotter source with time. The higher silica contents are probably caused by both the higher fluid source temperatures and the increased amounts of boiling occurring during upflow. Deposition of amorphous silica triggered by the increased silica concentrations would result in decreased permeability within the flow channels and contribute to increased pressures below constrictions present in the fluid pathways. Fluid

overpressures probably led to the rupturing of the sinter throttle at the mouth of the geyser, resulting in a rapid depressurization of the shallow part of the geyser plumbing, causing immediate boiling that triggered the hydrothermal explosion.

11.3.3.1 Comparison with Yucca Mountain

While the amounts of heat and fluid flow at Yellowstone are orders of magnitude greater than those expected for Yucca Mountain, the link between boiling, increased silica concentrations, and resulting precipitation of amorphous silica can still be applied to the Yucca Mountain system. Under the higher-temperature operating mode, where boiling temperatures are predicted to persist in the near-drift environment for 1,000 to 2,000 years, dissolved solids will precipitate as dryout occurs (BSC 2001 [154677], pp. 146–171). The amount and composition of minerals precipitated by dryout depends in part on the flux of fluids into the dryout front and the composition of these fluids. Development of a heat pipe above the emplacement drifts at Yucca Mountain could lead to increased fluid flow and chemical transport into the dryout area. Measured concentrations of dissolved silica in heated waters (26.5–51.7°C) collected from hydrology boreholes around the Yucca Mountain Drift-Scale Test (DST) are up to two times those of unheated porewater compositions (BSC 2001 [154677], Table 9). While the DST fluid concentrations (up to 139 ppm SiO_2) are still significantly lower than those observed for Porkchop Geyser (741 ppm), they demonstrate how heating can lead to increased silica concentration that ultimately results in the precipitation of amorphous silica. Sustained reflux of silica-bearing fluids into fractures within the dryout zone at Yucca Mountain could ultimately lead to plugging of high-permeability flow channels, thus changing fluid flow paths in the near-drift area. These changes could persist with time, so that when the near-drift area cools below boiling temperatures, seepage into the drifts is restricted to flow along unsealed fractures with larger apertures. Because of the unsaturated nature of the Yucca Mountain system, fluid overpressures will not develop, and thus hydrothermal explosions such as the one observed at Porkchop Geyser do not need to be considered for Yucca Mountain.

11.3.4 Silica Sealing at Yellowstone

Mineral dissolution and precipitation and associated changes in permeability resulting from water-rock interaction have been observed in a number of geothermal systems (Grindley and Browne 1976 [154531]; Fournier 1985 [154614]). One of the best examples of self-sealing is recorded in the subsurface hydrothermal mineralogy observed in Yellowstone drill cores (White et al. 1975 [154530], pp. 20–22). Keith et al. (1978 [106316], pp. A24–A25) present a summary of hydrothermal alteration studies conducted on cores from two scientific drilling locations in the northern part of the Upper Geyser Basin, located about 3 km northwest of Old Faithful Geyser. These drill holes are separated by only 130 m and have similar stratigraphies, but have significantly different temperature and pressure profiles. Keith et al. (1978 [106316], pp. A24–A25) interpret the contrasts in wellhead pressures at equivalent depths to indicate horizontal self-sealing resulting from hydrothermal alteration. Vertical pressure gradients found in the wells also suggest the presence of low-permeability flow barriers.

To determine the nature and extent of self-sealing at Yellowstone, lithologic and alteration descriptions, matrix permeability measurements, and fracture and vein characterization were conducted on core samples from the Y-5 and Y-8 boreholes (Dobson et al. 2001 [154547], pp.

283–287; [154503]). The Y-5 well, located in the Midway Geyser Basin, penetrates a thick section of Lava Creek rhyolite ash flow tuff that varies in texture from nonwelded to densely welded, with vapor-phase cavities present in some sections (Figure 11.3-5). The Y-8 core hole, located in the Upper Geyser Basin, has a more complex stratigraphy, consisting of volcaniclastic sediments, perlitic rhyolitic lava, and nonwelded pumiceous ash flow tuff (Figure 11.3-6). Both of these wells have an upper conductive gradient that changes into a nearly isothermal (~170°C) section at depths of 55–80 m (Figure 11.3-7). Detailed descriptions of the alteration mineralogy of both of these cores are presented in Keith et al. (1978 [106316], Figure 4, pp. A13–A24) and Keith and Muffler (1978 [152663], Figure 2, pp. 392–398).

Variations in porosity and permeability (Figures 11.3-8 and 11.3-9) correlate with lithology, degree of welding, and alteration (Dobson et al. 2001 [154547], pp. 285–286; [154503]). Perlitic rhyolitic lava samples have low porosities (mean of 10%) and very low matrix permeability values, as most samples were below the 0.1 millidarcy (md) detection limit of the minipermeameter. Volcaniclastic sediments typically have intermediate porosities (mean of 27%) and high permeabilities (>100 md), but silicified sediments have much lower permeabilities and a 50% reduction in porosity. Nonwelded pumiceous tuff samples from the Y-8 well have very high porosities (mean of 53%) and intermediate permeability values that range from 0.54–78.1 md (median value of 5.4 md). Nonwelded to weakly welded ash flow tuffs from the Y-5 well have intermediate porosities (mean of 34%) and permeabilities ranging from 5.57–1190 md (median value of 177 md). Moderately to densely welded tuffs have greatly reduced porosities (mean of 15%) and very low matrix permeabilities (0.002–18.5 md, with a median value of <0.1 md). The large difference in matrix permeability between nonwelded and densely welded tuffs is similar to that reported by Winograd (1971 [156254], Figure 5, p. 999).

Fractures observed in the Yellowstone core samples have a number of different origins, relating to the cooling of volcanic units, regional volcanic and tectonic processes, and hydrothermal activity. The distribution of veins and fractures in the Yellowstone cores (Figures 11.3-10 and 11.3-11) is correlated with texture and lithology (Dobson et al. 2001 [154547], pp. 286–287; [154503]). Veins and fractures are most abundant in the more densely welded tuffs, which have an average of about 5 fracture/vein features per meter of core over the studied interval (17.7–84.7 m for the Y-5 core). These fractures range from planar to irregular to hackly in form and have dips ranging from subhorizontal to near-vertical, and many of the fractures probably originated as joints formed during cooling of the tuff after emplacement (Winograd 1971 [156254], Figure 4, p. 997). The above correlation between fracture frequency and degree of welding is consistent with the observed fracture distribution at Yucca Mountain, where fractures are more abundant in welded Topopah Spring tuff (0.81–4.36 fractures/m) than in the nonwelded Paintbrush tuff (0.46–0.97 fractures/m) (CRWMS M&O 2000 [145771], Table 6).

In the Y-8 core, the perlitic rhyolitic lava has abundant, randomly oriented veinlets and microveinlets that form a stockwork configuration. In contrast, the volcaniclastic sediments and nonwelded to weakly welded tuffs have very few veins and fractures. Fracture and vein apertures range from <0.5 mm up to 20 mm. While most of the fractures observed in the core samples appear to be effectively sealed by mineralization, the presence of euhedral secondary mineral phases such as mordenite, analcime, and bladed calcite indicates that some fractures, veins, and vugs were open to fluid flow and may still serve as open pathways.

Several zones of hydrothermal breccia (Figure 11.3-12) were observed in the cores (Dobson et al. 2001 [154547]; [154503]). The breccia zones typically consist of a discrete, near-vertical vein that broadens upward and contains angular clasts of wall rock up to 5 cm in diameter that form a jigsaw texture in a brownish-red silica, montmorillonite, and Fe-oxide/hydroxide matrix. These breccias, found within the densely welded tuff, represent transient conduits of high fluid flow that are formed by the explosive release of overpressure in the underlying geothermal reservoir, and are subsequently sealed by supersaturated geothermal fluids (Grindley and Browne 1976 [154531], pp. 379–381). Numerous hydrothermal explosion craters have been identified at Yellowstone (Muffler et al. 1971 [156250], pp. 723–724), and a small hydrothermal eruption was observed in 1989 at Porkchop Geyser (Fournier et al. 1991 [156246], pp. 1114–1116). This type of eruption will not occur at Yucca Mountain, because the prevailing unsaturated conditions will preclude the pressure buildup required for this to occur.

Most fluid flow in the Yellowstone geothermal system is associated with high-permeability features, namely the matrix of high-permeability lithologies and open veins and fractures. While the initial permeability distribution is controlled by lithology, subsequent hydrothermal alteration has clearly modified both matrix and fracture permeability (Figure 11.3-13). Hydrothermal alteration resulted in the reduction of matrix permeability and focusing of flow along fractures, where multiple pulses of fluid flow and self-sealing have occurred.

Hydrothermal self-sealing appears to have generated the existing permeability barrier that delineates the top of the convecting geothermal system at Yellowstone. A steep increase in wellhead pressure observed during drilling between 49.7 (0.55 barg [bar gauge]) and 55.2 m (2.0 barg) in the Y-8 well suggests that a major low-permeability zone is located between these depths within the lower part of the volcaniclastic section (White et al. 1975 [154530], Table 5, pp. 18–22). The fluid responsible for this pressure increase probably entered the borehole immediately below the low-permeability silicified interval at 51.7–54.0 m and above the contact with the perlitic rhyolitic lava at 55.2 m. This depth also marks the transition between a steep conductive thermal gradient observed above and a near-isothermal section that extends to the well bottom. The presence of bladed calcite near this interval and elevated $\delta^{18}O$ values of hydrothermal quartz suggest that the silica seal may have formed in response to transient boiling events associated with depressurization (Sturchio et al. 1990 [154524], Table 1, pp. 30–34).

Silicification is not the only type of hydrothermal alteration that has affected fluid flow in the Yellowstone geothermal system. The presence of abundant clay minerals (montmorillonite and celadonite) and zeolites (clinoptilolite, mordenite, and analcime) as replacement minerals and in void spaces also probably reduced the matrix permeability for all of the rock units studied. Dissolution and replacement of obsidian likely led to localized increases in porosity and permeability, especially within the volcaniclastic sediments.

Hydrothermal sealing can occur fairly rapidly. Most of the USGS core holes at Yellowstone were partially or completely plugged by mineral precipitation within 25 years of having been drilled (Fournier et al. 1993 [154527], p. 33). However, the timing and duration of the mineralization observed in the Y-5 and Y-8 cores are not well constrained. Uranium-Thorium disequilibrium dating of Biscuit Basin rhyolite samples from the Y-8 core (Sturchio et al. 1987 [154525], pp. 2029–2030) suggests that uranium was mobilized and added to the rock around 19 ka. Subsequent hydrothermal alteration that decreased permeability (and thus ended uranium

mobility) in this unit is more recent. A radium disequilibrium study of hot spring waters at Yellowstone (Clark and Turekian 1990 [156780], p. 179) suggests that the mean water-rock reaction time (involving congruent rock dissolution and release of radium) in the high-temperature reservoir is 540 years, with a maximum calculated reaction time of 1,150 years.

The presence of multiphase veining in the Yellowstone cores suggests that there have been multiple episodes of fluid flow and self-sealing. A commonly observed vein assemblage for the perlitic rhyolitic lava is an outer band of celadonite, followed by chalcedony, and with most recent precipitation of mordenite. The sequential deposition of these phases indicates that there were progressive changes in fluid chemistry and/or temperature with time that resulted in this paragenetic sequence.

11.3.4.1 Comparison with Yucca Mountain

These observations from the Yellowstone geothermal system can be used to evaluate the coupled THC models developed for Yucca Mountain to predict whether, and in what time scale, permeability changes resulting from water-rock interaction could cause self-sealing at Yucca Mountain. While the Yellowstone system and the potential Yucca Mountain repository share many of the same THC processes, the effects of the processes are expected to differ significantly because of large differences in scale between the two systems, with much less extensive water-rock interaction predicted for the potential Yucca Mountain repository (Table 11.3-1).

Sturchio et al. (1987 [154525], p. 2029) estimate a conservative formational velocity of 1,500 m/yr (4.8×10^{-5} m/s) for the liquid-dominated, convecting Yellowstone geothermal system, about four to five orders of magnitude higher than those predicted for Yucca Mountain. Significantly higher fluid flow velocities occur along fractures, as evidenced by the high fluid discharge rates observed at many of the hot springs and geysers at Yellowstone. The initial heat flux value (67.7 kW/acre or 16.7 W/m^2) estimated for the higher-temperature operating mode at Yucca Mountain (BSC 2001 [155950], Section 3.3.5.4) is about one-third the calculated value (46 W/m^2) for the Firehole River drainage basin, where the Y-5 and Y-8 coreholes are located (Christiansen 2001 [156739], p. G52). However, the heat flux for Yucca Mountain will decline steadily with time as radioactive decay progresses, so that elevated temperatures at Yucca Mountain will not be sustained in the near-field environment beyond several thousand years.

The dissolution, transport, and precipitation of silica are highly dependent on system temperature, mineralogy, and liquid flux rate, as well as on whether boiling occurs. Rates of silica dissolution and equilibrium silica concentrations in geothermal fluids at Yellowstone are significantly higher than those predicted for Yucca Mountain because of the higher temperatures (170° to 240°C) encountered in the Yellowstone system (White et al. 1975 [154530], Table 3). Downhole water samples from the Y-7 and Y-8 wells have silica concentrations of 364 and 290 mg/L, respectively (Sturchio et al. 1989 [154529], p. 1028), more than three times greater than those predicted for the Yucca Mountain system (Kneafsey et al. 2001 [154460], Table 1) and more than twice the maximum measured value (139 ppm) of waters collected from higher-temperature intervals in the Drift-Scale Test (BSC 2001 [154677], Section 6.2.7.3.2). The rate of silica precipitation and concomitant permeability reduction depends not only on the rate of fluid flow, but also on processes such as boiling, cooling, and fluid mixing that result in silica supersaturation and subsequent mineralization. The presence of discrete zones of silicification at

Yellowstone suggests that the processes controlling mineralization are restricted both spatially and temporally.

11.3.5 Geochemical Modeling at Yellowstone

Meijer (1987 [101345]) reviewed four active hydrothermal systems (Newberry, Long Valley, Valles, and Yellowstone) hosted in tuffaceous rocks within the U.S. to select the system that best reflects the predicted geochemical and hydrologic behavior of the Yucca Mountain repository. Meijer (1987 [101345], p. 7) developed the following screening criteria:

- Host rocks are tuffaceous with zeolitic alteration
- Presence of an active hydrothermal system
- Availability of core samples with characterized subsurface alteration mineralogy.
- Availability of chemical analyses of thermal waters
- Availability of geologic and hydrologic data.

Based on these criteria, Meijer (1987 [101345], p. 10) selected the Yellowstone geothermal system as the best analogue case for Yucca Mountain.

Detailed studies of the downhole mineralogy at Yellowstone (e.g., Honda and Muffler 1970 [106045]; Keith et al. 1978 [106316]; Keith and Muffler 1978 [152663]; Bargar et al. 1981 [156244]; Bargar and Beeson 1984 [156241]; 1985 [156243]) show that a variety of secondary minerals are present. The observed hydrothermal mineralization includes the following phases: silica polymorphs (quartz, opal-CT, chalcedony, α-cristobalite), zeolites (clinoptilolite, mordenite, analcime, laumontite, heulandite, dachiardite), sheet silicates (montmorillonite, illite, chlorite, celadonite, kaolinite, lepidolite), carbonates (calcite, siderite, rhodochrosite), Fe-Mn oxides/hydroxides, pyrite, fluorite, adularia, albite, and minor accessory phases. The distribution and abundance of these minerals appears to be controlled by fluid and rock compositions and temperature.

Several thermal water compositions have been identified for the Yellowstone system on the basis of fluid samples collected from surface features and wells (Fournier 1989 [156245], pp. 18–20). Deep thermal waters have low sulfate and high chloride contents, and are near-neutral to slightly alkaline. Steam condensate waters have low chloride and high sulfate contents, and are acidic. Meteoric waters have low TDS contents and are similar to the waters currently found at Yucca Mountain.

Meijer (1987 [101345]) used reported fluid compositions and the EQ3/6 geochemical codes (Wolery 1979 [156741]) to calculate mineral assemblages for a fixed temperature. EQ3 speciates the dissolved constituents and calculates saturation indices for minerals, and EQ6 selects and precipitates phases to bring the fluids back to equilibrium conditions. A number of water samples were used for the geochemical modeling, including a sample with the highest silica content collected from Biscuit Basin that was chosen to represent the deep thermal water composition. Predicted mineral assemblages include silica polymorphs (chalcedony or cristobalite), zeolites (leonhardite or K-clinoptilolite), clays (Ca-nontronite, Ca-saponite) ± calcite and talc. These assemblages are similar to those found in the Yellowstone cores. Meijer attributed discrepancies between the predicted and observed mineralogies to: (1) some of the early-formed mineral

phases not being in equilibrium with the current fluids; and (2) the use of inappropriate thermodynamic data for some of the mineral phases, such as zeolites.

One important observation made from the core samples from Yellowstone is that the effects of hydrothermal alteration on welded devitrified tuffs for temperatures less than 170°C (and where the geothermal fluids are not acidic) appear to be relatively minor. From this observation, Meijer (1987 [101345], p. 48) concluded that the thermal pulse at Yucca Mountain would have only minor effects on the host rocks, limited to transport and redeposition of silica and precipitation of clays and zeolites in fractures, cavities, and the groundmass.

However, the key factor affecting fluid flow through the welded tuff repository horizon at Yucca Mountain is not the degree of alteration, but whether or not fluid flow through fractures is enhanced or restricted by mineral dissolution or precipitation. Meijer's study validates the use of geochemical modeling to predict changes in fluid and rock chemistry resulting from water-rock interaction, but it does not address how alteration of the Yellowstone cores might impact the overall permeability structure of the host rocks.

Comparison with Yucca Mountain

Recent geochemical modeling for the Yucca Mountain system (BSC 2001 [154677]) employs a more dynamic approach that couples heat and fluid flow with geochemical transport and reactions and resulting changes in porosity and permeability. The TOUGHREACT simulators (Versions 2.2 and 2.3) incorporate reactive chemistry and transport into the framework of the TOUGH2 Version 1.4 code, which simulates multiphase flow of gas and fluids together with tracer and heat transport through porous and fractured geologic media (Pruess 1991 [100413]). The TOUGHREACT code allows for the selection of kinetic or equilibrium thermodynamics to be used for mineral dissolution and precipitation, and it has several permeability law options available to relate porosity changes to changes in permeability. Simulations of fluid and heat flow and changes in permeability and porosity resulting from water-rock interaction were conducted for the near-drift region of the potential Yucca Mountain repository (BSC 2001 [154677]). The results of these simulations (conducted for thermal loads where boiling conditions persist for 1,000–2,000 years) suggest that only small changes in permeability and porosity will occur in the near-drift area (resulting from the precipitation of amorphous silica and calcite), and that these changes will not have a significant effect on repository performance.

The approach used for these simulations was validated through the modeling of the Yucca Mountain DST results (BSC 2001 [154677]) and by simulating a series of dissolution and precipitation experiments conducted using Topopah Spring tuff samples (BSC 2001 [155950], Section 4.3.6.7.4). These simulations were able to successfully predict observed changes in fluid and gas chemistry, mineral precipitation, and associated changes in porosity and permeability over the duration of these experiments.

11.3.6 Discussion and Conclusions

The Yellowstone geothermal system serves as a natural laboratory for studying a variety of important THC processes. The presence of abundant thermal features, such as Porkchop Geyser, afford the unique opportunity to track changes in fluid chemistry and temperature over time and

observe associated changes in mineral precipitation and reservoir permeability. Detailed studies of alteration mineralogy using continuous core samples from research holes drilled at Yellowstone reveal a detailed history of water-rock interaction. Observed variations in rock lithology, texture, and degree and nature of hydrothermal alteration can be used to identify correlations with variations in porosity and permeability. Densely welded tuffs have very low matrix permeabilities, but have more abundant fractures than nonwelded tuffs. A permeability seal encountered in the Y-8 core results from the precipitation of abundant secondary silica, which has greatly reduced the porosity and permeability of several intervals of volcaniclastic sandstones. Silica precipitation at Yellowstone results from both cooling and boiling processes, which serve to raise silica concentrations to above saturation levels. Geochemical modeling of fluid compositions has been used to successfully predict observed alteration mineral assemblages at Yellowstone.

THC processes are expected to have a much smaller effect on hydrogeological properties at Yucca Mountain than what is observed at Yellowstone, because of unsaturated conditions, lower temperatures, and much lower fluid fluxes that will result in less extensive water-rock interaction. Development of a heat pipe above emplacement drifts at Yucca Mountain under the higher-temperature operating mode could lead to increased chemical reaction and transport in the near field. Dissolved silica concentrations in waters from boreholes around the Yucca Mountain DST (with water boiling under heat-pipe conditions near 95°C) are up to two times those of ambient pore waters. Reflux and boiling of silica-bearing fluids within the near field at Yucca Mountain could cause fracture plugging, thus changing fluid flow paths. THC simulations conducted to date for the potential Yucca Mountain repository suggest that only small reductions in fracture porosity (1–3%) and permeability (<1 order of magnitude) will occur in the near field as a result of amorphous silica and calcite precipitation (BSC 2001 [155950], Section 4.3.6.4.2). These predicted changes in hydrogeological properties should not significantly affect repository performance.

11.4 PAIUTE RIDGE—A NATURAL ANALOGUE FOR THC COUPLED PROCESSES

11.4.1 Introduction

In addition to active geothermal fields described in Sections 11.2 and 11.3, sites of "fossil" hydrothermal alteration can be useful analogues to illustrate THC processes at Yucca Mountain. An example of this type of natural analogue is the Paiute Ridge intrusive complex, located on the northeastern boundary of the Nevada Test Site (NTS), Nye County, Nevada. The complex consists of late Miocene basaltic dikes and sills intruded into a partially saturated Rainier Mesa tuff and pre-Calico Hills Formation tuffaceous host rocks. The intrusions were emplaced at an estimated paleodepth of about 200 m, similar to the depth of the potential repository. The tuffaceous host rock surrounding the intrusions was hydrothermally altered to varying extent, depending on the distance from the intrusions (Matyskiela 1997 [100058], pp. 1115, 1117; Lichtner et al. 1999 [121006], p. 8).

Natural analogues provide a means of investigating the geologic processes characteristic of the potential repository (which take place over long time spans) and validating coupled-process models used to predict multicomponent flow, transport, and chemical reactions. The Paiute Ridge intrusive complex provides useful physical and chemical data for understanding the

influence of heat released from the repository on the tuff host rock and for THC modeling studies of the repository. Many other such intrusive complexes exist at the NTS and elsewhere that could provide an extensive data set for understanding and predicting the behavior of the potential Yucca Mountain repository.

To model mineral alteration processes properly in the highly fractured tuff host rock, mineral concentrations and associated surface areas in fractures and rock matrix must be distinguished, and kinetic rate constants—including nucleation kinetics associated with the transformation of metastable phases—must be known. In addition, mineral alteration may result in significant changes to hydrologic and transport properties such as permeability, porosity, and tortuosity of the repository host rock. Formation of mineral alteration zones on the scale of millimeters to centimeters could strongly affect the hydrologic properties of the repository host rock. As shown in Sections 11.2.12 and 11.3.4, fractures could become filled with silica minerals, forming a low-permeability zone, or cap rock, above the repository. Alternatively, the rock matrix bordering fractures could become sealed, thus reducing or preventing matrix imbibition and creating fast pathways for infiltrating water to reach the repository. Regardless of whether mineral alteration in the repository host rock is considered beneficial or detrimental to the integrity of the repository, potential changes in physical and chemical properties of the host rock create significant uncertainty in performance assessment models.

11.4.2 THC Coupled Processes Associated with a Yucca Mountain Repository

The tuffaceous host rocks at Yucca Mountain are composed primarily of volcanic glass (absent in the devitrified repository host units), silica polymorphs (cristobalite, tridymite, and opal-CT), feldspars, zeolites, clays, and calcite (Broxton et al. 1987 [102004], Table 2). An important question is to ascertain whether and at what rate this metastable assemblage will revert to a thermodynamically stable configuration as a result of heat introduced by the repository. This transformation can be accelerated with the addition of heat in the presence of liquid water in an otherwise closed system. Uncertainty exists in estimating the impact that heat produced by the decaying nuclear waste will have on the repository's performance over time (Lichtner et al. 1999 [121006], Section 6).

It is important to distinguish between changes in the near-field environment that take place in a closed system and changes resulting from fluid fluxes as a consequence of the heat generated from radioactive decay. For the higher-temperature operating mode, heat pipes may form above the repository drifts. Heat pipes (Section 11.2.4.5) are characterized by counterflow of liquid and vapor, with evaporation taking place at one end of the heat pipe and condensation of water vapor at the other, resulting in degassing of CO_2 and a consequent increase in pH and purging of oxygen (Lichtner and Seth 1996 [100771], pp. 3-140 to 3-141). Liquid water in the condensate zone is relatively dilute with reduced pH and chloride concentrations compared to the ambient groundwater composition. Within the heat-pipe zone, temperature is near boiling at atmospheric pressure. Salts are expected to form in the dryout zone where complete evaporation takes place. High salinities could result during the rewetting phase of the dryout zone, depending on the rate at which liquid water comes in contact with the deposited salts. This thermal period is expected to last for, at most, several thousand years with relatively low liquid fluxes (Lichtner and Seth 1996 [100771]; Hardin 1998 [100350], Figures 5-20 to 5-23; BSC 2001 [154677], Figures 70, 71, pp. 121–131).

Scenarios based on THC simulations range from little or no alteration to extensive alteration with the formation of a silica cap above the repository and alteration of feldspars, silica polymorphs, and glass to zeolites and clay minerals (Hardin 1998 [100350]; Whitbeck and Glassley 1998 [156452]; Nitao 1998 [117880]; BSC 2001 [154677]). The strong-alteration scenario could result in significant changes in porosity and permeability of the repository host rock that would affect its performance. The strong-alteration scenario represents a less probable case, because it assumes extremely small fracture porosity, and must occur over relatively short time spans (1,000–2,000 years) and at relatively low temperatures (~95–100°C). At such low temperatures, nucleation kinetics can inhibit certain reactions, such as precipitation of quartz, zeolites, or clays. As a consequence, there exists significant uncertainty as to which reactions will actually take place, and if so, at what rate. Generally, silicate minerals react relatively slowly at low temperatures, requiring geologic time spans (>10,000 yr) before significant alteration can take place.

Typically, THC calculations are performed using various forms of the dual-continuum model (DCM) to distinguish between fracture and matrix flow systems. The different DCMs are distinguished by the number of matrix nodes and their connectivity (Lichtner 2000 [156428]). Although fracture apertures used in DCMs can be on the order of millimeters or less, matrix block sizes are generally quite large—on the order of a meter to half a meter or larger—governed by the fracture spacing. Employing a DCM with a single matrix node of this size associated with each fracture node, it would be virtually impossible to describe processes taking place in the rock matrix at the millimeter to centimeter scale. DCMs that discretize the rock matrix are computationally intensive, and for this reason have not been used extensively in THC models applied to the Yucca Mountain repository.

11.4.3 Criteria for Selecting an Intrusive Body as a Natural Analogue for THC Processes

Several criteria should be satisfied for an intrusive body to serve as a natural analogue for THC processes at a potential Yucca Mountain repository. These criteria should include the following:

- The intrusive should be of sufficient size to produce enough heat to sustain boiling conditions for time spans of several thousand years. Typically, dikes and sills with widths greater than approximately 30 m (98 ft) will be required.

- The intrusive should be emplaced above the water table.

- Ideally, the host rock in which the intrusive is emplaced should be a volcanic tuff with compositional and physical properties similar to the Topopah Spring tuff at Yucca Mountain.

For the Paiute Ridge intrusive complex to serve as a natural analogue for the Yucca Mountain repository, it is beneficial to demonstrate that the time-temperature-saturation history surrounding an intrusive sill is similar to that predicted for the repository. The amount of heat stored in the intrusion is directly proportional to its width. Typical widths in the Paiute Ridge intrusive complex vary from tens to hundreds of meters. The typical emplacement temperature of a basaltic intrusion is approximately 1,000–1,200°C. This temperature is considerably higher than the maximum temperature of about 120°C estimated for the repository (BSC 2001

[155950], Section 4.3.5.3.3), and thus, the region very near to the intrusion cannot be expected to correspond to repository conditions. However, farther away from the intrusion, the temperature is expected to be buffered at the boiling temperature of water at atmospheric pressure. In this region, evaporation and condensation processes should be very similar to those encountered in a Yucca Mountain repository. Very likely, heat-pipe effects could have occurred with counter flow of liquid and vapor that were similar to those predicted to occur above and below the repository.

The Paiute Ridge intrusive complex satisfies the first two criteria; however, the tuff host rock in which it has intruded corresponds to the Rainier Mesa tuff and not the Topopah Spring tuff (see below). The Rainier Mesa tuff has different chemical and physical properties compared to the Topopah Spring tuff. The Rainier Mesa tuff at Paiute Ridge consists of nonwelded vitric rhyolitic tuff (Simmons 2002 [157578], SN-LANL-SCI-215-V1, pp. 90–94), whereas the Topopah Spring unit proposed for the repository horizon is a densely welded devitrified rhyolitic tuff. Because of this difference in welding, important physical properties, including fracture and matrix porosity and permeability and capillary properties, are different. The mineralogy is also different—the Rainier Mesa tuff contains abundant glass, compared to the devitrified, microcrystalline matrix of the welded Topopah Spring tuff. As a consequence, chemical alteration, as well as wetting and drying characteristics, can be expected to be different. Even so, given the difficulty in finding an exact analogue to the repository host rock, the Paiute Ridge complex can provide answers to many questions associated with THC processes at a potential repository.

11.4.4 Paiute Ridge Intrusive Complex as a Natural Analogue

11.4.4.1 Paiute Ridge Geologic Background

The study site is located about 40 km northeast of Yucca Mountain along the northeastern part of the Nevada Test Site (NTS), Nevada (Figure 11.4-1). The shallow (~200 m depth) Paiute Ridge complex consists of late Miocene (8.7 Ma) alkali basalt that was intruded into massive and bedded middle Miocene Calico Hills Formation, Paintbrush, and Timber Mountain Group tuffs (Byers and Barnes 1967 [101859], p. 2; Perry et al. 1998 [144335], p. 5-42). According to Crowe et al. (1983 [100972], p. 265), the basaltic intrusions are confined to a series of gently tilted fault blocks that are within a north-northwest-trending graben system of 15–20 km length (9.3–12.4 mi) and 4–8 km (2.5–5 mi) wide. Most of the faulting predates the basaltic intrusion in this area. For further details, the reader is referred to Lichtner et al. (1999 [121006]).

Fieldwork was conducted at Paiute Ridge for this study to characterize changes in tuff mineralogy, texture, and chemistry resulting from emplacement of the basaltic intrusions. While some variability in these properties may be attributed to pre-existing compositional, mineralogic, and textural zonation of the tuff (Broxton et al. 1989 [100024]; Mills et al. 1997 [157570]) and to low-temperature alteration associated with cooling of the ash-flow sheet and water-rock interaction since the tuff was deposited at 11.6 Ma, many of the changes in texture, degree of alteration, and whole-rock chemistry observed in the Rainier Mesa tuff samples described in Section 11.4 can be directly related to the proximity of these samples to the basaltic sill contact (Lichtner et al. 1999 [121006]; Matyskiela 1997 [100058]). Similar types of field relations were also observed at the Grants Ridge basalt intrusion (WoldeGabriel et al. 1999 [110071]). The goal of the studies described in Section 11.4 was to identify and characterize the changes in rhyolitic

tuff host rock caused by a thermal pulse analogous to the emplacement of waste packages within the potential repository at Yucca Mountain. The field observations were then used to constrain numerical simulations of the Paiute Ridge system (Section 11.4.7).

11.4.4.2 Field Studies

A reconnaissance field study focused on examining contact relations between basaltic sills, dikes, and plugs, as well as the volcanic tuff country rock. The field area consists of shallow-level intrusions exposed at Slanted Buttes and the valley to the east toward Carbonate Ridge (Lichtner et al. 1999 [121006], Section 3.1, pp. 4–7). Seventeen individual contact regions were investigated. Seven of these regions were within and around the Papoose Lake Sill, a region also studied by Matyskiela (1997 [100058]). Two of these regions were sites of detailed sampling.

The field studies focused on evaluating the possible effect of basaltic intrusions on the physical, mineralogical, and chemical characteristics of the volcanic tuff. The volcanic tuff was examined in the field for changes clearly related to contact metamorphic effects. The contact relations were found to vary with the type and thickness of the basaltic intrusion. As a result, the hydrothermal alteration is more extensive adjacent to thicker sills as compared with thinner dikes.

The most significant chemical and mineralogical alteration was associated with basaltic sills. Contact relations above, beneath, and adjacent to sills were observed on the southern flanks of the Slanted Buttes and at the Papoose Lake Sill. In the latter case, it was possible to observe volcanic tuff above the sill. Alteration was less evident adjacent to dikes compared with sills. This result may have been a consequence of the subvertical contact geometry, but was probably also affected by the relatively narrower aspect of the dikes compared with the sills, resulting in shorter-lived thermal events. Dikes were observed in two locations, on the southern and eastern flanks of Slanted Buttes, and at the Papoose Lake Sill (Figure 11.4-1, Locations B and O). A volcanic plug along the southern part of Slanted Buttes, which is probably the source for the dikes and offshoot sills at Paiute Ridge, was also examined (Figure 11.4-1, Location C). This plug showed the most significant physical interaction with the host tuff. The outcrop around the plug allowed direct observations of the contact, demonstrating plastic deformation of the tuff, brecciation along the contact zone, and stoping of the host tuff into the basalt flow. Unfortunately, the determination of the occurrence of alteration at a distance from the plug was not possible because of poor exposure and talus cover.

A variety of alteration features is readily observable adjacent to contacts. These features include the following:

- Fusion of tuff adjacent to contact with basalt. The tuff is transformed to a dense, glassy erosion-resistant mass adjacent to contact with larger intrusions.

- Formation of altered anastomosing opal vein zones (Figure 11.4-2). The tuff engulfed by these veins is altered in color, texture, and degree of induration. The veins are found both as isolated features and as complex structures that completely infiltrate the rock. In places, the center of the veins retains open fractures that may be lined with late-stage opal deposits.

- Development of silica-rich veins that penetrate the tuff with relatively little obvious alteration of the matrix. These veins may be traceable for many meters.

- Development of pipe-like alteration features. Silica-cored pipes (circular features) cross the tuff, producing concentric alteration halos. These features occur on the scale of a meter or two.

- Milky-white opal deposits along fractures. These appear to be late-stage deposits along open surfaces.

- Calcite-filled fractures widespread in the basaltic sill and adjacent altered tuff (Figures 11.4-3 and 11.4-4).

These alteration features are common and are particularly well developed adjacent to the sills observed in the area. In regions lacking outcrop, altered tuff can still be identified in weathered rock fragments scattered as float.

Two sites were selected for detailed sampling and assessment of the alteration geometry of the host tuff and the intrusive body (Table 11.4-1). These were the western limb of the Papoose Lake Sill (Figure 11.4-1 (Location H), Figure 11.4-5, and transect 7 of Matyskiela (1997 [100058])) and an exposure beneath a sill exposed on the southern part of Slanted Buttes (Figure 11.4-1, Location B). Most of the analytical work was conducted on samples collected from the Papoose Lake Sill and the adjacent host tuff. Hydrothermal alteration features are highlighted in the following sections, demonstrating significant changes above, adjacent to, and beneath the intrusive bodies. In all cases, the alteration effects diminish with distance from the contact.

11.4.4.3 Contact Metamorphic and Hydrothermal Features at Paiute Ridge Intrusive Complex

11.4.4.3.1 Alteration Adjacent to Papoose Lake Sill

The Papoose Lake Sill is approximately 27 m (90 ft) wide and trends N17E at the site of detailed investigation (Figure 11.4-5 and Location H in Figure 11.4-1). The exposure represents a vertical contact with the adjacent fused (vitrophyre) Rainier Mesa tuff along the western edge of the sill. The base of the sill is not exposed here and the host rock above the sill is partially eroded. The basalt along the contact is characterized by vertically jointed plates that are about an inch wide and oriented parallel to it. In contrast, the basal contact between the sill and the host rock as observed in other locations is mainly represented by horizontally jointed narrow plates (e.g., the southern part of Slanted Buttes, Figure 11.4-1, Locations B and E). A few feet from the contact, the Papoose Lake Sill is massive. Detailed descriptions of the samples mentioned in Section 11.4.4.3 are found in Table 11.4-1 (Simmons (2002 [157578], SN-LANL-SCI-215-V1, pp. 7–32, 90–94).

The basalt is generally sparsely vesicular with amygdules and veinlets of calcite. A sample (LANL# 3547) collected along the contact is purplish gray, fine grained, and sparsely porphyritic with partially altered pyroxene phenocrysts. The vitrophyre zone (i.e., fused volcanic tuff) adjacent to the contact varies in thickness from 0.5 to 2.1 m (1.5 to 7 ft) along strike of the

contact. It is generally black, glassy, and foliated with rare opal nodules, silica and calcite veins, and veinlets of reddish opaline tuff. Alteration of the tuff was investigated adjacent to the sill. Two vitrophyre samples (LANL# 3548 and 3549) separated by 8.2 m (27 ft) were collected along strike, 0.9 and 1.4 m (3 and 4.5 ft) west of the contact zone. The vitrophyre sharply transitions to a reddish, strongly indurated baked tuff several feet in width. A sample (LANL# 3550) was collected about 0.5 m (1.5 ft) west of the vitrophyre. It is porphyritic with quartz and plagioclase phenocrysts in a partially devitrified glassy matrix. The baked tuff grades to a nonwelded, pinkish, and weathered tuff (LANL# 3551) that crops out about 1.7 m (5.5 ft) west of the vitrophyre. The pink, weathered tuff sample occurs along the eastern edge of a narrow anastomosing opal vein zone. The 8 cm (3 in) wide pinkish orange opal veins (LANL# 3552 and 3554) trend north to south parallel to the sill contact. The host tuff (LANL# 3552 and 3553) engulfed by the opaline vein zone is pinkish and forms resistant knobs protected by the surrounding veins (Figure 11.4-2).

These anastomosing veins are found as close as 2.4 m (8 ft) from the contact. In places, the vein centers are open and contain white opal. The veins pinch and swell and wind around remnant knobs of tuff. They occur singly and as infiltrating masses. The veins are less common with distance from the contact and were not observed beyond about 14 m (45 ft). At 6.7 m (22 ft) west of the vitrophyre, the tuff (LANL# 3555) is altered. In the altered tuff, pumice clasts and the matrix appear to be totally silicified. In contrast, a sample collected about 0.12 m (0.4 ft) from LANL# 3555 is partially altered, and the pumice clasts are glassy. At 14 m (45 ft) from the contact, opal veins and veinlets are sparse. However, the moderately welded host tuff (LANL# 3557) is partially altered and contains glassy pumice clasts. Silica and calcite replacements occur side by side in the matrix (Figure 11.4-4).

Between 15 and 61 m (50 and 200 ft) from the contact, the nonwelded and unaltered tuff is friable and vitric and contains large pumice fragments. Narrow fractures contain calcite in some places, but no other alteration features were evident in cavities and/or vesicles (Figure 11.4-6). These contact relations represent the most complete record of alteration at close proximity to the intrusive bodies in the study area.

11.4.4.3.2 Alteration Patterns above the Papoose Lake Sill

Although well-preserved sections were not found above the sill, abundant evidence of pervasive alteration was observed in the overlying Rainier Mesa tuff. In some places, the alteration appeared more intense in terms of density of veining or discoloration and silicification of the host tuff. Several samples (LANL# 3560–3565) were collected above the sill between the western and eastern limbs, directly east of the detailed sampling section at Papoose Lake (Figure 11.4-1, Locations I, J, K, N, O, and P; Table 11.4-1). Because of poor exposure in the western half of the overlying tuff, most of the samples were collected closer to the eastern limb. More samples (LANL# 3538–3545) were also collected above the Papoose Lake sill at location K, about 490 m (1,600 ft) northeast of the main sampling location (Location H) along the western limb of the sill (Figure 11.4-1). At Location K, the exposed sill is about 15 m (50 ft) wide. The degree of alteration is similar to Location H, represented by dense anastomosing opal veining that is about 7.6 m (25 ft) wide. However, unlike the sill contact with the tuff at Location H, no vitrophyre or fused tuff was noted near the opal veins above the sill at Location K. The Location K area is not completely exposed, and thus a vitrophere zone that is obscured by talus may exist

in this area. Although the thickness of the veined zone is unknown, it is located about 45 m (150 ft) to the east of the exposed sill margin. The opal veins above the sill are generally oriented N20W, slightly different from the N-S trend noted adjacent to the sill at Location H.

11.4.4.3.3 Alteration Patterns beneath a Sill

The contact zone of a sill was examined in a gully located on the SW flanks of Slanted Butte (Figure 11.4-1, Locations A and B). The contact relations below the sill are generally well exposed and alteration patterns can be observed. The basaltic sill dips about 55° to the south. The sill is about 7.6 m (25 ft) thick at the point of investigation. The basalt is purplish gray, coarsely vesicular, and includes trains of fine vesicles. Amygdules filled with calcite and opal are common. Large altered mafic phenocrysts are also present. The basalt along the contact exhibits a thin chilled margin, consisting of horizontally jointed (with respect to the sill) and narrowly spaced plates along the contact with the underlying tuff. In contrast, at the Papoose Lake Sill in the northern part of Paiute Ridge, vertically jointed plates characterize the sill margin. These features clearly delineate the nature of the contact between the basaltic intrusions and the tuff host rocks. The country rock tuff units are pre-Rainier Mesa tuff and belong to the Wahmonie Formation and Crater Flat Group (Table 11.4-2). Two samples (LANL# 3570 and 3571) were collected from the contact and the top part of the sill (Figure 11.4-1, Location B). The pinkish tuff along the contact with the basalt does not form a foliated vitrophyre (as was noted at the Papoose Lake Sill in the northern part of the Paiute Ridge area), but exhibits a dense, coarse-grained granite-like texture, possibly as a result of slow cooling. Incipient mineral layering is noted within the fused tuff directly beneath the sill. About a foot beneath the contact, the tuff (LANL# 3572) grades from coarser to fine-grained crystalline material. This resistant contact zone extends for 1.2–1.5 m (4–5 ft) below the basalt. Unlike the sections sampled in the northern part of the Paiute Ridge area, there are at least five tuff units beneath the sill that are cut by a dike finger that is vertically wedged along a fault into the underlying tuff sequence. The fault zone is extensively altered to clay. Two tuff samples (LANL# 3573 and 3574), collected about 1.3 m (4.4 ft) beneath the contact, are generally nonwelded. A moderately welded, light gray tuff (LANL# 3575–3578) that contains brown and dark lithic fragments occurs about 4.6 m (15 ft) beneath the sill. At 6.4 m (21 ft) beneath the sill, the same unit (LANL# 3576 and 3577) contains multiple layers of white to reddish orange opal veins and veinlets mostly parallel to bedding and to lithologic contacts.

These opal veins are of different character than those observed at the Papoose Lake Sill section. They consist of white siliceous cores surrounded by a discoloration halo in some places and no observable halo in other places. They occur parallel to the sill-tuff contact and are about an inch in thickness.

These fractured veins pinch and swell along strike and mostly occur in a 0.6 m (2 ft) wide zone. About 1 m (3.4 ft) below the vein zone, the tuff (LANL# 3578) is nonwelded and contains no opal veins. A white crystal-rich tuff crops out about 11 m (35 ft) beneath the sill. It is coarse grained with pumice clasts and abundant feldspar, quartz, and biotite phenocrysts. On the south side of the dike that wedges down into the underlying tuff, the crystal-rich tuff is intruded by a 0.12–0.46 m (0.4–1.5 ft) wide opal vein that is 4.9 m (16 ft) beneath the sill. The vein trends obliquely to the tuff-sill contact and is traceable for more than 30 m (100 ft). This vein strikes

N-S and dips 65° to the east. In addition, siliceous pipes occur about 4.6 m (15 ft) below contact. They are well-indurated and characterized by a white core and circular reddish halo.

11.4.5 Original Depth of Intrusions

Paleozoic limestone, quartzite, and shale unconformably underlie middle Miocene tephra of the Timber Mountain and Paintbrush tuffs and older undivided tuff units at the Paiute Ridge study area (Byers and Barnes 1967 [101859]; Perry et al. 1998 [144335]). The Tertiary tuffs at the northern and southern study areas were extensively intruded by shallow late Miocene basaltic dikes, sills, and plugs. Based on reconstructed topography above the sills and dikes, it was suggested that the intrusive bodies were emplaced a few hundreds of meters from the paleosurface (Valentine et al. 1998 [119132], p. 5-29, Figure 5.16; Ratcliff et al. 1994 [106634], p. 413). This assumption is consistent with the presence of abundant vesicles along the edges of the sills and dikes, the localized nature of the contact metamorphic effects adjacent to the sill, and minimal amounts of hydrothermal alteration along the contacts (Valentine et al. 1998 [119132], pp. 5-41 to 5-44, 5-51).

However, based on detailed field observations of contacts between the intrusive bodies and host tuffs throughout the study area, it appears that the sills and dikes started at deeper levels close to the plugs and eroded centers and migrated up section into shallow levels away from the central part of the intrusive complex. For example, the sills generally branch out from major dikes and intruded into pre-Rainier Mesa tuff units in the southern part, whereas the Papoose Lake Sill in the north intruded into the Rainier Mesa tuff. This observation is corroborated by subsurface stratigraphic data from several drill holes (Figure 11.4-1) along the eastern part of Yucca Flats, which provide information about the type and thicknesses of the major tuff units deposited in the basin adjacent to Paiute Ridge during the Miocene (Drellack and Thompson 1990 [156446], pp. 1–11). The thicknesses of the tuff units encountered in these drillholes can be used to estimate the original thicknesses of the corresponding units that crop out in the adjacent Paiute Ridge area (Figure 11.4-1; Table 11.4-2).

According to the subsurface stratigraphic information, the major tuff units intersected in the upper part of the Yucca Flats drill holes consist of the Timber Mountain Group (i.e., Rainier Mesa tuff and Rainier Mesa tuff vitrophyre), the Lower Wahmonie Formation, and the Crater Flat Group in descending stratigraphic order. The Ammonia Tanks tuff at the top of the Timber Mountain Group, the Paintbrush Group, and the Calico Hills Formation units were not defined in the drill holes (Drellack and Thompson 1990 [156446]). Using the thicknesses of the different tuffs in the drill holes (from the surface to the top of the Rainier Mesa vitrophere unit), it is estimated that the late Miocene basaltic magma was intruded into a shallow environment of about 200 m depth.

Information on the degree of alteration of the tuffs encountered in the drill holes can be used to help differentiate between alteration caused by the basaltic sills from more regional alteration events. According to the Yucca Flats drill hole data (Table 11.4-2), pervasive zeolitization (interpreted to predate the intrusion of the basaltic sills) occurs in the lower half of the subsurface sequences, typically below the Rainier Mesa tuff unit. The presence of zeolites (such as clinoptilolite and chabazite; see Table 11.4-3) in Rainier Mesa tuff samples adjacent to the sill

contact (and above the regional zone of pervasive zeolitization) was thus attributed to hydrothermal alteration resulting from the sill intrusion.

11.4.6 Laboratory Methods and Results

Thin sections were prepared of almost all of the samples for petrographic descriptions, using optical and scanning electron microscopic techniques. Selected samples from the host tuff and basaltic sill in the Papoose Lake area were processed for bulk chemical and mineralogical analyses. Additional major-element glass chemistry was obtained for most of the tuffs selected for bulk analysis, using an electron microprobe. Most of the tuff samples selected for analysis were collected adjacent to the sill at Location H.

11.4.6.1 Petrographic Results

The mineralogical and chemical characteristics of the alteration are keys to understanding the conditions of hydrothermal processes. Petrographic observations identify opal and calcite veining associated with some of the alteration features (Simmons 2002 [157578], SN-LANL-SCI-215-V1, pp. 89–94). Calcite appears rather abundant in some sections. The vitrophyre found adjacent to the basalt contact contains significant volcanic glass and is largely free of hydrous mineral alteration. Some interesting observations were made of the anastomosing veins from the Papoose Lake Sill locality.

Preliminary petrographic examination of samples of Rainier Mesa tuff systematically collected at intervals from the contact zone to about 61 m (200 ft) west of the sill indicate variable physical and mineralogical alterations (Figure 11.4-1, Location H). Comparison of two tuff samples from above the sill collected at different distances from the sill outcrop (Figure 11.4-1, Locations K and N) indicated that the intensity of alteration above the sill decreases away from the sill margin. A light pinkish brown tuff (LANL# 3539) collected from a 7.6 m (25 ft) wide, densely veined zone about 46 m (150 ft) from the western edge of a sill northeast of the Papoose Lake Sill is sparsely porphyritic with plagioclase, albitic sanidine, quartz, biotite, and minor amounts of hornblende and clinopyroxene. Secondary minerals of silica, calcite, and minor clay replaced the matrix. These secondary minerals also occur in cavities and along fractures as veinlets, aggregate crystals, and radiating spherules, ranging in width from 25–105 μm. At Papoose Lake Sill (Location H), east of the main outcrop, a number of Rainier Mesa tuff samples collected above the sill are strongly indurated, moderately altered, and contain similar phenocryst assemblages. Secondary minerals of opal, calcite, and zeolite replaced the matrix and also occur in cavities and fractures. Shard fragments and pumice clasts are totally replaced by secondary silica.

Similar physical (e.g., color, hardness, welding, veining) and mineralogical (silica, zeolite, calcite) alteration patterns are noted in the basalt and host tuff samples collected from the main section adjacent to the Papoose Lake Sill. The basalt along the contact is fine grained, vertically jointed with uniformly spaced plates, purplish gray, and sparsely vesicular with minor calcite and/or opal amygdules. The altered basalt is porphyritic with plagioclase and sparse mafic minerals that are altered to reddish brown spots. The matrix is dominated with microlites and microcrystalline aggregates of pyroxene. Secondary calcite, silica, clays, and perhaps zeolites occur as veinlets and crystal aggregates in cavities and along fractures. The veinlets pinch and

swell and range in width from 90 to 135 μm. Some cavities or mineral pseudomorphs are partially filled with abundant microcrystalline aggregates of epidote and calcite (Figure 11.4-3).

Three main alteration zones were identified in the tuff near the basaltic intrusion: (1) a vitrophyre zone immediately adjacent to the sill contact, (2) a baked zone, and (3) an altered zone characterized by opal veining. The host tuff adjacent to the basaltic sill contact was fused and transformed to a foliated, perlitic vitrophyre with opal amygdules and silica veinlets. The phenocryst assemblage in the vitrophyre is similar to the overlying tuff. Secondary silica deposits, represented by overgrowth around phenocrysts up to 27 μm wide and veinlets that are 27 μm to 0.28 mm wide, are commonly noted parallel and transverse to welding fabric. Away from the contact, the intensity of alteration transitions from the 2.1 m (7 ft) wide vitrophyre at the contact to a baked interval and then to a 7.6 m (25 ft) wide zone that is characterized by dense, anastomosing opal veining (Figure 11.4-2). The tuff samples are sparsely porphyritic with variable degrees of welding. In one of the samples (LANL# 3554), the phenocrysts are segregated and form bands of crystals represented by quartz, plagioclase, sanidine, and minor biotite and hornblende. The sample is devoid of matrix, thereby creating a crystal-rich zone due to winnowing. The intensity of alteration and replacement of the matrix, pumice clasts, and phenocrysts by calcite, silica, zeolite, and clays decrease with distance from the vitrophyre interval. Within the altered zone, the secondary minerals generally occur as veinlets, cavity filling, or as aggregates within the matrix. For example, at about 13 m (43 ft) from the contact, the tuff is moderately welded, and the matrix replaced by calcite and silica in separate zones (Figure 11.4-4). In some cases, silica spherules crystallized in fractures, causing these fractures to be widened later by fluid flow and also narrowed by silica and calcite recrystallization along the walls. The sample (LANL# 3558) collected outside the altered zone contains similar phenocryst assemblages, but the amount of secondary silica and calcite significantly diminished. The cavities and vesicle walls are devoid of secondary minerals, suggesting no effect on these outer units furthest from the basaltic intrusion.

Examination of selected samples from the sill and the host tuff using a scanning electron microscope (SEM) shows the size and textural relations of the secondary minerals. For example, calcite occurs in the basalt along the contact in cavities and as 100 μm wide and several-millimeter-long veinlets in the matrix (Figure 11.4-3). Calcite and silica intergrowth is also noted in the matrix. Moreover, potassium-rich euhedral crystals (possibly zeolites) are also present in the altered basalt. Fractures in the vitrophyre adjacent to the sill are filled totally by zeolites that are rich in potassium and calcium. Some of these zeolite crystals are more than 10 μm long. Calcite and silica commonly occur in cavities, and in most cases, calcite postdates silica. Almost all of the tuffs proximal to the contact contain silica, calcite, and abundant zeolites in partially filled cavities and within the matrix (Table 11.4-3). However, two of the samples collected from 23 and 61 m (75 and 200 ft) from the sill show no alteration effects. The cavities and vesicles are clean and the shards show no visible signs of alteration (Figure 11.4-6).

11.4.6.2 Mineralogical Results

The mineralogy of selected basalt and tuff samples was identified using quantitative X-ray diffraction (XRD) analysis (Simmons 2002 [157578], SN-LANL-SCI-215-V1, pp. 56–59). The samples were ground for approximately 10 minutes using acetone in a Brinkmann automated

grinder to reduce the particle size and homogenize the sample and internal standard. The samples were analyzed using calibrated Siemens D-500 powder diffractometers.

Results of the XRD analysis are given in Table 11.4-3. Consistent with the petrographic results, the basalt from the contact and those tuffs collected within 14 m (45 ft) from the sill contain abundant secondary minerals dominated by clinoptilolite (Table 11.4-3). Although petrographic analysis reveals calcite and silica in the basalt, smectite was the only secondary mineral identified by XRD analysis. Despite clay-like alteration noted petrographically in most of the altered tuffs, the XRD results show only variable amounts of opal, tridymite, cristobalite, clinoptilolite, and chabazite in the various tuff samples.

11.4.6.3 Geochemical Results

Aliquots of powdered samples were used for major and trace element analyses using a Rigaku 3064 wavelength dispersive X-ray fluorescence (XRF) (Simmons 2002 [157578], SN-LANL-SCI-215-V1, pp. 63, 69–76). Analysis and statistics of the unknown samples are based on a model that uses intensities for 21 standard rocks. To assess whether the major and trace element variations of the tuff samples are genetic or a result of hydrothermal alteration related to the basaltic intrusion, major and trace element concentrations of bulk-rock samples were plotted against distance from the sill (Figures 11.4-7 and 11.4-8). An average Rainier Mesa rhyolitic tuff composition reported by Broxton et al. (1989 [100024]) is plotted with these data for comparison. A discussion of the major and trace element variability and its origin is presented in Section 11.4.6.4.

11.4.6.4 Discussion

Field and analytical results suggest that the Paiute Ridge basaltic dikes and sills intruded into at least two different tuff units, the Rainier Mesa tuff of the Timber Mountain Group and older bedded tuffs from the Lower Wahmonie Formation and Crater Flat Group that mostly crop out in the southern part of the study area. Generally, the host tuffs in the southern part of the study area are thin, mostly bedded, and crop out along gullies. Those outcrops in the northern part are massive, nonwelded, and occur mostly along ridge tops. Most of the analytical results were obtained on samples collected from the Papoose Lake Sill area at Locations H, N, and K (Figure 11.4-1). These tuffs are pinkish, sparsely porphyritic, variably welded, massive, and generally contain abundant pumice clasts. For example, a light pinkish brown tuff from above a sill at Location K contains plagioclase (30%), quartz (32%), sanidine (38%), and minor amounts of biotite, hornblende, and clinopyroxene. According to Byers et al. (1976 [104639]), mafic phenocrysts such as hornblende, clinopyroxene, biotite, plagioclase, and Fe-Ti oxides are common in the upper part of the Rainier Mesa tuff, and sanidine generally contains cryptoperthite rims. A vitrophyre (fused tuff) and a nonwelded tuff collected at Location H adjacent and at 61 m (200 ft) from the Papoose Lake sill, respectively, also have similar phenocryst assemblages with diagnostic albitic rims on sanidine, which is a characteristic feature of alkali feldspars in the Rainier Mesa tuff (Byers et al. 1976 [104639], p. 42).

Depending on proximity to the sill, variable degrees of alteration related to the intrusion are recorded in the tuff units. For example, the transformation of the nonwelded Rainier Mesa tuff to vitrophyre, hardening and discoloration resulting from baking, and the prevalence of

anastomosing opal veins within 12 m (40 ft) of the sill are macroscopic physical modifications related to the sill. However, such features are not uniformly apparent at all the contacts studied during the field investigation. At Location H of the Papoose Lake Sill area, the 12 m (40 ft) wide alteration aureole adjacent to the sill progressively changes from a 2.1 m (7 ft) wide vitrophyre at the contact to a comparable size of baked interval, and to a 7.6 m (25 ft) wide opal veining zone. However, such systematic alteration is not fully developed at Location K above the sill. There, hardening of the tuff and a 7.6 m (25 ft) wide opal vein zone are developed 46 m (150 ft) east of the western edge of the sill. At Location B in the southern part of the study area, the pre-Rainier Mesa tuff units are exposed beneath the sill and the alteration features are different from those noted at Locations H and K. The tuff directly beneath the sill was transformed into a granitic-like granular-to-fine-grained rock, suggesting slow cooling, following the fusion of the tuff. In contrast, the vitrophyre observed at location H represents a fused Rainier Mesa tuff that chilled rapidly adjacent to the sill. The type of the stratigraphic units and the nature of the fused tuff along the contact (e.g., vitrophyre or granular) suggests that the level of intrusion was deeper in the southern part compared with those sills and dikes along the northern boundary of the basaltic intrusive complex. In the southern part, multiple opal veins, ranging in thickness from a few inches to about a foot thick are present within 6 m (20 ft) below the contact. The opal vein zone (≤7.5 m or 25 ft wide) noted adjacent and beneath the sills at Locations B and H (Figure 11.4-1) represent mass silica mobilization from altered tuff within the hydrothermal aureole. Although other low-temperature secondary minerals are closely associated with opal, no systematic zonation is apparent from the effect of the basaltic intrusion. The anastomosing opal veins engulfed variable sizes of tuff clasts that are partially affected by these veins. Although there was voluminous mobilization of silica along fractures created during the basaltic intrusion, subsequent fluid flow was probably significantly reduced because of the impermeable opal veins. The alteration zone occurred at close proximity and parallel to the basaltic sill (≤14 m or 45 ft), likely creating a barrier between the intrusion and the outer tuff units.

Petrographic examination of samples from hydrothermal alteration zones at Locations H and K revealed other secondary features related to the intrusions. Silica, calcite, zeolite, and clay materials are present as veinlets along fractures, as clusters in cavities and matrix, and as overgrowths around feldspar and quartz phenocrysts. These features appear to contain abundant zeolite (clinoptilolite) and show precipitation layering within the veins (Figures 11.4-6a and 11.4-9b). The figures show a tabular crystal of zeolite overgrowing a second layer of zeolite having a scalloped or rounded morphology.

The presence of zeolite as multiple generations within fractures and cavities of the altered tuffs suggests that zeolites in addition to silica were deposited by hydrothermal alteration associated with the basaltic intrusion. However, older zeolitzed tuffs are present in the southern part of Paiute Ridge and in the lower half of the subsurface units intersected in the drill holes along the eastern part of Yucca Flats (Table 11.4-2; Drellack and Thompson 1990 [156446], pp. 60, 64, 66, 68–69; Valentine et al. 1998 [119132], p. 5-46, 5-55, Table 5.3). The silica and calcite veinlets that range in width from microns to millimeters and in length to several millimeters also formed during this process. The pumice clasts and the glassy matrix of the tuffs from the alteration zone are mostly devitrified and/or totally replaced by calcite and silica. A basalt sample from the contact at Location H is also moderately altered. The rock is purplish gray and contains clay, calcite, epidote, and silica along fractures and in cavities.

Published Rainier Mesa tuff chemical data from the lower part of the unit (Quinlivan and Byers 1977 [156450], Table 6; Broxton et al. 1989 [100024], Table 3) are correlative to the major and trace element concentrations of the tuff samples from Locations H, K, and N in the northern part of Paiute Ridge. This observation is also consistent with the petrographic results. Physical, mineralogical, and chemical variations noted in some of the Paiute Ridge samples collected from the hydrothermal aureole beneath, adjacent, and above the basaltic sills are attributed to the intrusions.

Localized chemical variations are noted in the host tuffs adjacent to the basaltic sills. Variations in major and trace element contents are more pronounced in samples collected near the contact (Figures 11.4-7 to 11.4-8). For less mobile components such as TiO_2, Al_2O_3, total iron, Nb, and Zr, little variation is observed throughout the suite of samples, with most variability occurring within a zone that extends 30–40 feet from the sill contact. While silica appears to be mobile (as observed by the presence of opal veins), the actual range of observed silica concentrations for all of the analyzed tuff samples is fairly small (74–81% SiO_2, normalized to anhydrous compositions). Significantly more variability is observed for the more mobile alkali and alkaline earth elements (Na, K, Rb, Ca, Sr). Most of the variability for Na, K, and Rb occurs within 30 ft of the sill contact, suggesting that the original tuff compositions were modified by hydrothermal alteration resulting from the sill intrusion. However, the distribution of Ca (and Sr to a lesser degree) is much more scattered. The measured CaO concentrations of the tuff samples (ranging from 0.5 to 5.6% CaO, normalized to anhydrous compositions) are generally higher than the average Rainier Mesa rhyolitic tuff composition (0.52 wt.%) of Broxton et al. (1989) [100024] (Table 3). The observed increase in CaO contents is in part caused by the presence of variable amounts of secondary calcite in the tuff samples. The calcite may originate from two separate events, one being the intrusion of the sill, while the other would be low-temperature precipitation of calcite from infiltrating groundwater over millions of years. One of the samples collected about 122 m (400 ft) above the sill at Location O (LANL# 3560) has higher Fe_2O_3, MgO, CaO, Sr, Zr, and Ba concentrations. This may reflect a difference in the bulk rock composition resulting from the presence of lithic fragments within the tuff (Simmons 2002 [157578], SN-LANL-SCI-215-V1, p. 25).

As shown in Table 11.4-3, abundant clinoptilolite with minor chabazite formed from the alteration of glass within the contact aureole of the basaltic sill at Papoose Lake Sill. Hydrolysis of volcanic glass, resulting in higher alkalinity and increased silica and alkali ion to hydrogen activity ratio in pore fluids, provided the necessary environment for the formation of zeolite (Hay 1978 [105967], pp. 135–136; Broxton et al. 1987 [102004], pp. 91, 93). Published field and experimental data suggest that clinoptilolite formation is favored over other zeolites, including chabazite in low alkalinity (pH = 7–9) environments (Mariner and Surdam 1970 [156449], p. 977; Barth-Wirsching and Höller 1989 [156445], Table 5, p. 493; Sheppard 1993 [156451], pp. 10–12). The close spatial association of clinoptilolite and opal within the alteration aureole suggests that the anastomosing opal veins are the result of hydrothermal alteration of glassy matrix and pumice clasts. For example, the most altered tuffs (LANL# 3552, 3554, and 3555) from the contact aureole contain higher silica and lower alkali contents (Simmons 2002 [157578], SN-LANL-SCI-215-V1, pp. 22–23, 71, 92–93). Smectite is absent from the altered tuffs. This may be related to relatively high alkali ion to hydrogen ion activity ratios and relatively high silica activities, which favor the crystallization of clinoptilolite over smectite (Barth-Wirsching and Höller 1989 [156445], Table 5, pp. 496–497; Sheppard 1993 [156451], p.

12). Moreover, the lack of smectite in the altered tuff may be attributed to the low Fe, Mg, and Ca contents in the altered tuff. These cations are important components for smectite formation.

In summary, the field study indicates zones of hydrothermal alteration generally occurred within 10–15 m (30–50 ft) of some of the larger basaltic intrusions, especially sills. In some parts of the contact zone, rather pervasive alteration with a zone of silica veins is observed. In other parts, veining is rather limited or absent. The confinement of these features to areas adjacent to contacts appears to demonstrate that the veining and alteration features were caused by the basaltic intrusions.

11.4.7 Thermal-Hydrologic-Chemical Modeling of Hydrothermal Systems

As mentioned in Section 11.4.3, the Paiute Ridge system meets most of the criteria established for serving as an appropriate analogue for THC processes that are expected to occur at the potential Yucca Mountain repository. The effect of a basaltic intrusion on alteration of the host rock in which it is emplaced and alteration of the intrusion itself was modeled using the computer code FLOTRAN (Lichtner 2001 [156429]). A one-dimensional geometry perpendicular to the intrusion was used for the simulations (Figure 11.4-10). Effects of gravity were not included in the simulations, although gravity could have important effects, depending on the geometrical relation between the intrusion and the host rock. Both equivalent and dual-continuum models were considered.

11.4.7.1 The Computer Code FLOTRAN

To estimate the thermal evolution of host rocks surrounding an intrusion emplaced above the water table, it is essential to take into account the two-phase behavior of the system. Latent heat of solidification of the intrusion is neglected, because this process is relatively fast compared to the time required for the intrusion to reach ambient conditions. Preliminary calculations were performed using the computer code FLOTRAN (Lichtner 2001 [156429]). FEHM (Zyvoloski et al. 1997 [100615]) is limited to temperatures less than approximately 300ºC and could not be used. Both FEHM and FLOTRAN are capable of describing two-phase nonisothermal fluid flow in variably saturated media for dual and single continua. A documentation of the mass- and heat-conservation equations in the dual-continuum model used in FLOTRAN, and their relation to the equivalent-continuum formulation, is presented in Simmons 2002 ([157578], SN-LBNL-SCI-108-V2, pp. 17–21).

Equation-of-state properties used in FLOTRAN for pure water were derived from the IFC (International Formulation Committee) (1967 [156448]). Constitutive relations must be provided as functions of pressure and/or temperature for the density, viscosity, saturated vapor pressure curve, internal energy, and enthalpy of pure water. The reported validity of the equation of state properties lies in the range of pressure p and temperature T: $0 < p < 165.4 \times 10^5$ Pa (165.4 Bars), and $0 < T < 800$ºC (IFC 1967 [156448], p. 1, Figure 2). Although this is satisfied for pressure, it is not satisfied for the temperature range needed to describe the intrusion. However, as demonstrated in Table 11.4-4, the calculated properties are quite close to the measured values reported by Haar et al. (1984 [105175], Table 3) at the maximum temperature of interest.

In the scoping calculations that follow, a one-dimensional (1-D) model was considered of a semi-infinite medium representing the host rock in contact with the intrusion (Figure 11.4-10). This approach is a simplified model in which the effects of gravity and surface infiltration are neglected. By symmetry, only half of the dike width need be modeled. A 30 m wide completely dry intrusion with an initial temperature of 1,200ºC is assumed to be emplaced instantaneously into unsaturated tuff at ambient temperature and pressure.

Rock properties and initial and boundary conditions used in the calculations for the equivalent continuum model are listed in Table 11.4-5. The values used for density, specific heat, and thermal conductivity for basalt are typical for basalts as listed in Drury (1987 [156447], p. 107). Very small values for porosity and permeability of basalt were chosen to simulate an essentially impermeable intrusion. The "tuff" values are representative of the nonwelded Paintbrush tuff (PTn) at Yucca Mountain (approximately analogous to the nonwelded tuffs at Paiute Ridge). (It should be noted that the host rock at Papoose Lake Sill is now believed to be composed of Rainier Mesa tuff, which had not been established at the time these calculations were performed.) Values for van Genuchten parameters (fracture/matrix equivalent continuum) are means for PTn values in Wu et al. (1997 [156453], Table A-1). Thermal properties of tuff are from Francis (1997 [127326], Table B-1). Values for density and porosity are from Peters et al. (1984 [121957], Table A-2). Saturation values ranging from 0.4 to 0.6 are observed for the PTn at Yucca Mountain, and corresponding calibrated model values were taken from Robinson et al. (1997 [100416], Table 5.2). Because of the extreme dryout conditions produced by the high temperature of the intrusion, the results are sensitive to the cutoff used to evaluate the characteristic curves near the residual saturation.

11.4.7.2 Dual-Continuum Model Calculations

Several cases are considered with varying coupling strength between fracture and matrix continua. Values for the fracture-matrix area factor of $\sigma_{fm} = 10^{-6}$, 10^{-4}, 10^{-2}, and 10^{2} are compared and contrasted. Results are shown in Figures 11.4-11 to 11.4-18 for fracture and matrix temperature and saturation as functions of distance for various times indicated in the figures. Boiling and condensation fronts propagate into the country rock as indicated by the 100ºC isotherm and changes in saturation. Liquid water is stable only for temperatures below the boiling point, corresponding to approximately 100ºC at atmospheric pressure. In the figures, boiling occurs at the leading edge where saturation increases from zero. The boiling front is followed by condensation further away from the intrusion, where both saturation and temperature return to ambient conditions. In the intervening region, the temperature is buffered at the boiling temperature of 100ºC. In this region, a heat pipe is present with counterflow of liquid and gas. High flow rates of liquid towards the contact are a consequence of capillary suction, as the country rock is dried out from heat released from the intrusion. At early times, liquid flow rates are on the order of 1,000 m/yr, with gas flow rates several orders of magnitude higher.

As can be seen from the figures, fracture and matrix saturations are very different, even for strong coupling between fracture and matrix, in order to preserve equality of the capillary pressure between the two continua. For $\sigma_{fm} = 100$ (shown in Figures 11.4-11 and 11.4-12), the dual-continuum results agree with the equivalent-continuum model. Fracture and matrix temperatures are identical, and saturations obey Equations II-19 and II-26 in Lichtner (2001

[156429]). With the fracture volume fraction $\varepsilon_f = 0.01$, fracture porosity $\phi_f = 1$, and matrix porosity $\phi_m = 0.47$, it follows that the equivalent continuum porosity $\phi_e \cong \phi_m$ and the equivalent continuum saturation $s_e \cong s_m$, the matrix saturation. The fracture saturation follows from Equation II-26 (Lichtner 2001 [156429]). As can be seen from the figures, fracture and matrix temperatures become significantly different from one another only in the extreme case of very weak coupling strength with $\sigma_{fm} = 10^{-6}$. For weaker coupling, the fracture network cools sufficiently to sustain liquid water at the intrusion-host rock interface for times up to one year, as shown in Figure 11.4-19. As heat is conducted from the matrix to the fracture, the water vaporizes and the fracture network remains dry until the rewetting phase begins. The matrix remains completely dry until rewetting commences.

The effect of fracture-matrix coupling on fracture saturation is shown in Figure 11.4-19, where the fracture saturation at the interface between the basalt intrusion and the tuff host rock is plotted as a function of time. Temporary rewetting of the fracture occurs near the basalt-host rock contact for times up to one year as the intrusion cools. During this time, the matrix remains completely dry and at elevated temperatures well above boiling conditions. The transient rewetting of the fracture, however, does not extend very deep into the intrusion. The fracture becomes dry as more heat is transferred from the matrix. As the intrusion cools, final rewetting requires longer times, ranging from several hundred to over 1,000 years as the coupling strength decreases.

Finally, the role of chemical reactions was investigated briefly by considering the redistribution of silica as the intrusion cools and heats up the surrounding host rock. The incorporation of chemical processes is complicated by the initial high temperature of the intrusion (~1,200ºC). This condition leads to phase changes as moisture is redistributed throughout the host rock (initially two-phase) and the intrusion (initially single-phase gas). In the computer code FLOTRAN, all chemical reactions are expressed in terms of a set of primary species that must be chosen from the set of aqueous species linked by homogeneous reactions in local chemical equilibrium. Thus, an aqueous phase must be present at all times to treat chemical processes. Fortunately, it is not necessary to obtain thermodynamic constants at these high temperatures because liquid water is never present, on account of the low pressures involved (on the order of one bar).

To accommodate conditions of phase changes from two-phase to single-phase gas and vice versa, the approach used in FLOTRAN is to freeze the solution composition at some saturation cutoff value, specified by the user, as the system becomes a single-phase gas. For the reverse process, involving the transition from single-phase gas to two-phase, this frozen composition is released back to solution. Solid that precipitates from solution at a boiling front remains as is until that part of the system cools sufficiently for liquid water to once again become stable, after which the solid is allowed to react. It is necessary to make certain that the results obtained are not sensitive to the value of the saturation cutoff used.

For the simplified scoping calculation presented here, the matrix of both the host rock and the intrusion is considered to be composed of pure amorphous silica representing glass, and the fracture continuum is considered to be completely devoid of solid. As the glass matrix dissolves, reprecipitation of amorphous silica takes place in the fracture continuum. It should be noted that a more detailed description of the chemical system is required to distinguish between the

different chemical compositions of the basaltic intrusion and the tuff host rock; however, this level of detail was not attempted in this preliminary study. Fast kinetics were assumed with reaction rates close to local equilibrium. The value for the saturation cutoff used in the calculation was 0.001. Figure 11.4-20 shows the volume fraction of amorphous silica in the fracture at different times for the case of $\sigma_{fm} = 10^{-2}$. As the boiling front propagates into the host rock, silica precipitates from solution in the fractures. The source of silica is derived from the matrix upstream where dissolution of amorphous silica occurs (not shown). This result appears to be consistent with field observations at the Papoose Lake Sill.

11.4.7.3 Discussion

Although the field observations for mineral alteration are not inconsistent with the dual-continuum model predictions, there still remain a number of puzzling features. First, the close confinement of the alteration of the tuff host rock to zones adjacent to the intrusion is difficult to understand. This is the region that would be expected to be dry over the long term until the system cooled and rewetting took place. Whether the alteration could have occurred during the relatively rapid and transient passage of the boiling front as it swept through the host rock is still unresolved. It would appear difficult, however, to explain the extent of alteration of the matrix as caused by such a short-duration, transient event. Unfortunately, alteration of the matrix is not properly described by the dual-continuum connected-matrix model used here. A better approach would appear to be the dual-continuum disconnected-matrix formulation, which was beyond the scope of the present study.

A second puzzling feature is the sporadic appearance of alteration along the contact rather than a more uniform appearance, as modeling would predict. This feature could have several explanations. One is that nucleation kinetics were involved, and in most places, the reactions simply did not take place, although they were thermodynamically favored. This could be a result of low permeability and porosity values present in portions of the tuff (especially those that were fused) which would thus restrict the amount of water that could interact with the rock. Another possibility is that dehydration reactions of the basaltic dike released volatiles that reacted with the tuff host rock. Additionally, the host tuff may have had variable physical and chemical properties prior to the intrusion of the sill that might have resulted in non-uniform alteration.

Sensitivity analyses would help improve future models of the Paiute Ridge system. A number of the model input parameters are uncertain, and a sensitivity analysis would be useful to determine which parameters have the most impact on model results. In this regard, it should be emphasized that, for example, the van Genuchten parameters used for the intrusion and tuff country rock were not based on field measurement but were generic values that are approximate at best. The initial saturation condition of the tuff host rock plays an important role in moisture and heat redistribution, but is difficult, if not impossible, to know saturation values at the time the intrusion was emplaced.

11.4.8 Conclusions of Paiute Ridge Study

Magmatic intrusions in tuffaceous rock above the water table offer a unique opportunity to study conditions analogous to the potential Yucca Mountain high-level nuclear waste repository following emplacement of waste. The Paiute Ridge intrusive complex in partially saturated tuff

appears to offer a possible natural analogue site. A new result of this study is that the Papoose Lake Sill apparently intruded into Rainier Mesa tuff, and the resulting hydrothermal process was characterized by low-temperature alteration of glass to clinoptilolite and opal. The key observations of this study suggest that:

- The intrusion generally occurred at shallow levels and decreased in depth away from the central intrusive complex.
- The basalt along the contact is sheeted into narrow vertically or horizontally jointed plates, depending on whether the host tuff is exposed adjacent to or beneath the sill.
- Variable cooling patterns (e.g., glassy or crystallized fused tuff) occurred as noted along the intrusive contact.
- Alteration of nonwelded tuff to clinoptilolite and opal is similar to that observed in diagenetic processes at Yucca Mountain.
- Fractured zones in the tuff created by the basaltic intrusion were sealed by extensive silica remobilization during hydrothermal processes, resulting in low-porosity, highly indurated tuffs adjacent to the intrusive body.
- Hydrothermal alteration was confined to a narrow zone close to the contact zone, as indicated by major and trace element chemical data.

Field observations at the Paiute Ridge intrusive complex and results from laboratory analysis of altered and unaltered tuffs illustrate the intensity of hydrothermal alteration and extent of THC processes associated with thermal perturbation of rhyolitic ash flow tuffs. The secondary mineral assemblages are similar to those present at Yucca Mountain, and the presence of these minerals in the tuff at Paiute Ridge indicates the extent of the alteration. The pervasive anastomosing opal veins and associated secondary minerals (e.g., clinoptilolite, calcite, cristobalite) appear to have reduced matrix or fracture permeability in the immediate vicinity of the basaltic intrusion. The observed mineral zonations can be used to evaluate coupled process models. The widespread opal veins along fracture-matrix margins provide a means for evaluating porosity/permeability relationships and descriptions of fracture-matrix interaction employed in THC codes.

Preliminary results were presented for a one-dimensional THC dual-continuum model of the interaction of country rock with heat released from an intrusive complex emplaced above the water table. A simplified chemical system was considered involving precipitation and dissolution of amorphous silica. Results demonstrated the possibility of forming opal-filled veins with the source of silica derived from the matrix of the host rock. However, because of the irregularities caused by kinetic barrier effects associated with reaction of glass, it is important to compare and contrast a number of different natural analogue sites to be able to derive general conclusions regarding mineral alteration and, specifically, the effect of heat generated by a potential repository in tuff at Yucca Mountain.

Finally, an unexplained observation of this study is the proximal confinement of alteration of the tuff host rock to the intrusion. Additional modeling studies, and analytical data such as isotopes,

would elucidate the mechanisms responsible for the observed alteration patterns. A more extensive treatment of chemical processes, combined with the dual-continuum disconnected matrix formulation of the dual-continuum model, would allow for discretization of the rock matrix, thus resulting in more representative simulation results.

11.5 ANALOGUES TO THC EFFECTS ON TRANSPORT

The Marysvale hydrothermal uranium-molybdenum ore deposit in Utah has been evaluated as a natural analogue for evaluating the effects of water-rock interaction and radionuclide transport. Depletions in igneous rock $\delta^{18}O$ values were interpreted to result from exchange with circulating meteoric waters (Shea and Foland 1986 [156672], p. 281). The largest ^{18}O depletions were observed along an intrusive contact, where enhanced fluid flow was thought to have occurred. Uranium mineralization related to the hydrothermal event associated with the intrusion appears to be concentrated along faults and fractures (Shea 1984 [156673], p. 327). Uranium is primarily concentrated in uranium-bearing mineral phases, such as uraninite and coffinite, but is also found associated with sericite and chlorite along zones of microfracturing. The observed distribution of uranium was interpreted to be due to both bulk-flow and diffusion-transport processes, with most transport (and subsequent deposition) occurring within the fracture network.

Wollenberg et al. (1995 [157467]) used gamma-ray spectrometry and fission-track radiography to examine the location and abundance of uranium and thorium in tuffaceous rocks encompassing hydrothermal systems at the Long Valley caldera, California, and the Valles caldera, New Mexico. In the lateral flowing hydrothermal system at the Long Valley caldera, where temperatures range from 140–200°C, uranium is concentrated to 50 ppm with Fe-rich mineral phases in brecciated tuff fragments. In the vapor zone of the Valles caldera's hydrothermal system (temperature ~100°C), the concordance of high uranium, low Th/U, and decreasing whole-rock oxygen-isotope ratios suggests that uranium was concentrated in response to hydrothermal circulation when the system was formerly liquid-dominated. In the underlying present-day liquid-dominated zone (temperature to 210°C), up to several tens of parts per million uranium occurs with pyrite and Fe-oxide minerals, and in concentrations to several percent with a Ti-Nb-Y rare-earth mineral.

In the Valles caldera's outflow zone, uranium is also concentrated in Fe-rich zones, as well as in carbonaceous-rich zones in the Paleozoic bedrock that underlies the Quaternary tuff. Thorium, associated with accessory minerals, predominates in breccia zones and in a mineralized fault zone near the base of the Paleozoic sedimentary sequence. Relatively high concentrations of uranium occur in springs representative of water recharging the Valles caldera's hydrothermal system. By contrast, considerably lower uranium concentrations occur in hot waters (>220°C) and in the system's outflow plume, suggesting that uranium is being concentrated in the hotter part of the system. The Long Valley and Valles observations indicate that uranium and radium are locally mobile under hydrothermal conditions, and that the reducing conditions associated with Fe-rich minerals and carbonaceous material are important factors in the adsorption of uranium and its attenuation in water at elevated temperature. The Valles and Long Valley studies provide evidence for at least localized mobility of uranium and its daughters in tuff and underlying sedimentary rocks at temperatures comparable to those expected in a nuclear waste repository environment.

11.6 ANALOGUES TO THM EFFECTS

11.6.1 Insights from Field Tests

Results of heater tests conducted at the NTS in granite and tuff and at the Stripa Swedish underground laboratory in granite showed a decrease in fracture permeability as a result of thermal expansion. The Climax spent fuel test at the NTS was conducted in a 426 m deep shaft in granite. During the three-year test, temperatures in the monitored region of the rock mass reached 80°C (Hardin and Chesnut 1998 [150043], pp. 4-1 to 4-3). No significant changes in mineralogy or microfracturing occurred as a result of heat or irradiation. Monitored permanent displacements were on the order of 0.1–1 mm (Hardin and Chesnut 1998 [150043], p. 4-3). The sense of displacement was consistent with the regional extensional tectonic regime.

Four heater experiments were conducted in G-tunnel, within Rainier Mesa, NTS. In the heated-block test, rock-mass mechanical and thermomechanical properties were measured in tuff under controlled thermal and stress-loading conditions. The block was subjected to maximum temperatures ranging from 76–145°C, and equal biaxial stresses with magnitudes up to 10.6 MPa (Zimmerman et al. 1986 [138273], pp. vii–ix). The permeability of a single, near-vertical fracture was measured. The largest changes in permeability were associated with excavation of the block, when the apparent permeability increased from 76 to 758 microdarcies. Subsequent compressive loading decreased the permeability but did not completely reverse the unloading conditions, and the apparent permeability ranged from 252–332 microdarcies over a stress range of 3.1–10.6 MPa (Hardin and Chesnut 1998 [150043], p. 4-6). Increased temperature under biaxial confinement decreased the fracture aperture, lowering the apparent permeability from 234 to 89 microdarcies during heating.

In addition to full-scale heater tests that investigated short-term near-field effects from thermal loading, a time-scaled heater test was also performed at the Stripa underground laboratory to investigate the long-term thermomechanical response to thermal loading (Robinson 1985 [157445]). In the full-scale and time-scale heater tests, heat flow was not affected by fractures or other discontinuities in the granitic rock mass. Thermoelastic deformation of the rock mass was nonlinear and less than predicted. Fracture closure in response to thermal expansion was confirmed by observation of diminished water inflow to the heater and instrument boreholes (Nelson et al. 1981 [150092], pp. 78–80) and by increased compressional wave velocity during heating (King and Paulsson 1981 [157444], p. 699).

11.6.2 Krasnoyarsk

Krasnoyarsk-26 (K-26) is an underground facility in south-central Siberia where nuclear power has been generated by three underground reactors for approximately four decades, with a byproduct of weapons-grade plutonium. The power generated by these reactors is used to provide heat, electricity, and hot water for the city of Zheleznogorsk. Although K-26 differs from Yucca Mountain in geology and hydrologic regime, with K-26 located in saturated, fractured Archean-Proterozoic gneisses, it is the longest “heater test” on record, with a 40-year record of thermal measurements.

A schematic of the underground workings is shown in Figure 11.6-1. The depth of the underground workings has not been reported precisely, but is estimated to be at ~200–300 m below the surface in saturated bedrock (Gupalo 2001 [157471], p. 9). Large sources of heat are present in the P-2 and P-4 underground workings, where air temperatures reach 60–65°C (Gupalo 2001 [157471] p. 15). Based on temperatures measurements in 125 boreholes around the heat sources over 30 years, the dynamics of the rock-mass heating have been obtained. The maximum temperature of the rock is 63°C. The 30°C isotherm is established at a distance of 30 m from the heat sources (Gupalo 2001 [157471], pp. 52, 83).

Facilities at B-3 and B-4 were constructed for "technological works" in 1960, but they have not been used. This makes it possible to monitor coupled processes in both types of underground facilities, those that have and have not been impacted by heat. The dimensions of the chambers containing the heat source are approximately 20 m wide × 60 m long × 40 m in height (Gupalo 2001 [157471], pp. 24, 83; 1999 [157470], p. 9). All chambers have a 1.6 m thick concrete lining.

The geologic conditions of the P-2, P-4, B-3, and B-4 facilities are quite different. Chamber P-2 is located in the footwall of a steeply dipping zone of cataclasis and is surrounded by schistose zones. Chambers P-4 and B-4 are located in fractured gneiss (Gupalo 2001 [157471], p. 15).

The convergence of underground chamber walls as a result of manmade disturbances has been small over the 40-year lifetime of the facility. The largest values of convergence were measured in chamber P-2, where convergence ranged from 16.9–21.5 mm. In chamber P4, maximum convergence of walls is half that of P-2. In B-4, maximum convergence of walls amounted to 1.55 mm, one order of magnitude less than the heated facilities in P-2 and P-4. Approximately similar heat sources operate in P-2 (T = 45°C) and P-4 (T = 62°C), such that their impact on the host rock is similar. The increased deformation in P-2, as compared to P-4, is attributed to the unfavorable mining and geologic conditions, compared to the rock mass in pillars surrounding chamber P-4 (Gupalo et al. 1999 [157470], p. 45).

According to the velocity of ultrasonic waves measured from logging seven boreholes, three zones of deformation can be distinguished in the rock mass: (1) a zone of concrete lining (0.0–1.6 m) and adjacent rock layer with high disturbance level (1.6–2.0 m); (2) a zone of contour rock layer of intermediate disturbance (1.6–2.0 m); (3) the undisturbed rock mass (over 4.0 m) (Gupalo et al. 1999 [157470], p. 80). The vertical component of convergence was determined to be 2.1 mm (+0.09 mm/yr from 1976 to 1998). (Gupalo 2001 [157471], p. 80).

The effect of thermal loads on rock-mass deformation was found to be significant in the disturbed zone. Within a homogeneous rock mass, convergence of chamber walls over a 40-year observation period was 1.0 mm in the absence of thermal impacts, but dislocations increased 8 to 10 times under increased temperature effects (Gupalo 2001 [157471], p. 81).

There is a clear temperature-related effect of the underground facilities on fracture-vein waters. The area of enhanced temperatures of underground water reaches 38–70 m above the roof of the workings, and maximum recorded temperatures of the underground waters is 36°C. (Gupalo 2001 [157471], p. 83).

Although the K-26 example is more analogous to preclosure conditions rather than postclosure performance at Yucca Mountain, it provides an example of relative thermomechanical stability under sub-boiling conditions in a more heterogeneous rock mass than that found at Yucca Mountain. It also provides a test case that compares a thermomechanically disturbed regime to one that is merely mechanically disturbed in the same rock mass, to determine the thermal component of disturbance.

11.6.3 THM Insights from Geothermal Fields

During the 1970s and 1980s, The Geysers geothermal region was rapidly developed as a site of geothermal power production. The likelihood that this could cause significant strain within the reservoir, with corresponding surface displacements, led to a series of deformation monitoring surveys from 1973 to 1996. For the period 1980-1994, peak volume strains occurred in excess of 5×10^{-4}. Changes in reservoir steam pressures were well correlated with volume strain and contraction of the reservoir (Mossop and Segall 1999 [157466], p. 29,113).

Seismicity has been induced by oil and gas production in areas where pore pressures have decreased, in some cases by several tens of MPa (Segall and Fitzgerald 1998 [157464], p. 117). Induced earthquakes are also common in geothermal fields, such as The Geysers, where strong correlations between earthquake activity and both steam production and condensate injection, have been observed. Stress measurements within hydrocarbon reservoirs show that the least horizontal stress decreases with declining reservoir pressure, as predicted by poroelasticity. Production-induced stressing may promote frictional sliding on pre-existing faults. However, it is not expected that this magnitude of stress would occur at Yucca Mountain.

Studies of hydraulic fracturing experiments in hot dry rock suggest that under thermal conditions, mechanical stresses in the rock at Yucca Mountain will occur along preexisting fracture zones and will develop in the direction of maximum principal stress. The Hijori hot dry rock site in Yamagata, Japan, was the site of hydraulic fracturing experiments in 1988 that were accompanied by microseismic events (Sasaki 1998 [157465], p. 171). The microseismic events were thought to have been caused by shear failures induced by high pore-fluid pressures occurring on planes of weakness in the rock surrounding the main hydraulic fracture. The experiment indicated a migration of the induced microseismic events that eventually distributed along a vertical plane, with the strike of seismicity nearly parallel to the direction of the maximum principal stress. The vertical orientation and east-west strike of the seismic events are essentially coplanar with the caldera ring-fault structure in the southern portion of the Hijiori Caldera. This indicates that a preexisting fracture zone was being reopened and developed in the direction of maximum principal stress.

11.7 SUMMARY AND CONCLUSIONS

Geothermal systems illustrate a variety of THC processes that are relevant to Yucca Mountain. They include advective and conductive heating, fracture-dominated fluid flow, chemical transport, boiling and dryout, condensation, and mineral alteration, dissolution, and precipitation. Yellowstone and other geothermal systems in welded ash flow tuffs or other low-permeability rocks indicate that fluid flow is controlled by interconnected fractures. Alteration in low-permeability rocks is typically focused along fracture-flow pathways. Only a small portion of the

fracture volume needs to be sealed in order to retard fluid flow effectively. At Yucca Mountain, fluid flow and low-temperature water-rock interaction over the past 10 m.y. have resulted in the precipitation of minor amounts of opal and calcite on fracture and lithophysal cavity surfaces.

The main minerals predicted to precipitate in the near field of the potential Yucca Mountain repository are amorphous silica and calcite, which are also commonly found as sealing minerals in geothermal systems.

Sealing in geothermal fields can occur over a relatively short time frame (days to years). Precipitation of minerals can be triggered by a variety of processes, including boiling, water-rock interaction, heating and cooling of fluids, and fluid mixing. The unsaturated conditions, lower temperatures, and much lower fluid-flow rates predicted for the Yucca Mountain system in comparison to geothermal systems, should result in less extensive water-rock interaction than is observed in geothermal systems.

Fracturing and sealing occur episodically in geothermal systems. Different generations of fracture mineralization indicate that there are multiple pulses of fluid flow, recording distinct temperature conditions and fluid compositions, throughout the lifespan of a geothermal system. Most mineralization at Yucca Mountain is predicted to occur soon after waste emplacement (1,000–2,000 yr), when temperatures would reach boiling (for the higher-temperature operating mode) above the emplacement drifts.

The effects of processes such as boiling, condensation, dissolution, and precipitation on the higher-temperature operating mode for Yucca Mountain will be restricted to the near-field environment. Silica precipitation at Yellowstone results from both cooling and boiling processes, which serve to raise silica concentrations to above saturation levels. Geochemical modeling of fluid compositions has been used to successfully predict observed alteration of mineral assemblages at Yellowstone.

As shown in Section 11.3, THC processes are expected to have a much smaller effect on hydrogeological properties at Yucca Mountain than on those observed at Yellowstone. However, development of a heat pipe above emplacement drifts at Yucca Mountain under a higher-temperature operating mode could lead to increased chemical reaction and transport in the near field. Reflux and boiling of silica-bearing fluids within the near field at Yucca Mountain could cause fracture plugging, thus changing fluid-flow paths. THC simulations conducted to date for the potential Yucca Mountain repository suggest that only small reductions in fracture porosity (1–3%) and permeability (<1 order of magnitude) will occur in the near field as a result of amorphous silica and calcite precipitation (BSC 2001 [155950], Section 4.3.6.4.2). Changes in permeability, porosity, and sorptive capacity are expected to be relatively minor at the mountain scale, where thermal perturbations will be minimal; this also applies to the lower-temperature (sub-boiling) design. These predicted changes in hydrogeological properties should not significantly affect repository performance.

Magmatic intrusions in tuffaceous rock above the water table, such as the Paiute Ridge intrusive complex studied in Section 11.4, offer a unique opportunity to study conditions analogous to the predicted postclosure repository conditions at potential Yucca Mountain. The Papoose Lake Sill intruded into Rainier Mesa tuff, and the resulting hydrothermal effects were characterized by

low-temperature alteration of glass to clinoptilolite and opal, similar to those present at Yucca Mountain. Hydrothermal alteration was confined to a narrow zone close to the contact zone. The pervasive anastomosing opal veins and associated secondary minerals (e.g., clinoptilolite, calcite, cristobalite, etc.) appear to have reduced matrix or fracture permeability in the immediate vicinity of the basaltic intrusion.

The widespread opal veins along fracture-matrix margins provide a means for testing and validating porosity/permeability relationships and descriptions of fracture-matrix interaction employed in THC codes. Preliminary results of a one-dimensional THC dual-continuum model of the interaction of country rock with heat released from an intrusive complex emplaced above the water table demonstrated the possibility of forming opal-filled veins with the source of silica derived from the matrix of the host rock. However, because of the irregularities caused by kinetic barrier effects associated with the reaction of glass, it is important to compare and contrast a number of different sites to be able to derive general conclusions regarding mineral alteration and, specifically, the effect of heat generated by a potential repository in tuff at Yucca Mountain.

Examples provided in Section 11.5 indicate that the observed distribution of uranium resulting from hydrothermal conditions at Marysvale was a result of advective transport and diffusion, with most transport-subsequent precipitation of uranium occurring within the fracture network. This observation was also borne out at portions of the Long Valley and Valles calderas. The latter two studies also provided evidence for at least localized mobility of uranium-series radioisotopes at temperatures more comparable to those expected under higher-temperature thermal-loading conditions in a nuclear waste repository environment.

THM effects at Yucca Mountain (Section 11.6) are expected to be less extreme than those operating in geothermal fields where microseismicity is detected. Although rock type, hydrogeology, and design configurations differ from those at Yucca Mountain, the closest analogue identified so far is K-26, which is particularly relevant to lower-temperature design scenarios. Although the 40-year record of experiments should be interpreted cautiously with respect to extrapolation to long time periods, thermomechanical effects, such as drift convergence, might be in the same range of magnitude (on the order of a few mm) as that at Krasnoyarsk for the preclosure period.

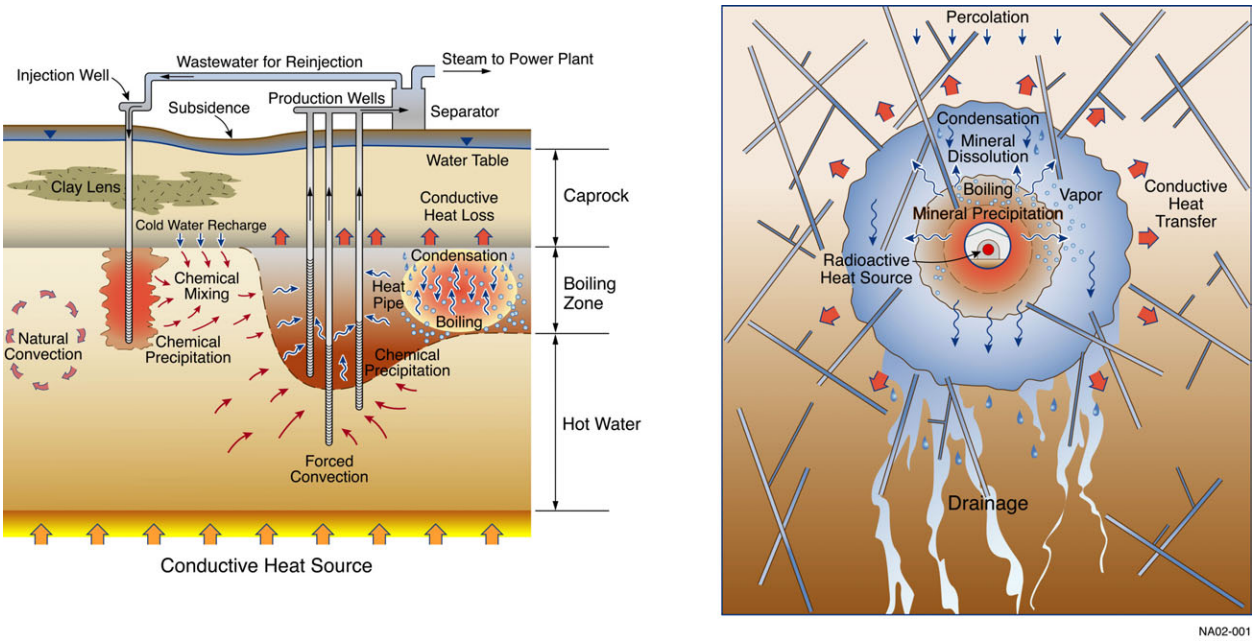

NOTE: Similar processes include boiling and condensation, advective liquid flow, mineral dissolution and precipitation, mixing, recharge (percolation), and heat conduction. A heat pipe is depicted on the right side of the geothermal system, showing countercurrent liquid and vapor flow resulting from boiling and condensation.

Source: Left figure adapted from Bodvarsson and Witherspoon (1989 [156337]), right adapted from CRWMS M&O (2000 [151940]).

Figure 11.2-1. Comparison of Processes in Geothermal (Left) and Anthropogenic (Right) Thermal Systems Created by Emplacing Heat-Generating Nuclear Waste in an Unsaturated Fractured Rock Mass

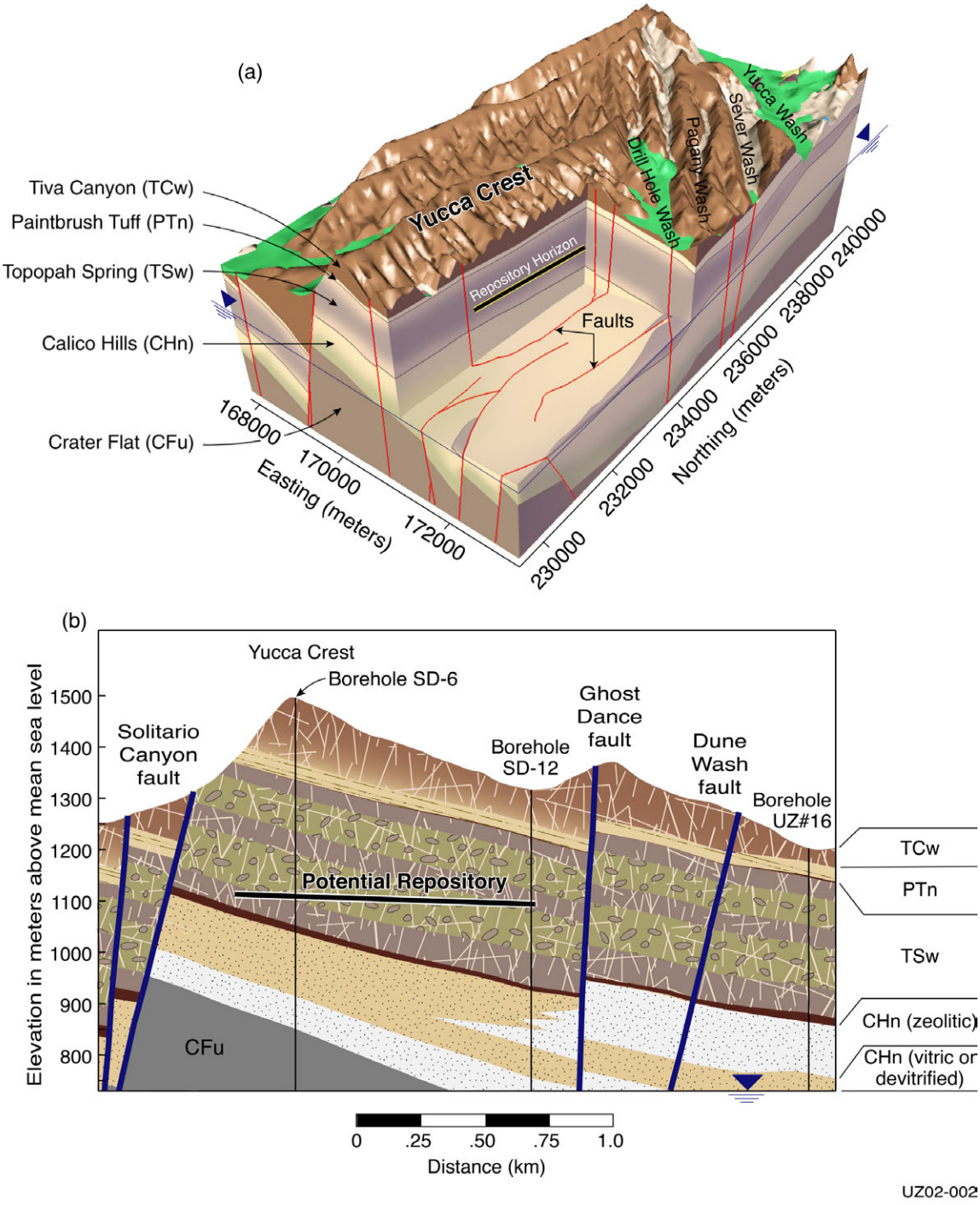

NOTE: In both (a) and (b), the water table is indicated by a blue downward-pointing triangle.

Source: CRWMS M&O 2000 [151940], Figure 3.2-1.

Figure 11.2-2. Schematic Diagram (a) and Cross Section (b) of the Yucca Mountain Lithology and Topography, Including Surface Features and Major Geologic Strata

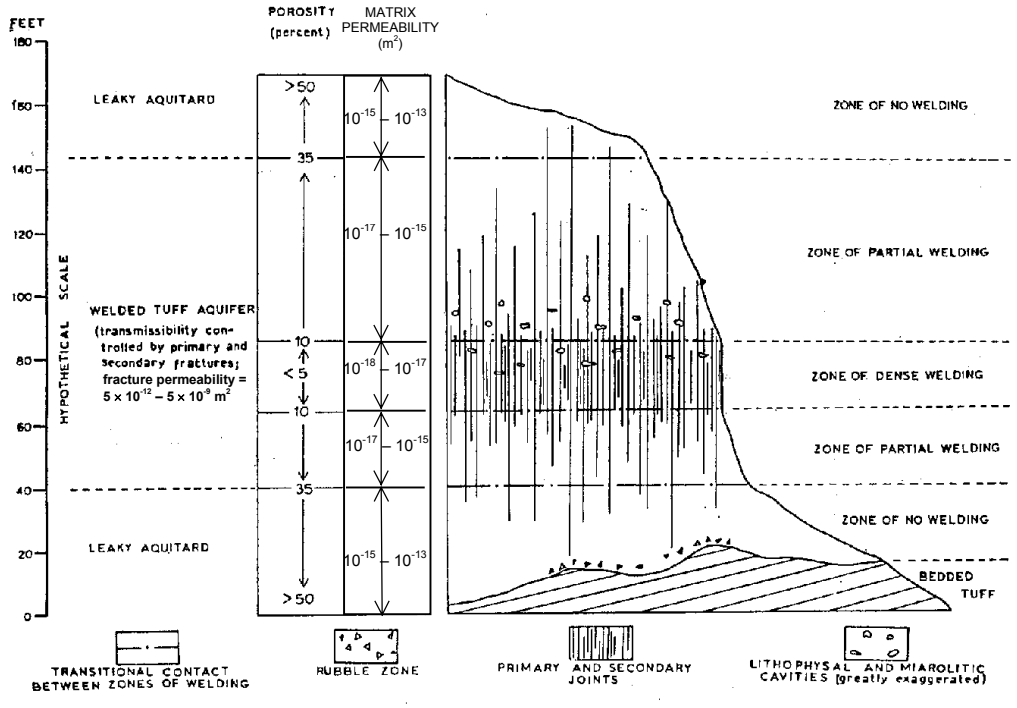

NOTE: While zones of dense welding have intrinsically low matrix permeabilities, these zones also have much more abundant fractures, resulting in higher overall permeability than nonwelded (and unfractured) tuff.

Source: Generic profile modified from Winograd (1971 [156254], Figure 5).

Figure 11.2-3. Typical Variations in Permeability and Porosity in Welded and Unwelded Ash Flow Tuff

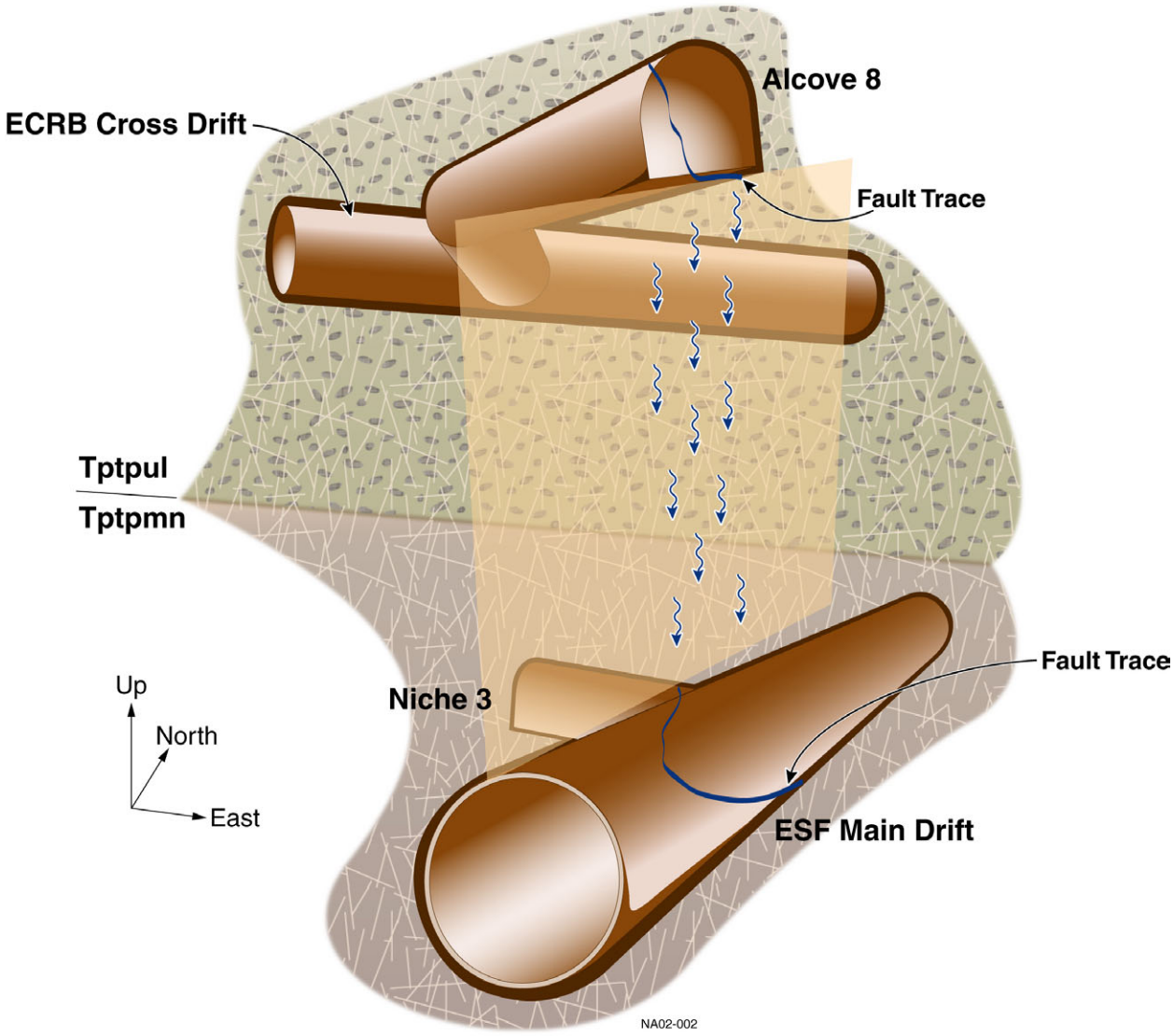

NOTE: Water is introduced into the fault in Alcove 8 and collected in and near Niche 3.

Source: Modified from BSC 2002 [157606], Figure 2.

Figure 11.2-4. Schematic Diagram of Flow Test at Yucca Mountain

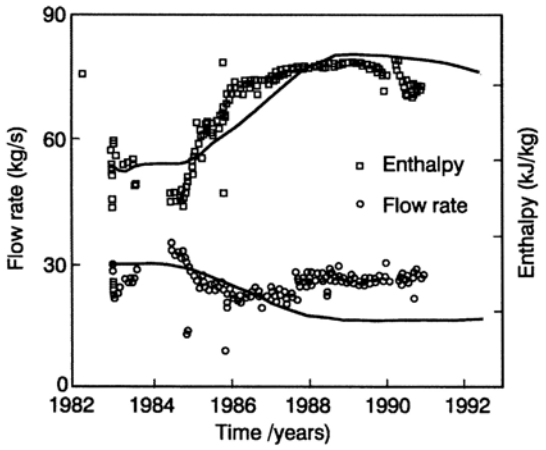

NOTE: Flow rates are slightly greater and enthalpy is slightly less than predicted by the 1986 model from 1988 to 1992.

Source: Steingrimsson et al. 2000 [156686], p. 2904.

Figure 11.2-5. Comparison between Predicted and Observed Flow Rates and Enthalpies for Well 6 of the Nesjavellir Geothermal Field (Iceland)

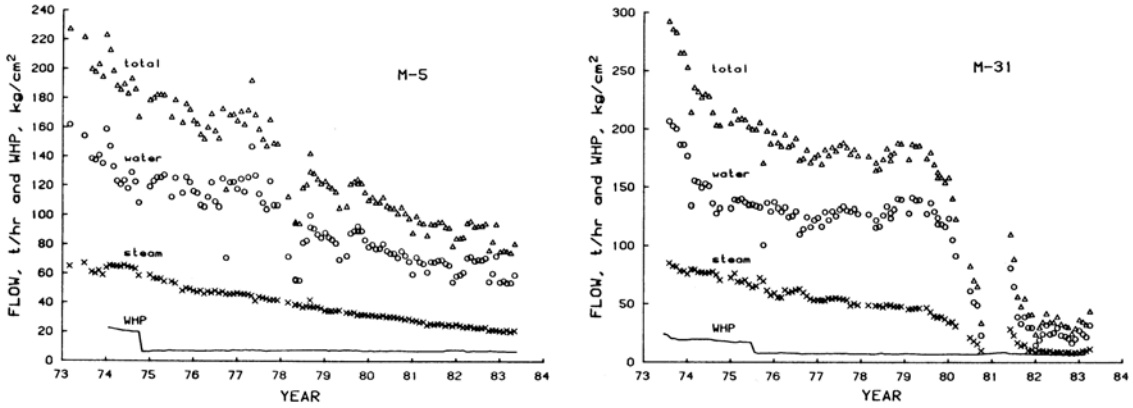

NOTE: Well M-31 experienced near-well boiling with abundant mineral deposition. Cleaning well M-31 in 1981 yielded a short-lived increase in production. WHP = well head pressure.

Source: Truesdell et al. 1984 [156350], p. 227.

Figure 11.2-6. Comparison of Production between Wells M-5 and M-31 at the Cerro Prieto Geothermal Field

NOTE: The botryoidal texture of the quartz indicates that it was deposited as chalcedony or amorphous silica, and that this deposition occurred at >300°C due to rapid decompression. qtz = quartz, qtz(chal) = chalcedony, py = pyrite, act = actinolite, and ep = epidote

Source: Moore et al. 2000 [156319], p. 261.

Figure 11.2-7. Photomicrograph of Fracture Minerals in the Karaha-Telaga Bodas System, Indonesia

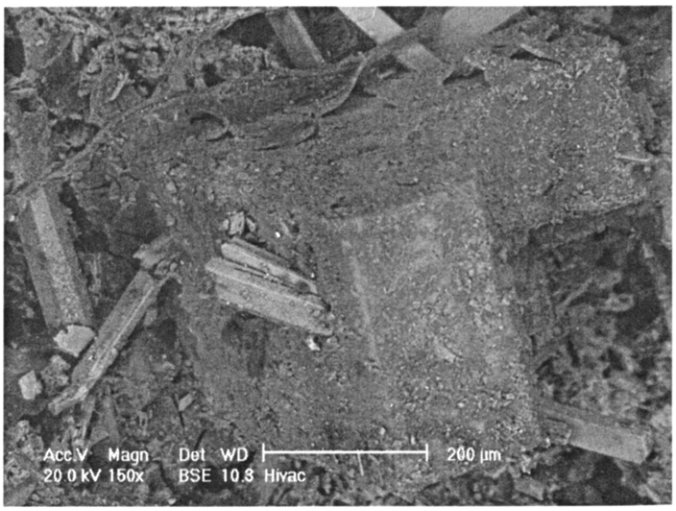

NOTE: Titanium-rich scale coats anhydrite and fine needles of actinolite. The scale is peeling off the top of the crystal.

Source: Moore et al. 2000 [156319], p. 260.

Figure 11.2-8. Scanning Electron Microscope Backscattered Image of Fracture Minerals in the Karaha-Telaga Bodas System, Indonesia

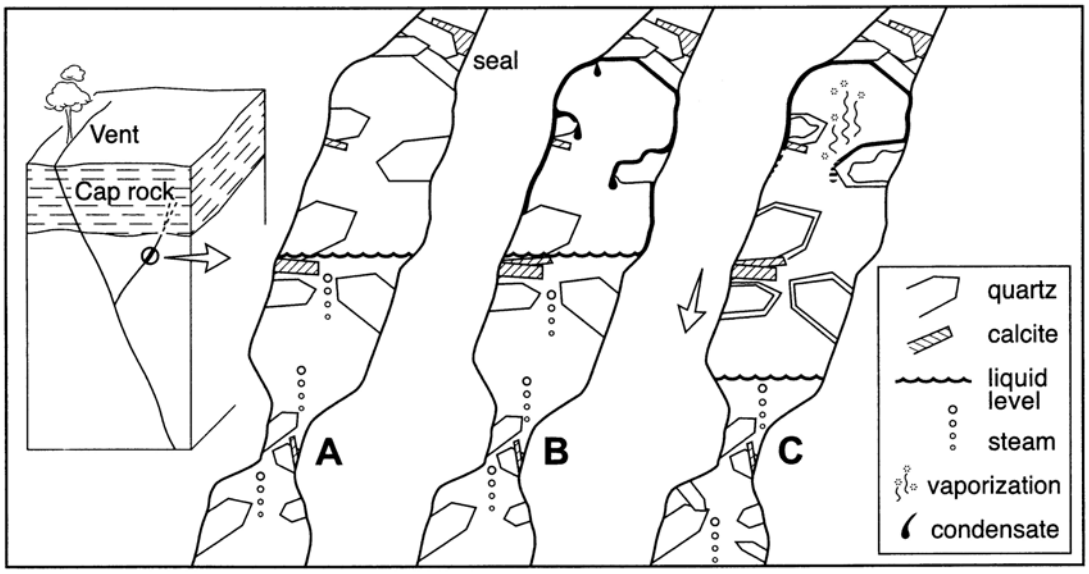

NOTE: In A, quartz and calcite are deposited as the result of boiling possibly due to depressurization in the system. Initially, the rock is too hot for condensation to occur. In B, the top portion of the vein has cooled sufficiently so that condensation occurs. Steam from below migrates through the vein until it reaches the cooler rock where condensation occurs. Corrosion of quartz and calcite occurs near the site of condensation. In C, subsequent lowering of the water table (indicated by the arrow) due to venting results in quartz and calcite deposition due to condensate boiling. Mineral deposition may also occur as condensate reaches the lower, superheated region, and in the liquid-dominated portion of the vein.

Source: Moore et al 2000 [156318], p. 1731.

Figure 11.2-9. Schematic Illustration Showing the Transition from a Liquid Dominated System to a Vapor-Dominated System, Showing only a Portion of the Vein

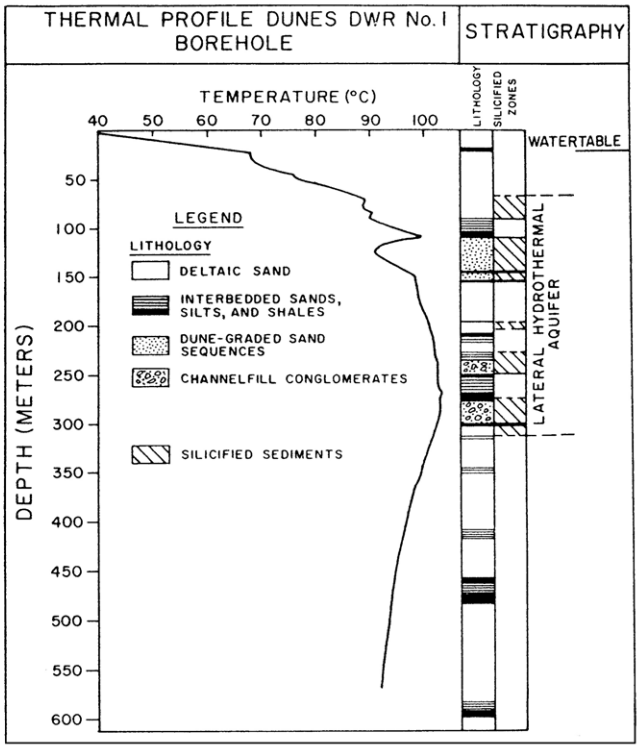

NOTE: The silicified regions are identified in the right column by cross hatching.

Source: Bird and Elders 1976 [154601], p. 286.

Figure 11.2-10. Temperature Profile and Lithology of Borehole DWR No. 1 at the Dunes Geothermal System, California

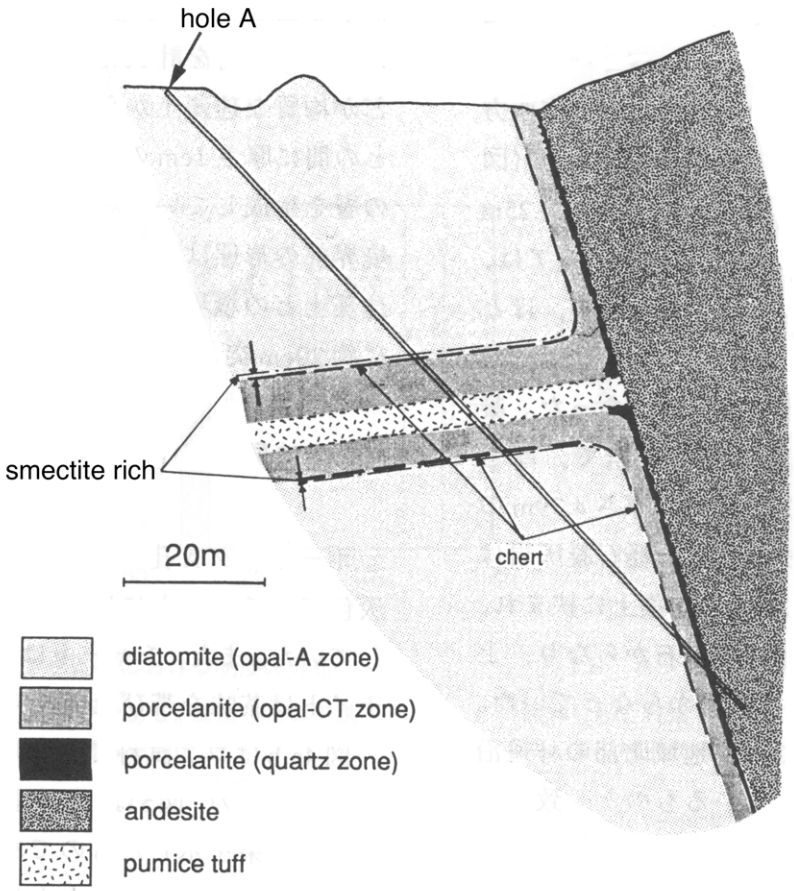

NOTE: The diatomite was altered to porcelanite and chert as a result of a hydrothermal system induced by the intrusion of an andesite dike. The thicknesses of the porcelanite and chert layers range from 20 cm to 20 m (porcelanite) and 5 cm to 20 cm (chert).

Source: Chigira and Nakata 1996 [156349], p. 15.

Figure 11.2-11. Schematic of Lithology near Borehole A in the Miocene Iwaya Formation, Japan

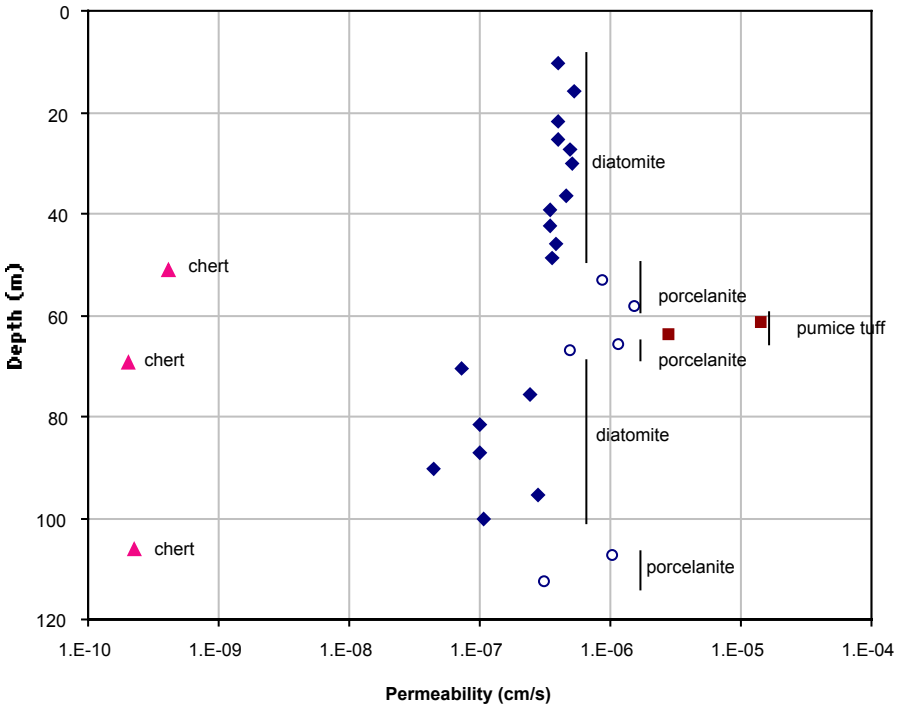

NOTE: Alteration mineral porcelanite has a similar permeability to the original diatomite, but the chert is far less permeable.

Source: Data from Chigira and Nakata 1996 [156349], p. 11.

Figure 11.2-12. Permeability Profile of Samples along Borehole A in the Miocene Iwaya Formation, Japan

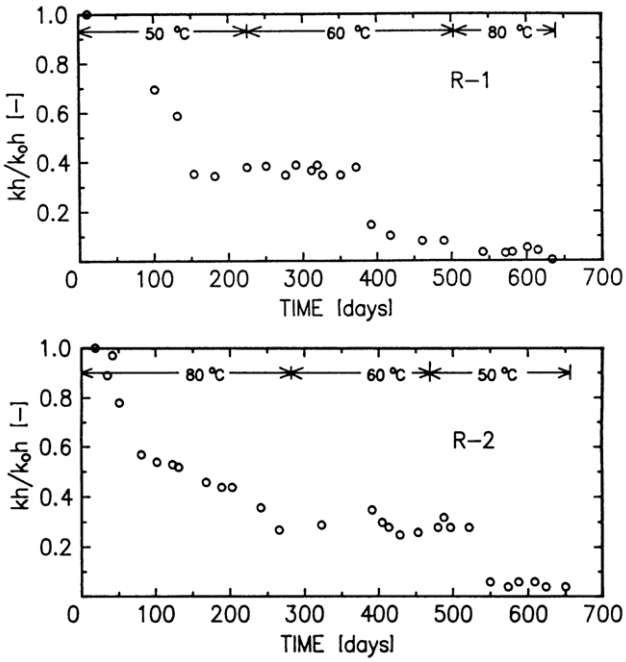

NOTE: The temperatures indicate the temperature of the injected water. The permeability-thickness product (kh) in Well R-1 decreased from 224 darcy-m to 0.79 darcy-m over 624 days. In Well R-2, the permeability-thickness product decreased from 91 darcy-m to 5 darcy-m over 637 days.
kh = permeability-thickness product
$k_o h$ = initial permeability-thickness product

Source: Itoi et al. 1987 [156346], pp. 543–544.

Figure 11.2-13. Reduction in Permeability in Wells R-1 and R-2 over the Duration of a Reinjection Experiment

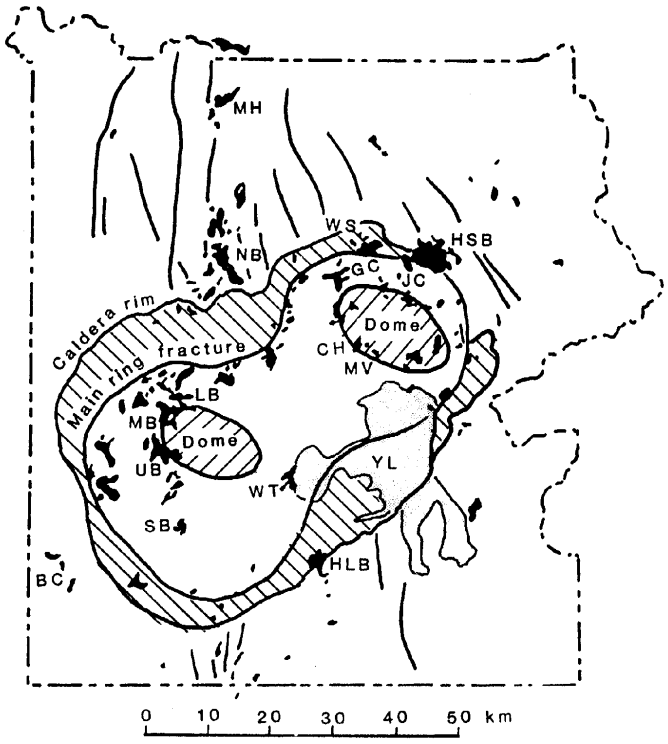

NOTE: Areas abbreviated as follows: BC = Black Creek, CH = Crater Hills, GC = Grand Canyon, HLB = Hart Lake Basin, HSB = Hot Springs Basin, JC = Joseph's Coat Hot Spring, MH = Mammoth Hot Springs, NB = Norris Geyser Basin, LB = Lower Geyser Basin, MB = Midway Geyser Basin, UB = Upper Geyser Basin, SB = Shoshone Geyser Basin, MV = Mud Volcano, WT = West Thumb, WS = Washburn Hot Springs, YL = Yellowstone Lake.

Source: Fournier 1989 [156245], Figure 2.

Figure 11.3-1. Map of Yellowstone National Park, with Outline of 0.6 Ma Caldera Rim

DTN: LB0201YSANALOG.001 [157569]

NOTE: Large sinter blocks had been ejected by 1989 explosion. The pool has an opalescent color, indicating presence of colloidal silica (photo by R. Fournier, USGS).

Source: Simmons 2002 [157578], SN-LBNL-SCI-185-V1, p. 7-1.

Figure 11.3-2. Porkchop Geyser (July 1991)

DTN: LB0201YSANALOG.001 [157569]

Source: Simmons 2002 [157578], SN-LBNL-SCI-185-V1, p. 7-1.

Figure 11.3-3. Block from 1989 Porkchop Geyser Eruption, with Gelatinous, Botryoidal Silica Coating Outer Margins and Cavities (photo from T.E.C. Keith, USGS)

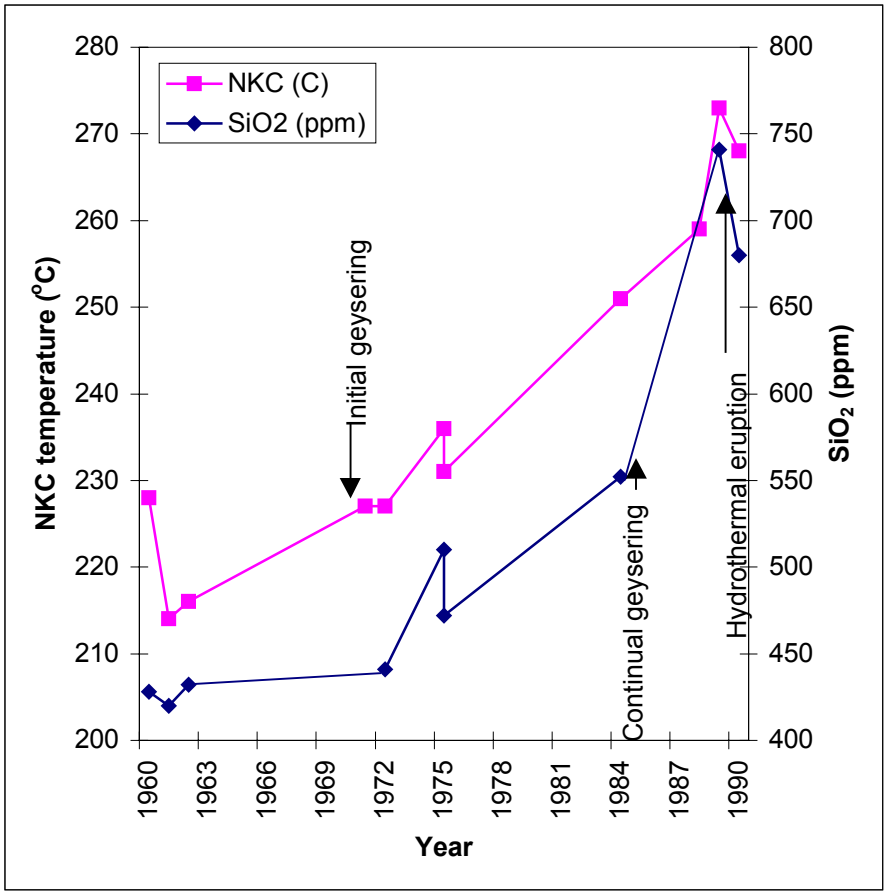

NOTE: Change in flow behavior interpreted to be linked to precipitation of amorphous silica, resulting in the clogging of flow channels.

Source: Fournier et al. 1991 [156246], p. 1116.

Figure 11.3-4. Changes in Calculated Sodium-Potassium-Calcium (NKC) Reservoir Temperatures and Silica Concentrations for Waters Sampled from Porkchop Geyser

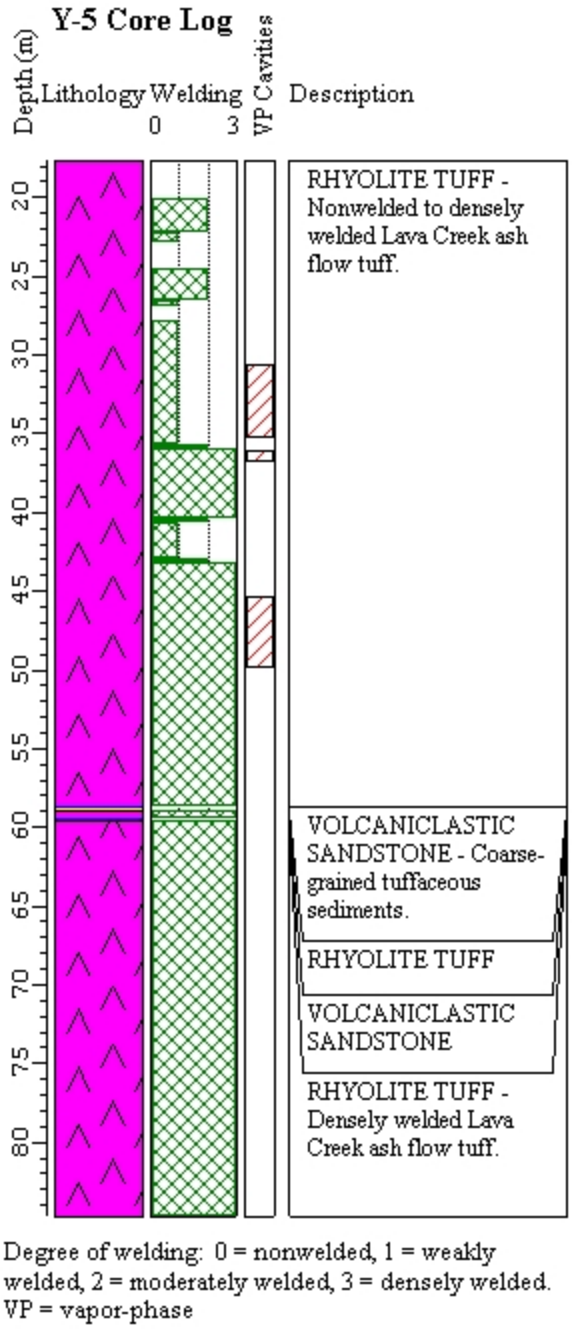

DTN: LB0201YSANALOG.001 [157569]

Source: Dobson et al. 2001 [154547], Figure 2.

Figure 11.3-5. Simplified Geologic Log of the Y-5 Core

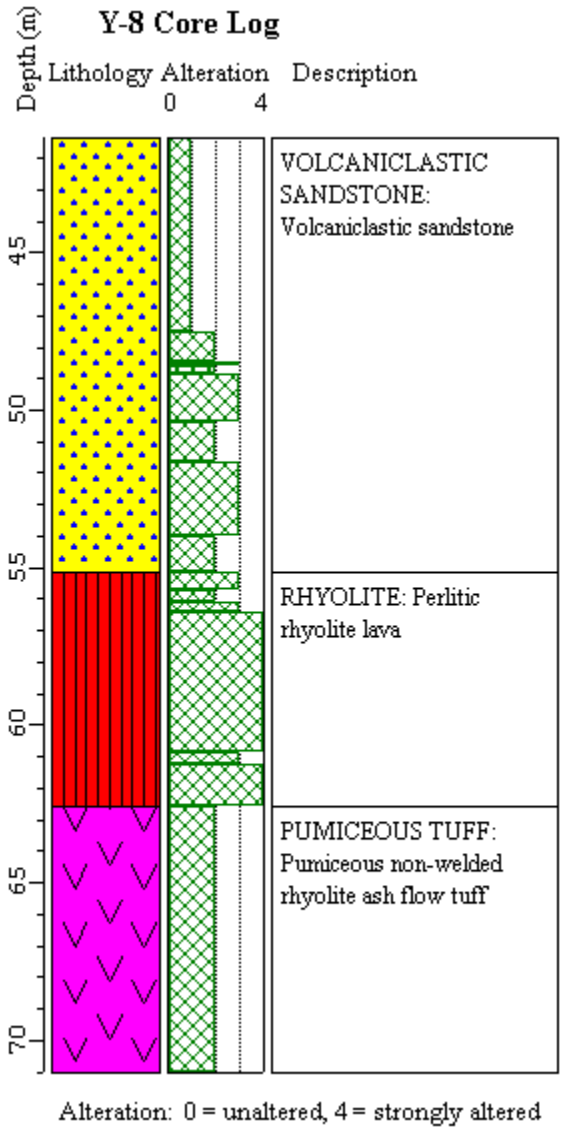

DTN: LB0201YSANALOG.001 [157569]

Source: Dobson et al. 2001 [154547], Figure 3.

Figure 11.3-6. Simplified Geologic Log of the Y-8 Core

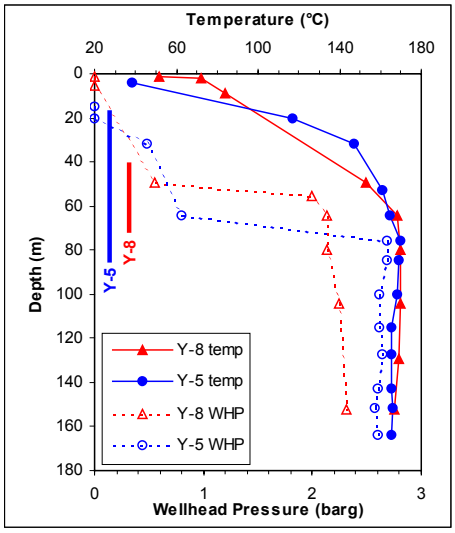

DTN: LB0201YSANALOG.001 [157569]

NOTE: Vertical bars at left indicate studied core-depth intervals. Temperature and pressure data from White et al. 1975 [154530].

Source: Dobson et al. 2001 [154547], Figure 1.

Figure 11.3-7. Downhole Temperature (Solid Lines) and Wellhead Pressure Variations (Dotted Lines) in the Y-5 and Y-8 Wells

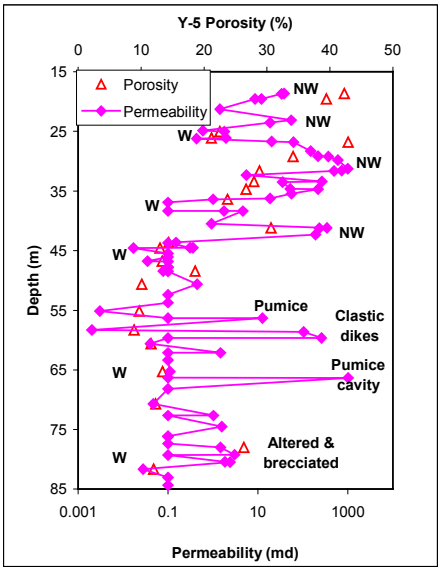

DTN: LB0201YSANALOG.001 [157569]

NOTE: W= moderately to densely welded tuff, NW = nonwelded to weakly welded tuff. The 0.1 md values represent the lower detection limit for minipermeability measurements; actual values are lower.

Source: Dobson et al. 2001 [154547], Figure 4.

Figure 11.3-8. Porosity and Permeability Variations in the Y-5 core

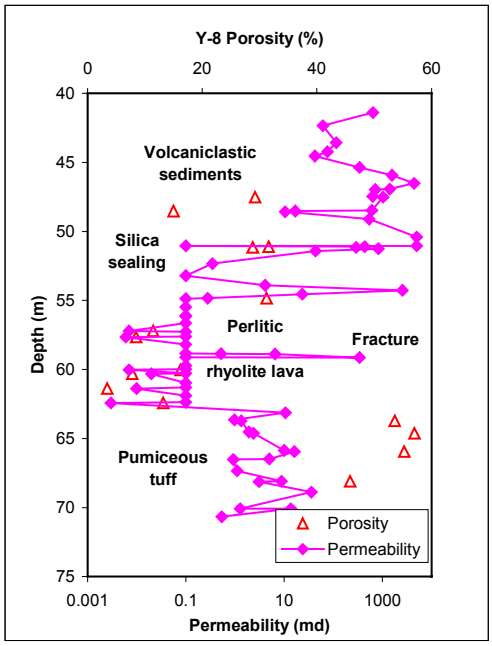

DTN: LB0201YSANALOG.001 [157569]

Source: Dobson et al. 2001 [154547], Figure 5.

Figure 11.3-9. Porosity and Permeability Variations in the Y-8 Core

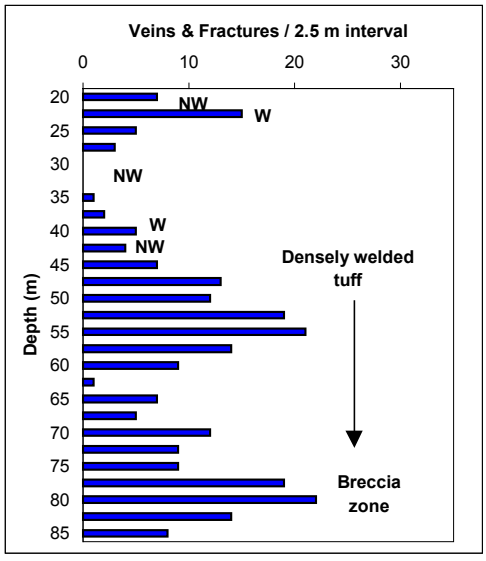

DTN: LB0201YSANALOG.001 [157569]

NOTE: W= moderately to densely welded tuff, NW = nonwelded to weakly welded tuff

Source: Dobson et al. 2001 [154547], Figure 6.

Figure 11.3-10. Veins and Fractures in the Y-5 Core

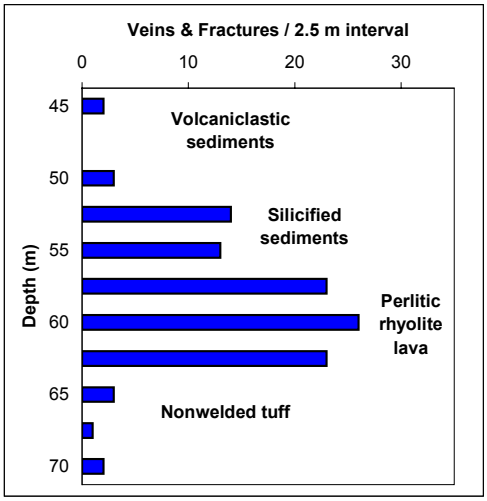

DTN: LB0201YSANALOG.001 [157569]

Source: Dobson et al. 2001 [154547], Figure 8.

Figure 11.3-11. Veins and Fractures in the Y-8 Core

DTN: LB0201YSANALOG.001 [157569]

NOTE: Core width is 4.4 cm. Permeability values of welded tuff clast (A) and matrix (B) are both below the minipermeameter detection limit (0.1 md).

Source: Dobson et al. 2001 [154547], Figure 7.

Figure 11.3-12. Hydrothermal Breccia from the Y-5 Core at 47.7 m (156.5 feet)

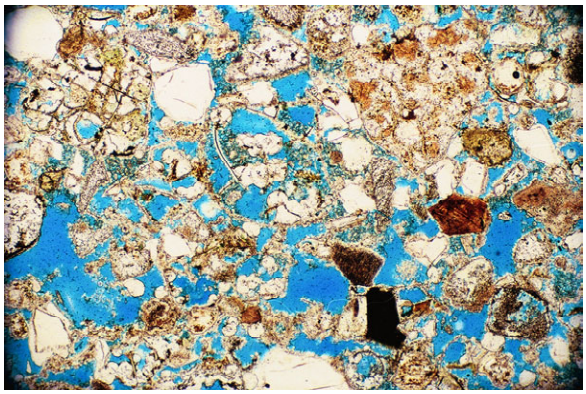

Y-8, 155.9’

Permeability = 1030 md

Porosity = 29.2%

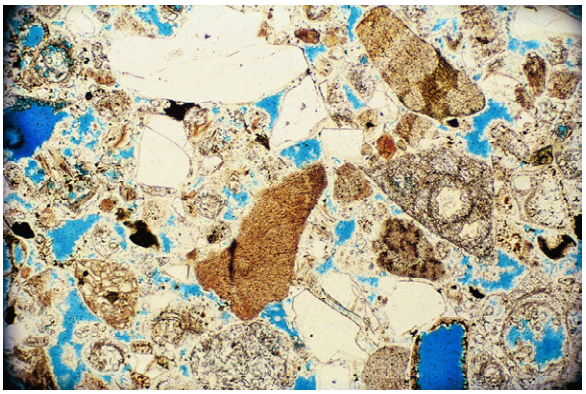

Y-8, 159.2’

Permeability = 16.9 md

Porosity = 15.0%

DTN: LB0201YSANALOG.001 [157569]

NOTE: Silicification of the sample from 159.2’ has resulted in a 50% reduction in porosity (change in abundance of blue epoxy denoting porosity) and decrease in permeability of nearly two orders of magnitude.

Source: Simmons 2002 [157578], SN-LBNL-SCI-185-V1, Roll 17, Photos 2 and 4.

Figure 11.3-13. Photomicrographs of Volcaniclastic Sandstone Unit from Y-8 Core

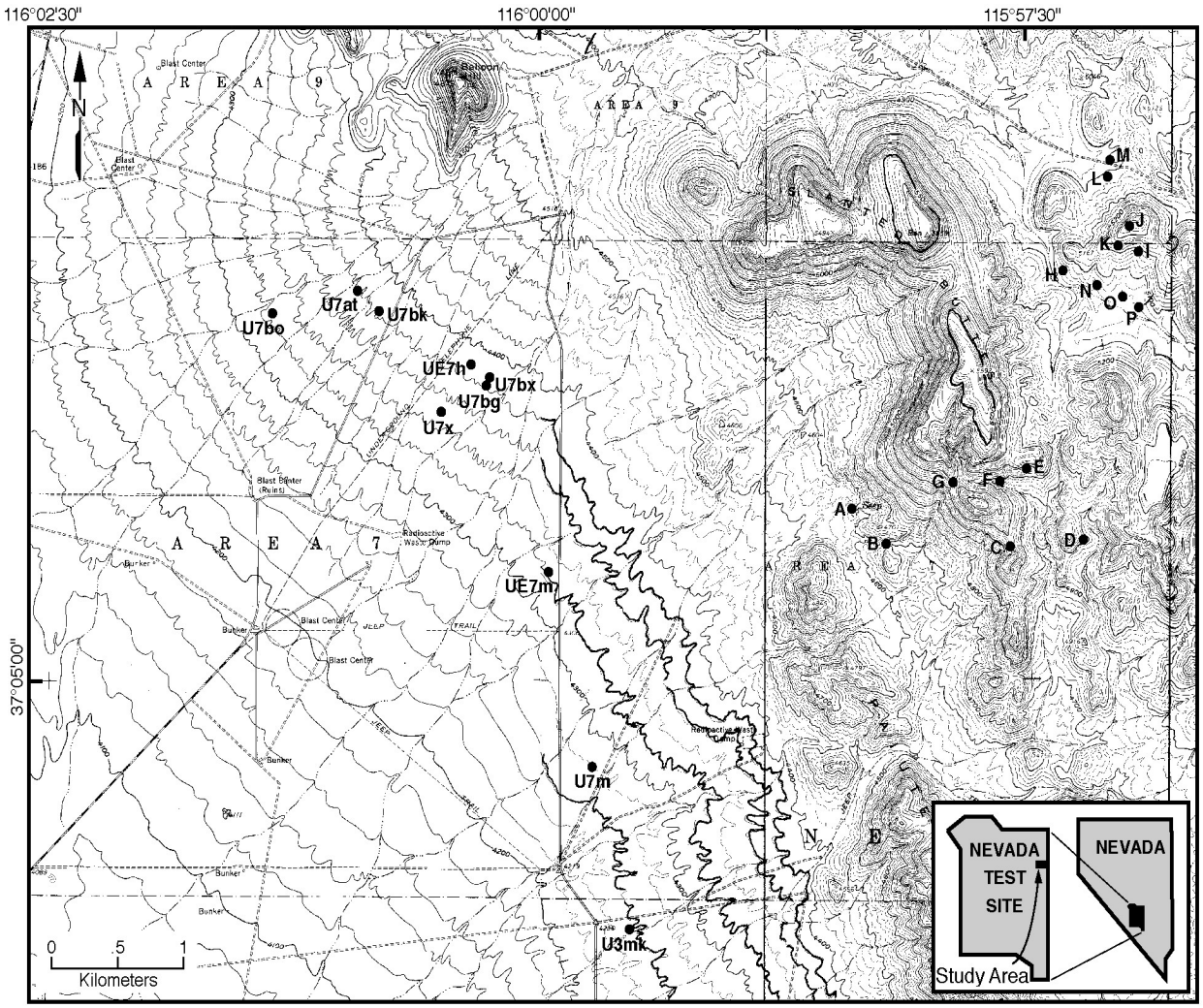

NOTE: Sampling sections, labeled with single letters, and drill holes, which all start with U, are indicated on the right and left sides of the figure, respectively. The stratigraphic units of the drill holes are given in Table 11.4-2.

Source: Simmons 2002 [157578] SN-LANL-SCI-215-V1, p. 6.

Figure 11.4-1. Location Map of the Paiute Ridge Basaltic Intrusion Complex in the Nevada Test Site

NOTE: These veins are within 8 ft (2.4 m) from the basaltic intrusion contact adjacent to the Papoose Lake Sill in the northern part of Paiute Ridge. The vein zone is about 25 ft (7.6 m) wide.

Source: Simmons 2002 [157578]; SN-LANL-SCI-215-V1, p.44, Figure 16B.

Figure 11.4-2. Anastomosing Opal Veins Adjacent to Papoose Lake Sill

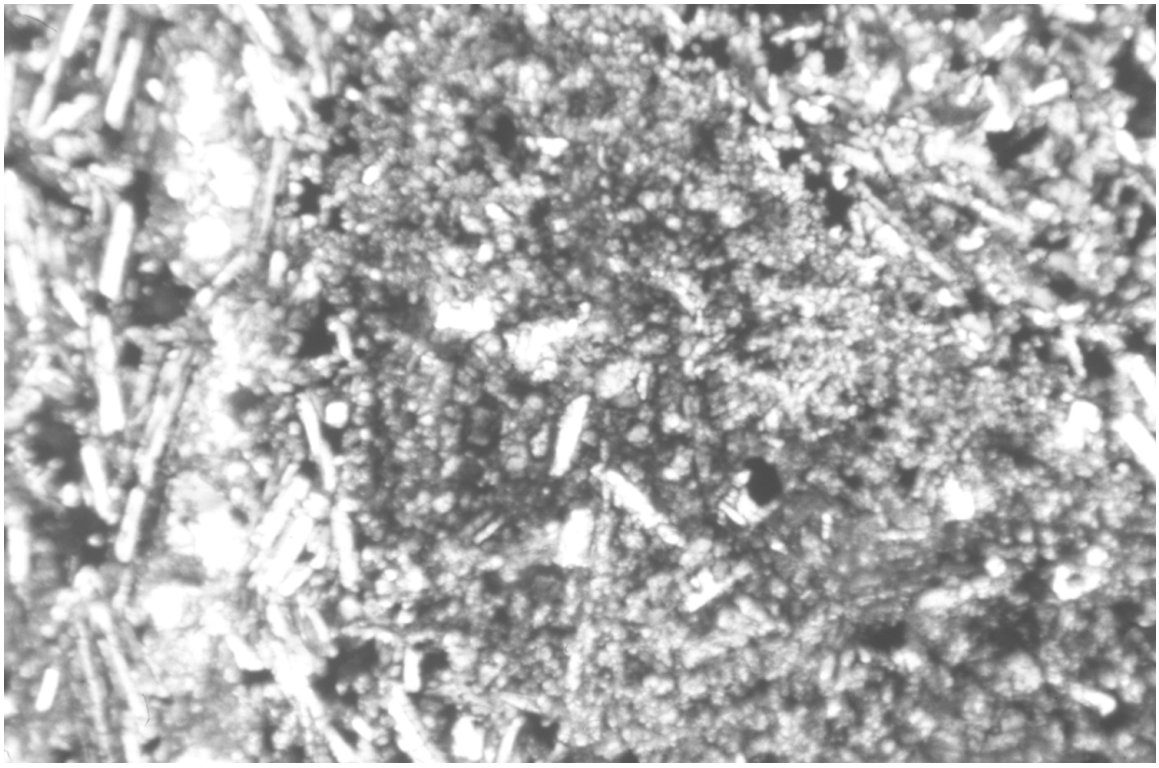

NOTE: Calcite veins along fractures and cavities and epidote grains in cavities are present in the photomicrograph of basalt (LANL# 3547) (view is 170 x 255 μm).

Source: Simmons 2002 [157578], SN-LANL-SCI-215-V1, p. 130.

Figure 11.4-3. Photomicrograph of Basalt from the Contact Zone of the Papoose Lake Sill in the Northern Part of Paiute Ridge

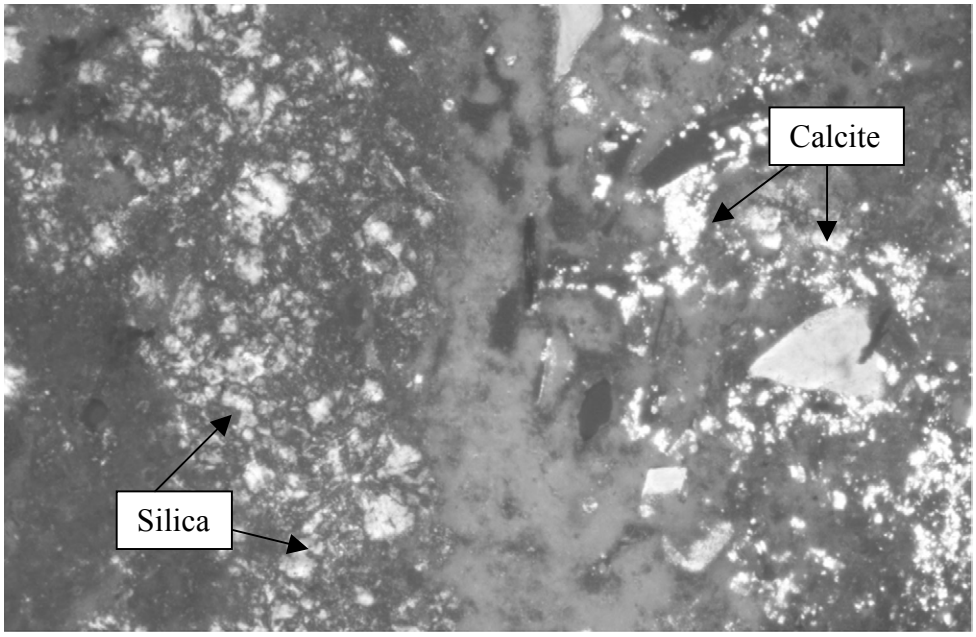

NOTE: This sample (LANL# 3557) was collected 43 ft (13.1 m) from the Papoose Lake Sill contact. Brighter patches of silica (left) and calcite (right) separated by opaque material replace the vitric matrix (view is 70 x 110 μm).

Source: Simmons 2002 [157578]; SN-LANL-SCI-215-V1, p. 131.

Figure 11.4-4. Photomicrograph of Altered Rainier Mesa Tuff

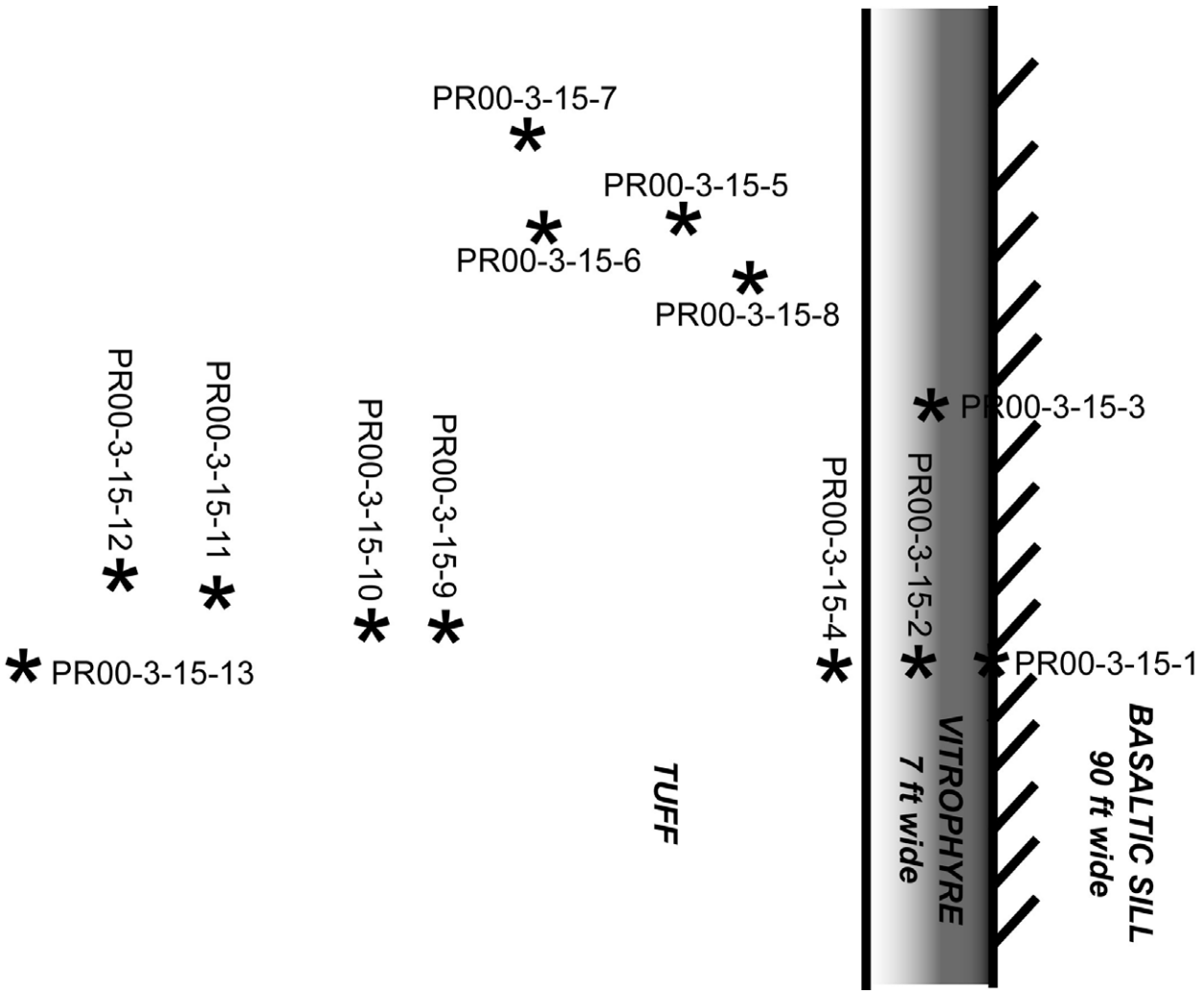

NOTE: Map not to scale; compiled from field notes; see Table 11.4-1 for sample descriptions and measured distances from sill margin.

Source: Simmons 2002 [157578], SN-LBNL-SCI-108-V2, p. 23.

Figure 11.4-5. Schematic Map of Location H, Papoose Lake Basaltic Sill, Paiute Ridge, Nevada Test Site

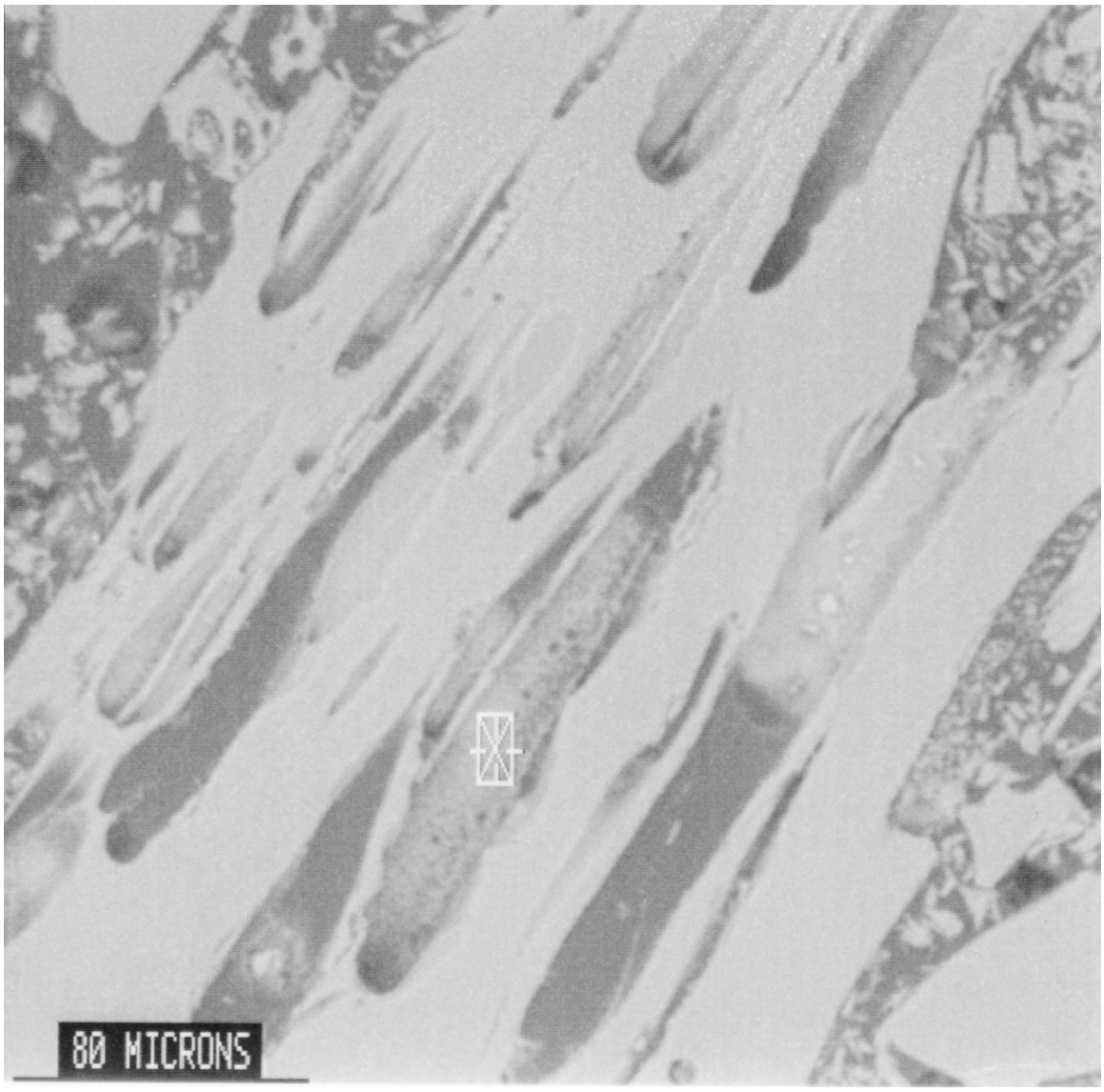

NOTE: This sample of nonwelded Rainier Mesa Tuff (LANL# 3559) was collected 200 ft (61 m) from the basaltic sill contact. It is apparent that the vesicles are devoid of secondary minerals from devitrification after deposition or from the hydrothermal process related to the basaltic intrusion.

Source: Simmons 2002 [157578]; SN-LANL-SCI-215-V1, p. 101.

Figure 11.4-6. Scanning Electron Microscope Image of Vesicles in Nonwelded Rainier Mesa Tuff

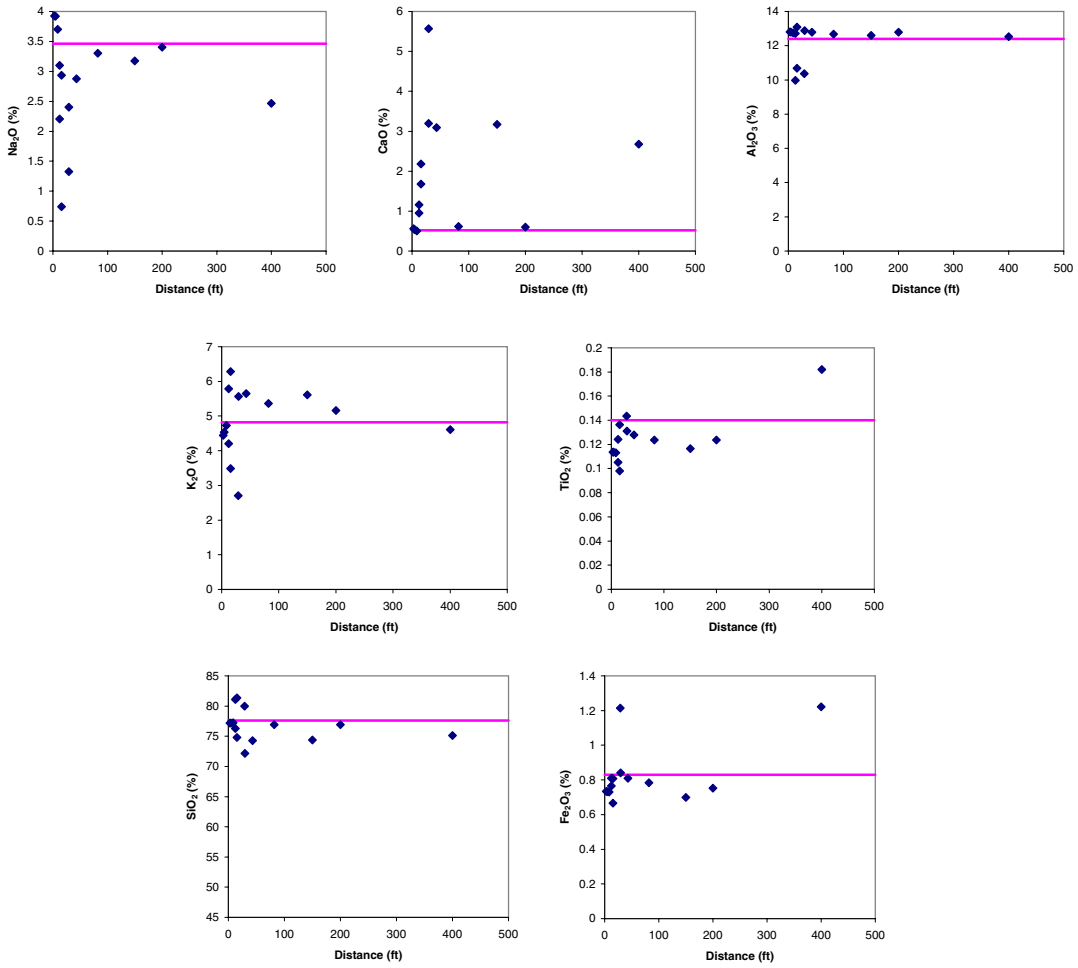

NOTE: These variation diagrams use data in feet for distance and wt% for Na_2O, K_2O, Al_2O_3, CaO, SiO_2, TiO_2, and Fe_2O_3 of tuff samples from the northern part of Paiute Ridge. Major-element contents are calculated to 100% volatile free. Total iron reported as Fe_2O_3. Line indicates average composition of Rainier Mesa rhyolitic tuff reported by Broxton et al. (1989 [100024], Table 3).

Source: Simmons 2002 [157578]; SN-LANL-SCI-215-V1, pp. 63, 69–76.

Figure 11.4-7. Variation Diagrams of Distance Versus Na_2O, K_2O, Al_2O_3, CaO, SiO_2, TiO_2, and Fe_2O_3

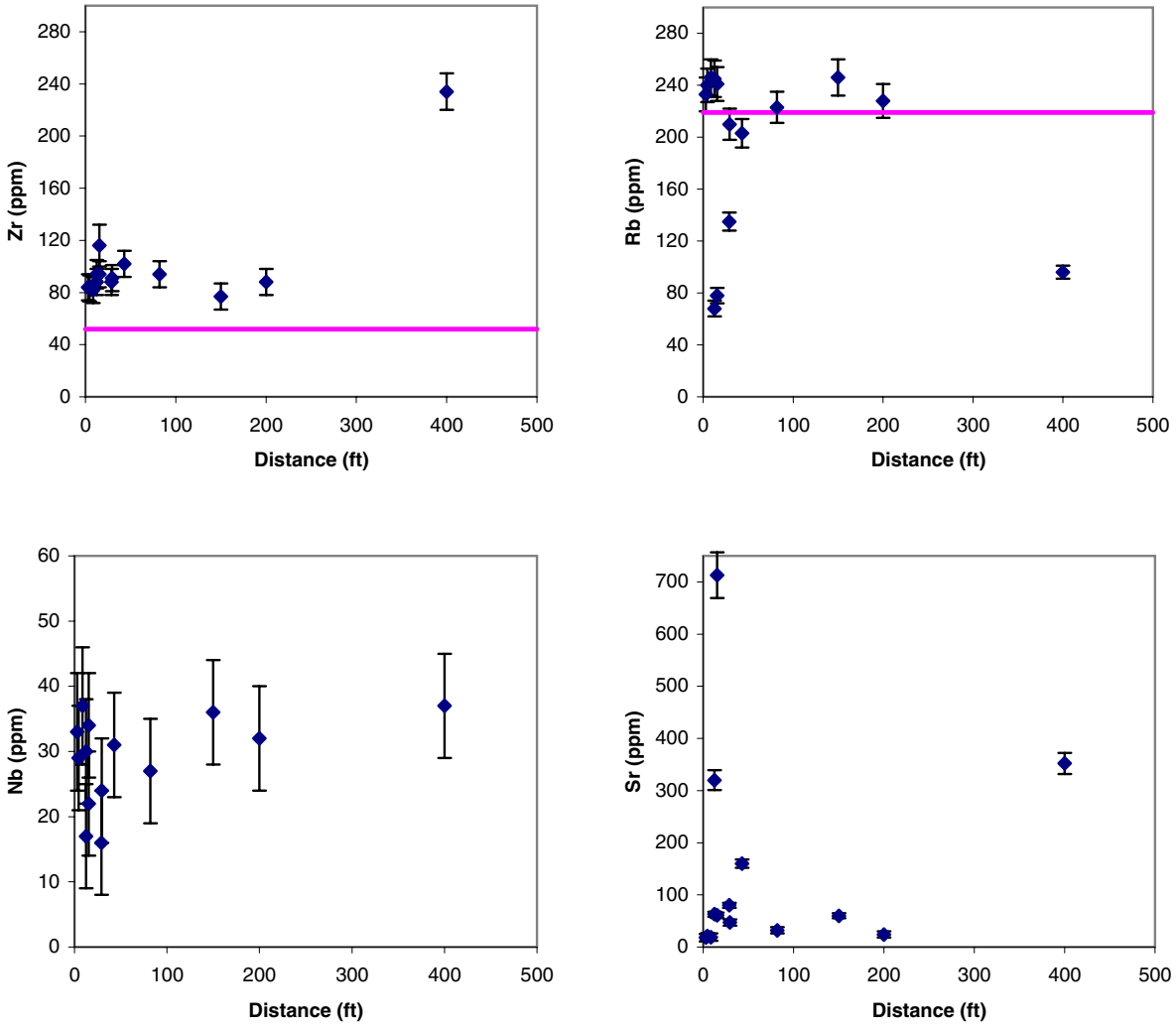

NOTE: These variation diagrams use data in feet for distance versus ppm for Zr, Rb, Nb, and Sr of tuff samples from the northern part of Paiute Ridge. Line indicates average composition of Rainier Mesa rhyolitic tuff reported by Broxton et al. (1989 [100024], Table 3).

Source: Simmons 2002 [157578]; SN-LANL-SCI-215-V1, pp. 63, 69–76.

Figure 11.4-8. Variation Diagrams of Distance Versus Zr, Rb, Nb, and Sr

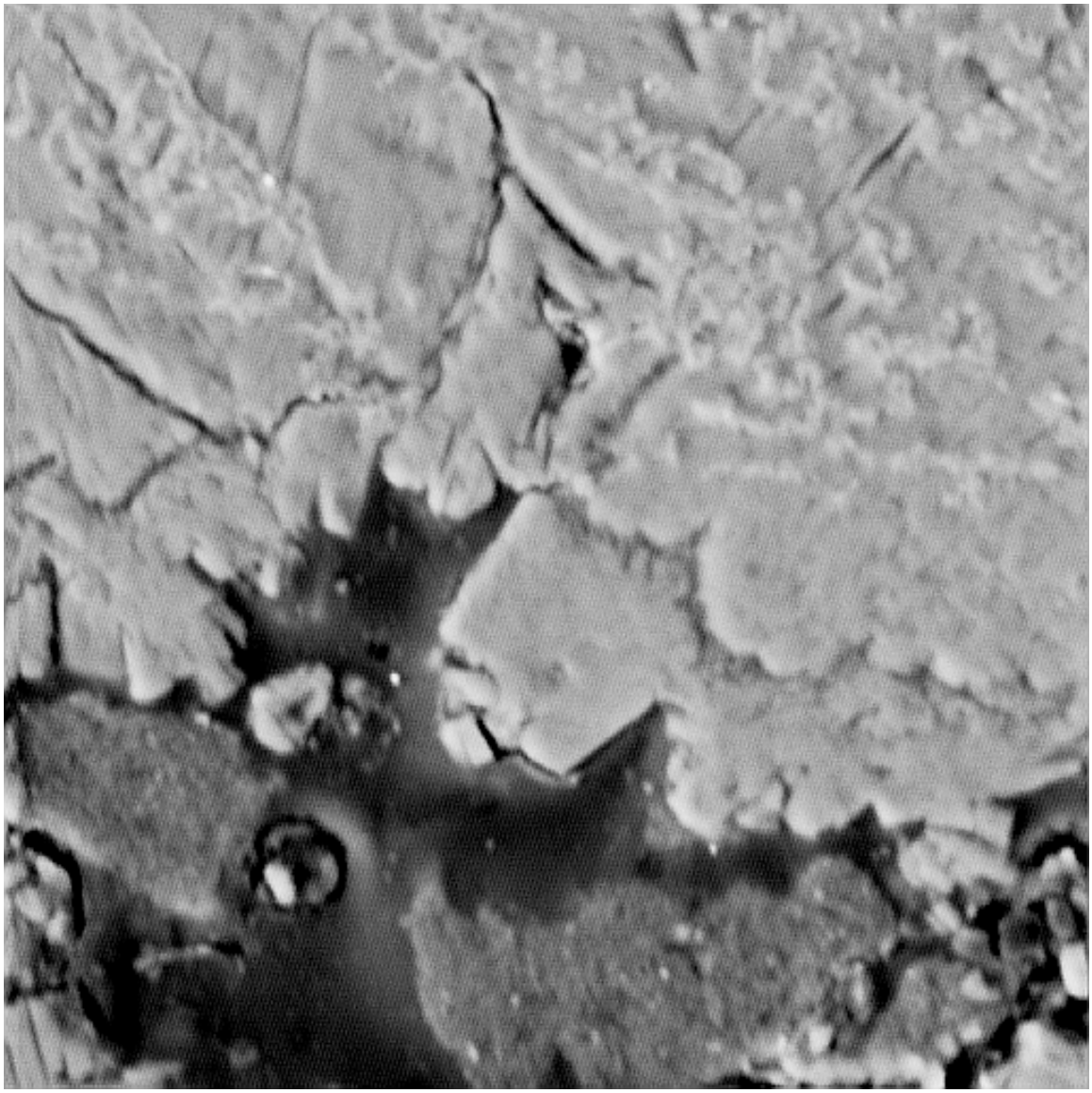

NOTE: 500 μm scale

Source: Simmons 2002 [157578]; SN-LANL-SCI-215-V1, p. 128.

Figure 11.4-9a. Tabular Crystal of Clinoptilolite Overgrowth on a Second Layer of Clinoptilolite with Scalloped or Serrated Edges (LANL# 3552)

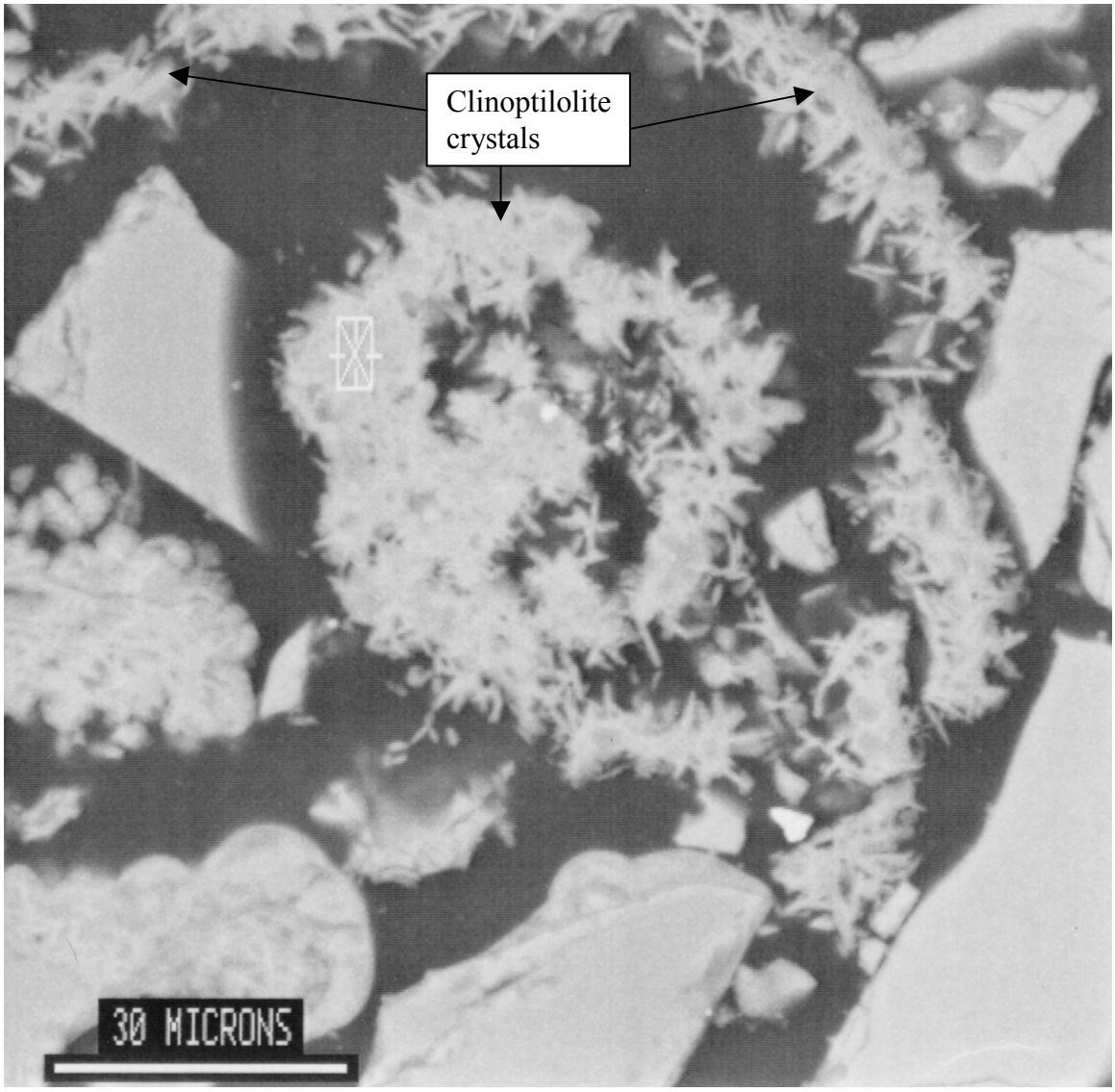

NOTE: This sample of Rainier Mesa Tuff (LANL# 3550) was collected 8.5 ft (2.6 m) from the Papoose Lake Sill contact in the northern part of Paiute Ridge. It is apparent that the cavity is partially filled by clinoptilolite.

Source: Simmons 2002 [157578]; SN-LANL-SCI-215-V1, p. 100.

Figure 11.4-9b. Scanning Electron Microscope Image of Clinoptilolite Crystal Aggregates in a Cavity of Rainier Mesa Tuff

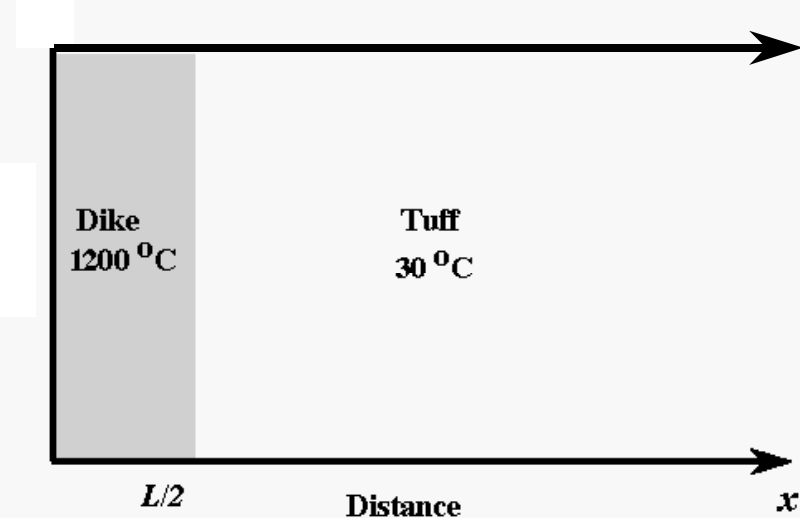

NOTE: This diagram of the half-space computational domain indicates the initial temperature of the intrusion of thickness *L* and tuff country rock for a one-dimensional simulation perpendicular to the intrusion.

Source: Simmons 2002 [157578], SN-LBNL-SCI-108-V2, p. 22.

Figure 11.4-10. Schematic Diagram of the Half-space Computational Domain

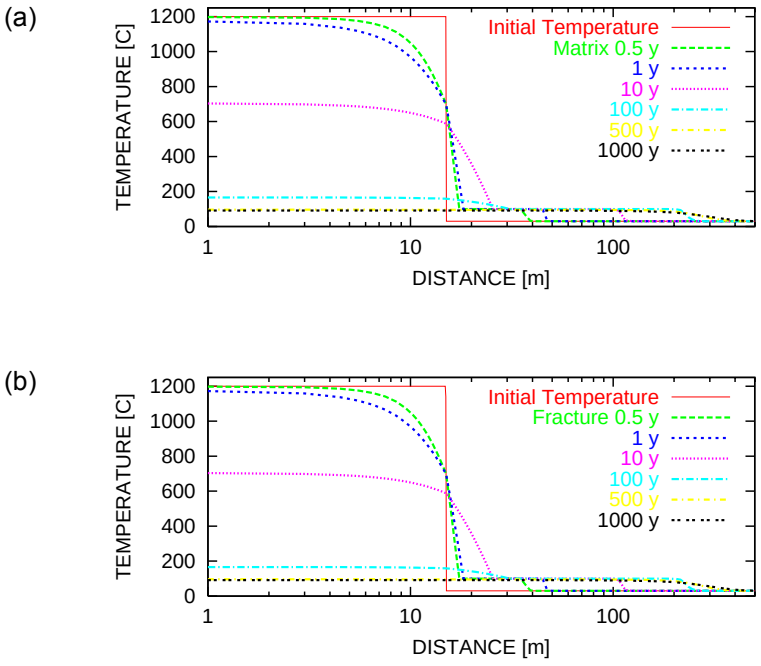

NOTE: $\sigma_{fm} = 10^2$

Source: Simmons 2002 [157578]; SN-LANL-SCI-215-V1, p. 112.

Figure 11.4-11. Matrix (a) and Fracture (b) Temperature Profiles as a Function of Distance at the Indicated Times for the Dual-Continuum Model with Strong Fracture-Matrix Coupling

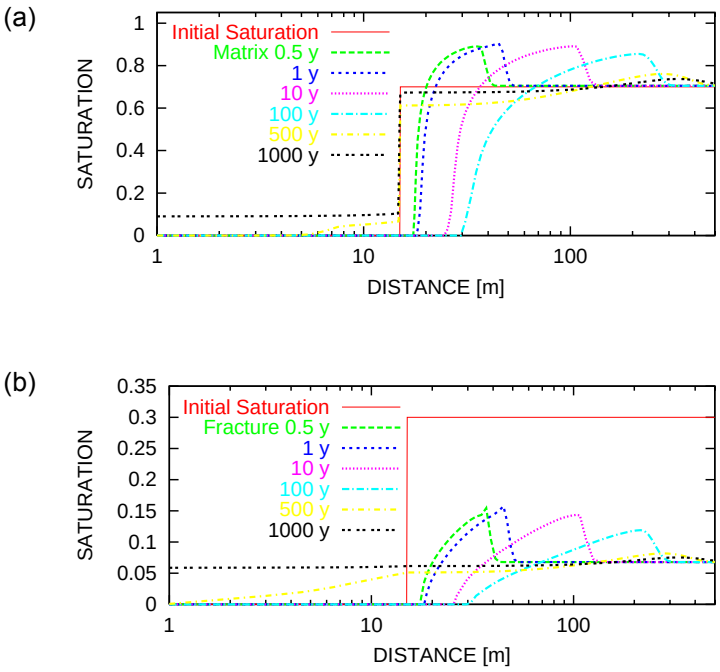

NOTE: $\sigma_{fm} = 10^2$

Source: Simmons 2002 [157578]; SN-LANL-SCI-215-V1, p. 112.

Figure 11.4-12. Matrix (a) and Fracture (b) Saturation Profiles as a Function of Distance at the Indicated Times for the Dual-Continuum Model with Strong Fracture-Matrix Coupling

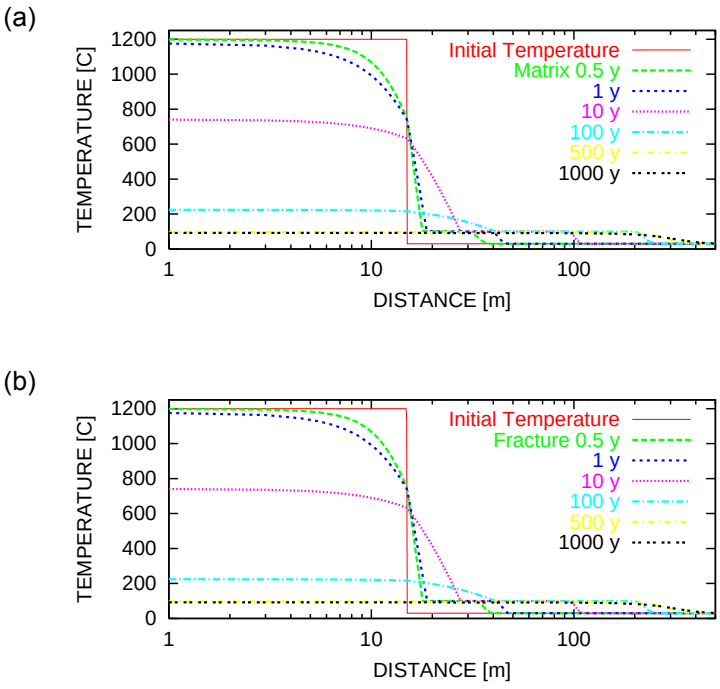

NOTE: $\sigma_{fm} = 10^{-2}$

Source: Simmons 2002 [157578]; SN-LANL-SCI-215-V1, p. 111.

Figure 11.4-13. Matrix (a) and Fracture (b) Temperature Profiles as a Function of Distance at the Indicated Times for the Dual-Continuum Model with Moderate Fracture-Matrix Coupling

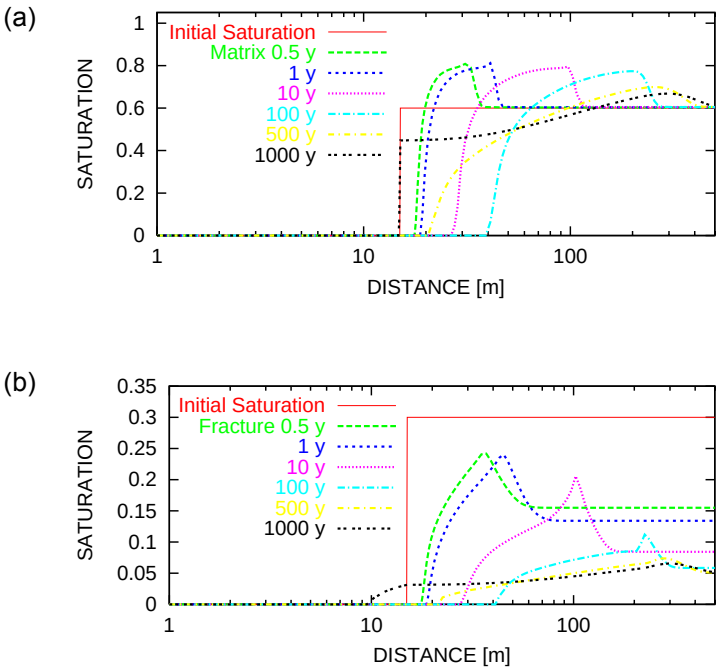

NOTE: $\sigma_{fm} = 10^{-2}$

Source: Simmons 2002 [157578]; SN-LANL-SCI-215-V1, p. 111.

Figure 11.4-14. Matrix (a) and Fracture (b) Saturation Profiles as a Function of Distance at the Indicated Times for the Dual-Continuum Model with Moderate Fracture-Matrix Coupling

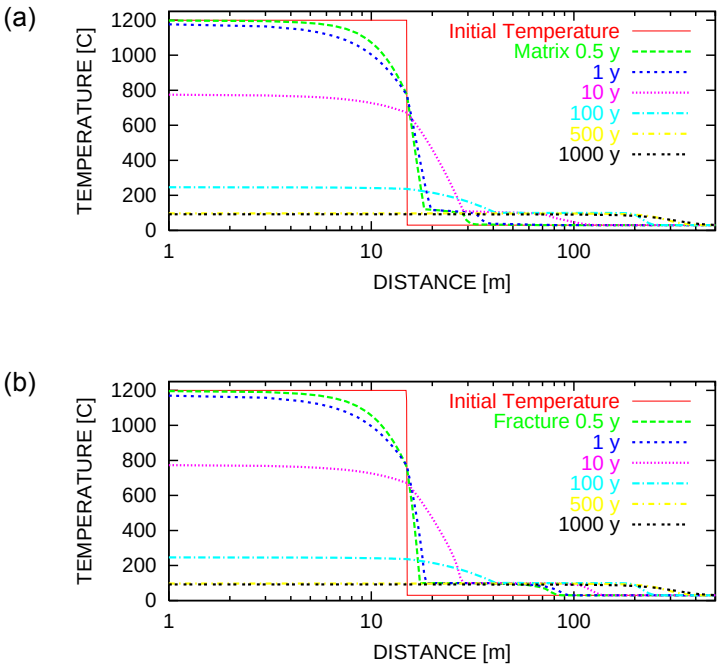

NOTE: $\sigma_{fm} = 10^{-4}$

Source: Simmons 2002 [157578]; SN-LANL-SCI-215-V1, p. 110.

Figure 11.4-15. Matrix (a) and Fracture (b) Temperature Profiles as a Function of Distance at the Indicated Times for the Dual-Continuum Model with Weak Fracture-Matrix Coupling

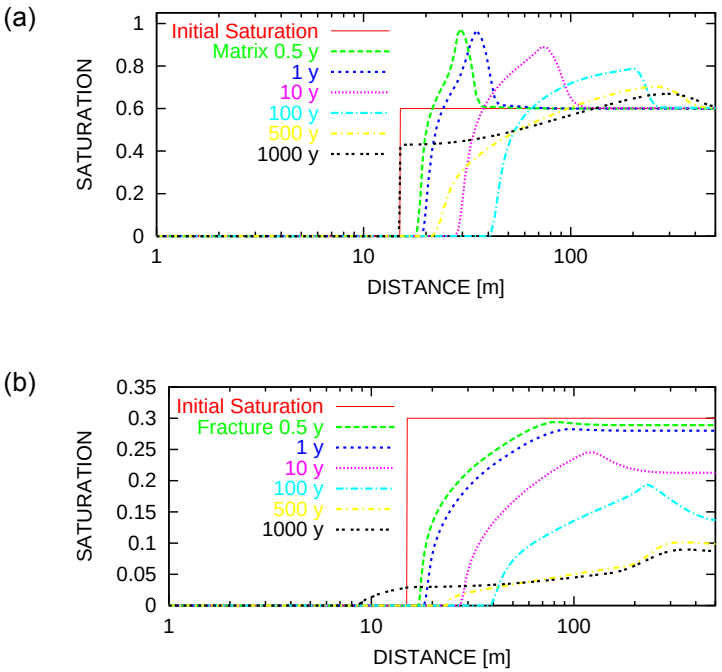

NOTE: $\sigma_{fm} = 10^{-4}$

Source: Simmons 2002 [157578]; SN-LANL-SCI-215-V1, p. 110.

Figure 11.4-16. Matrix (a) and Fracture (b) Saturation Profiles as a Function of Distance at the Indicated Times for the Dual-Continuum Model with Weak Fracture-Matrix Coupling

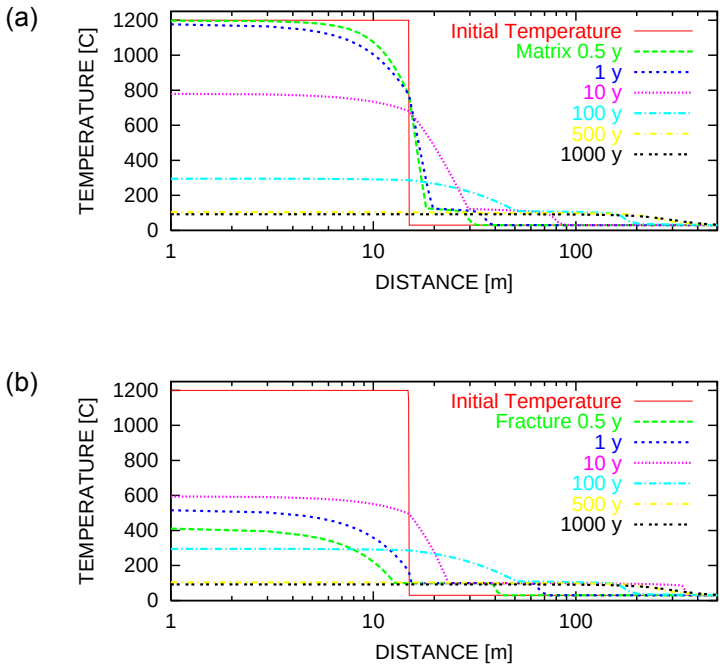

NOTE: $\sigma_{fm} = 10^{-6}$

Source: Simmons 2002 [157578]; SN-LANL-SCI-215-V1, p. 107.

Figure 11.4-17. Matrix (a) and Fracture (b) Temperature Profiles as a Function of Distance at the Indicated Times for the Dual-Continuum Model with Very Weak Fracture-Matrix Coupling

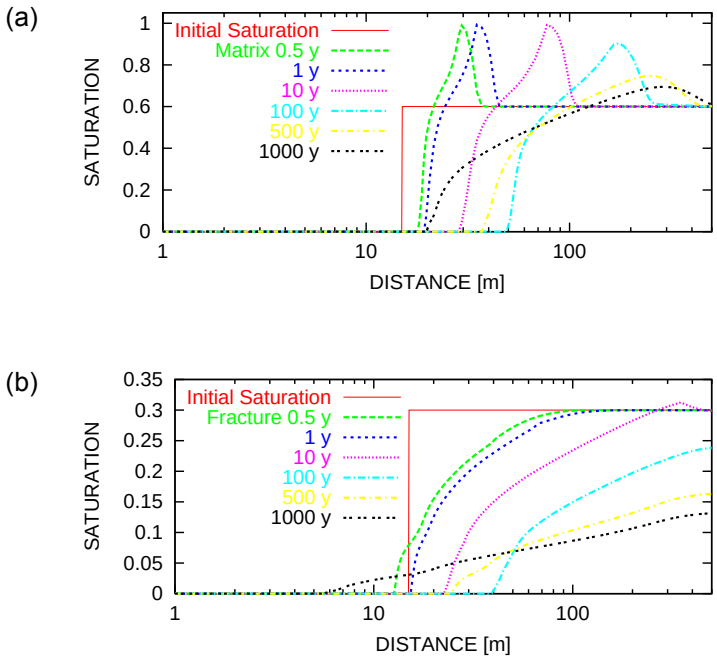

NOTE: $\sigma_{fm} = 10^{-6}$

Source: Simmons 2002 [157578]; SN-LANL-SCI-215-V1, p. 107.

Figure 11.4-18. Matrix (a) and Fracture (b) Saturation Profiles as a Function of Distance at the Indicated Times for the Dual-Continuum Model with Very Weak Fracture-Matrix Coupling

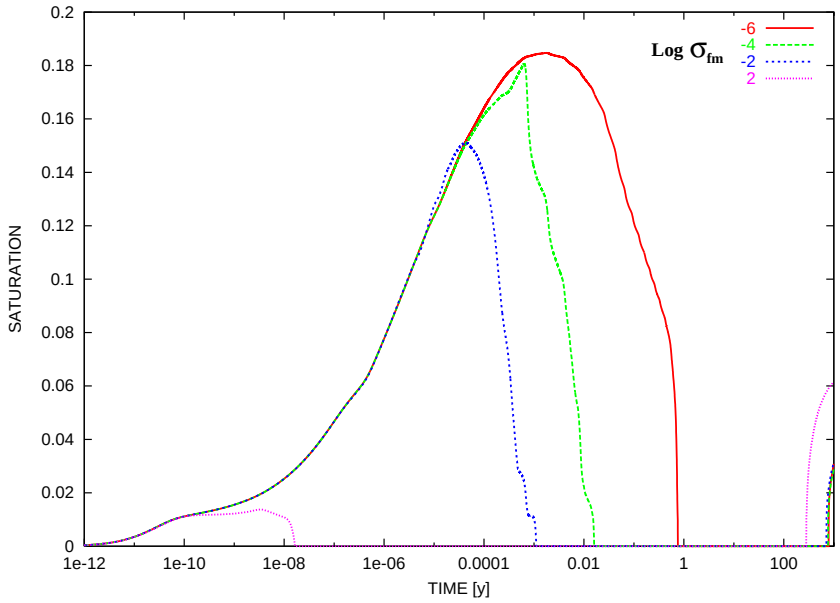

Source: Simmons 2002 [157578]; SN-LANL-SCI-215-V1, p. 118.

Figure 11.4-19. Fracture Saturation as a Function of Time at the Boundary between the Intrusion and Country Rock for Different Fracture-Matrix Coupling Strengths

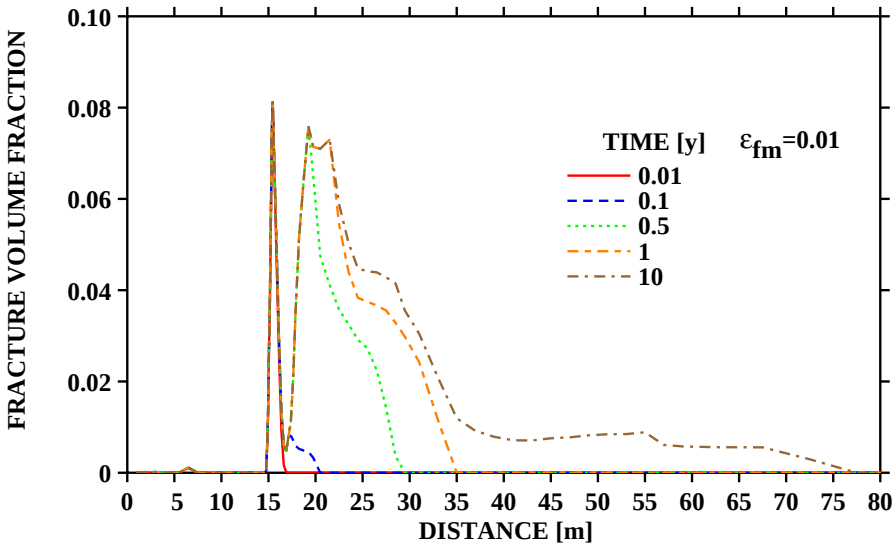

NOTE: $\sigma_{fm} = 10^{-2}$

Source: Simmons 2002 [157578]; SN-LANL-SCI-215-V1, p. 117.

Figure 11.4-20. Fracture Volume Fraction of Amorphous Silica Precipitation as a Function of Distance for Various Times with Moderate Fracture-Matrix Coupling

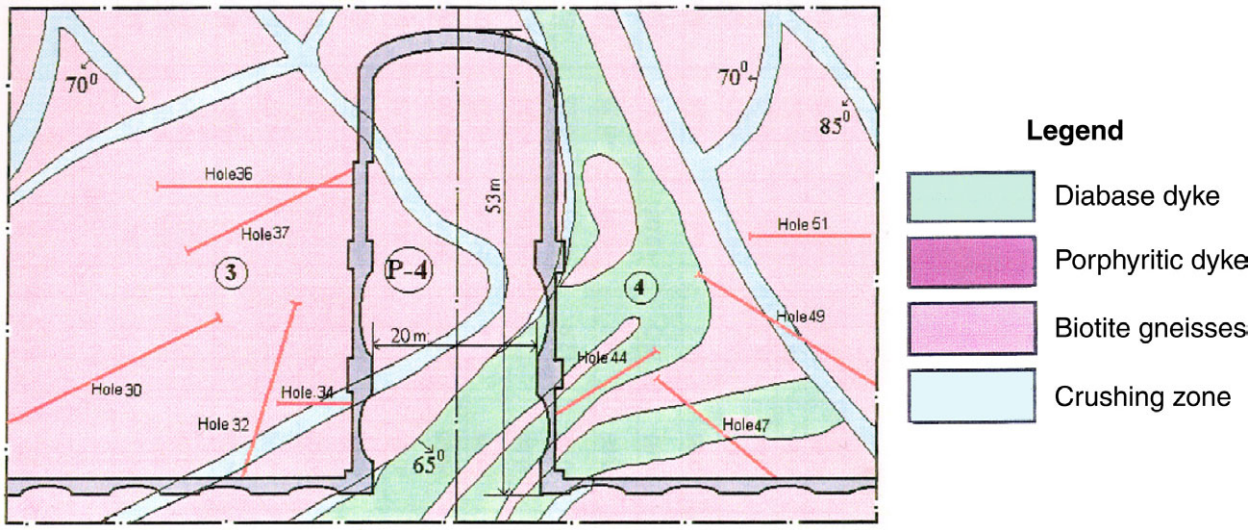

Source: Gupalo et al. 1999 [157470], Figure 2.16.

Figure 11.6-1. Schematic of the Underground Workings at Facility P-4 at K-26, Siberia, in Cross Section

Table 11.2-1. THC Processes in Geothermal Systems and Their Applicability to Yucca Mountain

THC process	Geothermal system component	Geothermal examples	Applicability to Yucca Mountain	Potential impact to repository performance
Advective heating	Heat transfer within convecting geothermal reservoir: develop near-isothermal vertical thermal profiles	Nearly ubiquitous: examples include Yellowstone (Wyoming), Salton Sea (California), Wairakei (New Zealand)	Would only occur very locally in high-temperature (>100°C) design (within heat pipe)	Could result in localized zone of enhanced water-rock interaction and chemical transport
Conductive heating	Heat transfer within low-permeability and unsaturated portions of geothermal systems	Nearly ubiquitous: examples include hot dry rock resources, upper portions of San Vicente (El Salvador), Amatitlan (Guatemala)	Main mechanism of heat transfer at Yucca Mountain (unsaturated conditions)	Heating leads to more rapid chemical reactions. Thermal expansion of rocks could alter fracture permeability
Fracture-dominated fluid flow	Fluid flow in fractured reservoir rocks with low matrix permeability	Silangkitang (Indonesia), Dixie Valley (Nevada), Los Azufres (Mexico)	Main mechanism for fluid flow within welded ash flow tuffs at Yucca Mountain	Could permit rapid movement of fluids along fast flow paths (evidenced by bomb-pulse tritium)
Chemical transport	Advective and diffusive transport of dissolved constituents in fluids. Tracer tests used to determine fluid flow paths and rates.	Ubiquitous. Well-documented tracer tests for many geothermal systems, including The Geysers (California), Dixie Valley (Nevada), Coso (California), Awibengkok (Indonesia)	Advective transport within fractures, and advective and diffusive transport between fractures and matrix	Potential mechanism for movement of radioactive waste materials from repository
Boiling	Development of two-phase and steam zones in geothermal systems due to depressurization and heating	Occurs in most high-temperature liquid-dominated geothermal systems with production, e.g., Awibengkok (Indonesia), Coso (California), and occurs naturally in steam-dominated systems, e.g., The Geysers (California), Karaha-Telaga-Bodas (Indonesia).	Would only occur in high-temperature design near drift walls for limited time	Would create dryout zone around drift for high-temperature design, and could lead to development of heat pipe. Fracture permeability could be modified by precipitation caused by boiling.
Dryout	Occurs during transformation from liquid-dominated to steam-dominated geothermal system	Documented for The Geysers (California), Karaha-Telaga-Bodas (Indonesia)	Would only occur in high-temperature operating mode near drift walls for limited time	Dryout zone would prohibit seepage into drift for early stages of high-temperature operating mode. Would lead to precipitation of dissolved solids in area that could be redissolved as cooling and rewetting occurred.

Table 11.2-1. THC Processes in Geothermal Systems and Their Applicability to Yucca Mountain (Cont.)

THC process	Geothermal system component	Geothermal examples	Applicability to Yucca Mountain	Potential impact to repository performance
Condensation	Occurs during transformation from liquid-dominated to steam-dominated geothermal system, and in upper levels of geothermal systems where rising vapor contacts cooler meteoric waters	Observed in many geothermal systems where rising gas and steam is cooled and mixes with near-surface meteoric fluids, resulting in development of bicarbonate and acid-sulfate springs. Documented for Yellowstone (Wyoming), Wairakei (New Zealand), Waiotapu (New Zealand)	Would mainly occur in high-temperature design above drift areas for limited time; can also occur in low-temperature design, but at a reduced level	Condensation above drift could lead to recycling of fluids, thus resulting in a higher volume of fluids passing through near-field area. This could also result in localized zones of near-saturation conditions and increase water-rock interaction. Condensation could also take place in the drift, resulting in dripping on waste packages.
Mineral dissolution	Occurs typically in condensation zones, or where acid fluids are present	Difficult to document, but observed at The Geysers (California) and Karaha-Telaga-Bodas (Indonesia)	Would occur primarily where condensation occurs	Mineral dissolution associated with condensation zone could lead to local increases in porosity and permeability.
Mineral alteration and precipitation	Occurs in numerous portions of geothermal systems, especially in zones with abundant fluid flow that have undergone heating	Ubiquitous. Degree and type of mineralization depends on rock and fluid compositions, water-rock ratios, and temperature. Boiling can result in significant mineralization. Alteration mineralogy well-characterized at Wairakei (New Zealand), Salton Sea (California), Silangkitang (Indonesia), Krafla (Iceland)	Alteration and precipitation likely to be confined to near-field environment, where boiling and increased fluid flux occur. These effects may be negligible for low-temperature design.	Alteration could lead to changed sorption properties (zeolite and clay formation). Precipitation of silica minerals and calcite in fractures could locally reduce permeability, or lead to focussed flow within a few larger fractures.

Source: Simmons 2002 [157578], SN-LBNL-SCI-108-V2, pp. 14–15.

Table 11.2-2. Estimated Process Time Scales for Potential Repository and Geothermal Reservoirs

Process	Repository Time Scale (yr)	Geothermal Reservoir Time Scale (yr)
Duration of heating (magma or nuclear waste)	1000s	10,000s
Dryout	100s to 2,000	10,000s
Fast-path flow from ground surface to repository or geothermal system	10's	10s
Water recycling in "heat pipe" (cyclic liquid-vapor counterflow)	<<1	1s to 10s
Intermittent flow events	<<<1	<<<1
Physical changes due to dissolution and precipitation	<1 to 1,000s	<1 to 10,000s
Mineralogic changes	<1 to 1,000s	<1 to 10,000s
Climate change	10,000s	10,000s

Source: Simmons 2002 [157578], SN-LBNL-SCI-108-V2, p. 15.

Table 11.3-1. Comparison of Yellowstone and Yucca Mountain Systems

	Potential Yucca Mountain Repository	Yellowstone Geothermal System
Boiling zone temperatures	~95°C	92–270°C
SiO_2 in fluids	<200 ppm	200–700 ppm
Duration of boiling conditions	<1,200 yr (high T) 0 years (low T)	≥15,000 yr
Fluid-flow conditions	Unsaturated	Saturated
Estimated fluid flux	10^{-9} to 10^{-10} m/s	4.8×10^{-5} m/s
Estimated heat flux	16.7 W/m^2 (in near-field area around waste packages)	46 W/m^2 (Firehole River Drainage Basin) 1.7 W/m^2 (Yellowstone Caldera)

Source: Simmons 2002 [157578], SN-LBNL-SCI-108-V2, p. 15.

Table 11.4-1. Samples, Lithologic Types and Descriptions, and Measured and Estimated Distances of Tuff Samples from a Basaltic Intrusion

Sample Number	Distance to Contact (ft) [m]	Lithology	Sample Description
Adjacent and west of Papoose Lake Sill			
PR00-3-15-1 (LANL# 3547)	Contact	Basalt	Purplish gray, fine grained, platy, and altered
PR00-3-15-2 (LANL# 3548)	4.5 [1.4]	Vitrophyre	Fused tuff, glassy, foliated, and 7 ft (2.1 m) wide
PR00-3-15-3 (LANL# 3549)	3.0 [0.9]	Vitrophyre	Fused tuff, glassy, foliated, and contains silica veinlets
PR00-3-15-4 (LANL# 3550)	8.5 [2.6]	Baked tuff	Hardened, pinkish orange, and devitrified
PR00-3-15-5 (LANL# 3551)	12.5 [3.8]	Tuff	Partially welded, cavernous, and pinkish orange
PR00-3-15-6 (LANL# 3552)	15.5 [4.7]	Opal vein	3” wide, NS trend parallel to contact, and reddish
PR00-3-15-7 (LANL# 3553)	15.5 [4.7]	Tuff	Within opal vein zone, pinkish, contains few opal nodules
PR00-3-15-8 (LANL# 3554)	12.5 [3.8]	Opal vein	N20E trend, crystalline, variable thickness, cuts nonwelded tuff
PR00-3-15-9 (LANL# 3555)	29 [8.8]	Tuff	Altered, silicified, pinkish and fine grained
PR00-3-15-10 (LANL# 3556)	29.4 [9.0]	Tuff	Nonwelded, collected within silicified zone, pinkish
PR00-3-15-11 (LANL# 3557)	43 [13.1]	Tuff	Nonwelded, cut by few opal veins, pinkish
PR00-3-15-12 (LANL# 3558)	82 [25]	Tuff	Nonwelded, pinkish, pumice-rich
PR00-3-15-13 (LANL# 3559)	200 [61]	Tuff	Nonwelded, pinkish, friable, pumice-rich, and cavernous
Above and east of Papoose Lake Sill			
PR00-3-14-2 (LANL# 3538)	~150 [46]	Tuff	Pale pink tuff cut by opal veins, dark red halo, pumice clasts
PR00-3-14-3 (LANL# 3539)	~150 [46]	Tuff	Same as LANL# 3538 with thicker veins and alteration
PR00-3-14-4 (LANL# 3540)	~150 [46]	Tuff	Same tuff with pumice clasts and nodule
PR00-3-14-5 (LANL# 3541)	~150 [46]	Tuff	Same tuff with corroded pumice clasts and devitrified
PR00-3-14-6 (LANL# 3542)	~150 [46]	Opal vein	1 cm wide in a similar tuff, contains fresh pumice clasts
PR00-3-14-7 (LANL# 3543)	~150 [46]	Tuff	Same tuff with dense pumice
PR00-3-14-8 (LANL# 3544)	~150 [46]	Tuff	Same tuff with thick opal veins
PR00-3-14-9 (LANL#3545)	>150 [46]	Tuff	Tuff east of opal vein zone, gray, no veins, pumice less distinct
PR00-3-15-14 (LANL# 3560)	~400 [122]	Tuff	Nonwelded, matrix silicified, few opal veins, reddish brown
PR00-3-15-15 (LANL# 3561)	~400 [122]	Tuff	Nonwelded with nodules, pumice-rich, grayish, cavernous
PR00-3-15-16 (LANL# 3562)	~500 [152]	Tuff	Dark reddish orange, nonwelded, friable, massive

Table 11.4-1. Samples, Lithologic Types and Descriptions, and Measured and Estimated Distances of Tuff Samples from a Basaltic Intrusion (Cont.)

Above and east of Papoose Lake Sill (continued)			
PR00-3-15-17 (LANL# 3563)	720 [220], 60.0 [183] west of dike	Tuff	Moderately welded with opal nodules, grayish
PR00-3-15-18 (LANL# 3564)	695 [212], 38.5 [11.7] west of dike	Tuff	Moderately welded with opal nodules, orangish
PR00-3-15-19 (LANL# 3565)	660 [201], 3.0 [0.9] west of dike	Fused tuff	Fused with fiamme and nodules, pinkish brown
Beneath sill (Figure 11.4-1, Section B)			
PR00-3-16-1 (LANL# 3570)	Top part of sill	Basalt	25 ft (7.6 m) thick, sparsely porphyritic, amygdules
PR00-3-16-2 (LANL# 3571)	Contact	Basalt-tuff	Platy basalt, fused granular tuff, no vitrophyre
PR00-3-16-3 (LANL# 3572)	1 [0.3]	Tuff	Pinkish gray, medium grained, partially fused
PR00-3-16-4 (LANL# 3573)	4.4 [1.3]	Tuff	Nonwelded, bedded, coarse, and crystal-rich
PR00-3-16-5 (LANL# 3574)	4.4 [1.3]	Tuff	Fine grained, pinkish gray, tilted 20°S
PR00-3-16-6 (LANL# 3575)	15 [4.6]	Tuff	Moderately welded, light gray, contains lithics
PR00-3-16-7 (LANL# 3576)	21 [6.4]	Opal vein	2 ft (0.6 m) wide, fractured, orange and white veins
PR00-3-16-8 (LANL# 3577)	30.8 [9.4]	Opal vein	Host tuff fractured, same as LANL# 3576
PR00-3-16-9 (LANL# 3578)	34.2 [10.4]	Tuff	Nonwelded, light gray, and contains lithics
PR00-3-16-10 (LANL# 3579)	35 [10.7]	Tuff	Crystal-rich, coarse, pumice-rich, matrix-free
PR00-3-16-11 (LANL# 3580)	16 [4.9]	Opal	0.4-1.5 ft (0.1 to 0.5 m) thick, N-S trend, dips 65°E, (98 ft) (30 m) long
PR00-3-16-12 (LANL#3581)	8 [2.4]	Tuff	Host tuff for the (98 ft) (30 m) long opal vein

Source: Simmons 2002 [157578], SN-LANL-SCI-215-V1, pp. 13–27, 90–94.

Table 11.4-2. Subsurface Stratigraphic Information from Drill Holes along the Eastern Part of Yucca Flats Adjacent to Paiute Ridge

Stratigraphic Units (upper one third of section)		Drill Holes: Interval Thickness, *I* (m), and Depth to the Tops of Formations, *D* (m)																			
		U 3mk		U 7at		U 7bg		U 7bh		U 7bk		U 7bm		U 7bo		UE7h		UE 7m		U 7x	
		I	*D*	*I*	*D*	*I*	*D*	*I*	*D*	*I*	*D*	*I*	*D*	*I*	*D*	*I*	*D*	*I*	*D*	*I*	*D*
Qal (Qta)		65.5		82.3		48.8		54.9		41.1		92.4		138.7		51.8		61		67.1	
Tma	Ammonia Tanks	none	None	none	none	29	48.8	21.3	54.9	none	none	none	none	none	none	18.3	51.8	none	none	none	none
Tmab	Bedded Ammonia Tanks	none	None	none	none		70.1		68.6	none	none	none	none	none	none		62.5	none	none	none	none
Tmr	Rainier Mesa	56.4	65.5	21.3	82.3	67.1	77.7	48.8	76.2	54.9	41.4	95.1	92.4	47.2	138.7	82.3	70.1	94.5	61	73.2	67.1
Tx (Tmrl/Ta)	Rainier Mesa/ Vitrophyre	24.4	**121.9**	35.1	**103.6**	32	**144.8**	39.6	**125**	38.1	**96**	59.4	**187.5**	39.6	**185.9**	4.6	**152.4**	39.6	**155.4**	≥73.1	**140.2**
Tpc	Tiva Canyon	nd	nd	nd	nd	nd	nd	nd	nd	nd	nd	nd	nd	nd	nd	nd	nd	nd	nd	nd	nd
Tpt	Topopah Spring	nd	nd	nd	nd	nd	nd	nd	nd	nd	nd	nd	nd	nd	nd	nd	nd	nd	nd	nd	nd
Tac	Calico Hills	nd	nd	nd	nd	nd	nd	nd	nd	nd	nd	nd	nd	nd	nd	nd	nd	nd	nd	nd	nd
Tw	Lower Wahmonie	24.4	146.3	21.3	138.7	18.3	176.8	19.8	164.6	21.3	134.1	18.3	246.9	15.2	225.6	18.3	157	21.9	195.1	nd	nd
Tc	Crater Flat	56.4	170.7	51.8	160	43.3	195.1	82.3	184.4	44.2	155.4	80.8	265.2	51.8	240.8	59.4	175.3	51.2	217	nd	nd
Tcb	Bull Frog	nd	nd	nd	nd	nd	nd	nd	nd	nd		nd	nd	nd		nd		nd	nd		
	Surface elevation (m)		1297.8		1336.6		1337.5		1338.7		1333.5		1291.7		1319.2		1338.7		1315.2		1328.9
	Drill hole depth (m)		381		460.4		396.2		396.2		376.4		472.4		609.6		780.6		587		533.4
Depth to pervasive zeolitization (m)			281.9		182.9		167.6		157		198.1		243.8		262.1		152.4		240.8		222.5

NOTE: nd means “not defined.” Values in bold-type indicate depth to Rainier Mesa Vitrophere Unit.

Source: Drellack and Thompson 1990 [156446], pp. 60, 64, 66, 68–69, 118, 122, 124, 126–127.

Table 11.4-3. Quantitative Mineral Abundances by XRD for Selected Tuff Samples Adjacent to Papoose Lake Sill in the Northern Part of Paiute Ridge

Sample	Smec-tite	Clino-ptilote	Chab-azite	Tridy-mite	Crist-obalite	Opal-CT	2ndary Quartz	K-Spar	Plagio-clase	Glass	Hem-atite	Bio-tite	Horn-blende	Augite	Cal-cite	Total
PR00-3-15-01, LANL# 3547	18.5	—	—	—	—	—	—	8.1	52.8	—	3.0	2.1	—	16.5	—	101.0
PR00-3-15-02, LANL# 3548	—	—	0.8	0.9	0.4	—	5.7	1.0	8.2	79.8	—	0.2	—	—	—	97.1
PR00-3-15-03, LANL# 3549	—	—	1.0	3.4	0.9	—	3.7	3.5	13.9	75.2	—	0.5	—	—	—	102.0
PR00-3-15-04, LANL# 3550	—	—	—	1.4	1.9	—	3.6	3.2	11.4	75.4	—	0.2	—	—	—	97.1
PR00-3-15-05, LANL# 3551	—	—	—	—	—	—	5.3	4.7	7.5	82.8	0.3	1.5	—	—	—	102.2
PR00-3-15-06, LANL# 3552	—	55.9	—	—	1.0	27.7	2.4	7.0	5.6	—	—	0.1	—	—	—	99.6
PR00-3-15-07, LANL# 3553	—	2.8	—	—	—	—	2.9	8.3	8.0	71.8	0.2	2.7	—	—	4.5	101.3
PR00-3-15-08, LANL# 3554	—	26.5	—	—	—	18.7	22.7	13.5	16.9	—	—	0.4	0.1	—	—	98.8
PR00-3-15-09, LANL# 3555	—	64.6	—	—	0.9	23.5	2.3	4.6	8.3	—	—	0.1	—	—	—	104.3
PR00-3-15-10, LANL# 3556	—	6.8	4.6	—	—	—	4.5	6.4	6.4	65.5	0.1	0.9	—	—	2.9	98.2
PR00-3-15-11, LANL# 3557	—	3.8	—	—	—	—	7.3	5.1	8.4	74.5	—	1.5	—	—	1.3	102.0
PR00-3-15-12, LANL# 3558	—	—	—	—	—	—	3.6	2.9	6.5	84.7	0.1	0.4	—	—	—	98.1
PR00-3-15-13, LANL# 3559	0.1	—	—	—	—	—	3.8	3.9	7.1	85.2	0.2	1.4	—	—	—	101.6

NOTES: Mineral abundances are in weight percent — means “not detected”

Source: Simmons 2002 [157578]; SN-LANL-SCI-215-V1, p. 59.

Table 11.4-4. Comparison of Equation of State Properties of Pure Water at 1,200ºC

p (bars)	Density (kg/m^3)		Enthalpy (kJ/kg)		Energy (kJ/kg)		Viscosity (μPa s)	
	FLOTRAN	**HGK**	**FLOTRAN**	**HGK**	**FLOTRAN**	**HGK**	**FLOTRAN**	**HGK**
1	0.14709	0.14708	5,131.03	5,150.0	4,451.18	4,470.1	40.66	40.38
5	0.7356	0.7354	5,130.4	5,149.2	4,450.7	4,469.4	40.89	40.39
10	1.4714	1.4710	5,129.7	5,148.2	4,450.1	4,468.4	41.18	40.42

NOTES: The comparison is between Haar et al. (1984 [105175]) (the HGK columns) and the equation of state used by FLOTRAN based on the International Formulation Committee of the Sixth International Conference on Properties of Steam (IFC 1967 [156448]) with the reported range of validity of $0 < p < 165.4 \times 10^5$ Pa (165.4 Bars) and $0 < T < 800$°C.

Source: Simmons 2002 [157578]; SN-LANL-SCI-215-V1, pp. 102–103.

Table 11.4-5. Basalt and Tuff Hydrothermal-Model Parameters for Fracture (f) and Matrix (m) and Dual-Continuum Parameters Used in the THC Simulations

Property	Symbol	Units	Mafic Intrusion	Tuff Host Rock
Fracture Permeability	k_f	m^2	2.74×10^{-9}	2.74×10^{-9}
Matrix Permeability	k_m	m^2	1.0×10^{-20}	4.66×10^{-14}
Fracture Porosity	ϕ_f	—	1.0	1.0
Matrix Porosity	ϕ_m	—	0.05	0.47
Rock Density	ρ_r	kg m^{-3}	2,830	2,410
Specific Heat	C_p	J kg^{-1} K^{-1}	1,010	1,100
Thermal Conductivity	C_{wet}	J m^{-1} s^{-1} K^{-1}	1.93	0.61
Thermal Conductivity	C_{dry}	J m^{-1} s^{-1} K^{-1}	1.93	0.61
Gaseous Diffusivity	D	m^2 s^{-1}	2.13×10^{-5}	2.13×10^{-5}
Temperature Exponent	θ	—	1.8	1.8
Tortuosity	τ	—	1.0	1.0
Residual Saturation	s_r	—	0.04	0.04
van Genuchten Parameter	α_f	Pa^{-1}	8.92×10^{-4}	8.92×10^{-4}
van Genuchten Parameter	α_m	Pa^{-1}	4.15×10^{-5}	4.15×10^{-5}
van Genuchten Parameter	λ_f	—	0.449	0.449
van Genuchten Parameter	λ_m	—	0.327	0.327
Initial Temperature	T_0	ºC	1,200	30
Initial Saturation	s_l^0	—	0.0	0.4
Dual Continuum Parameters				
Fracture Volume Fraction	ε_f	—	0.01	0.01
Matrix Block Size	l_m	m	0.5	0.5
Frature-Matrix Area Factor	σ_{fm}	—	100	0.1

Source: Simmons 2002 [157578]; SN-LANL-SCI-215-V1, p. 104.